POLITECNICO DI MILANO

Scuola di Ingegneria Civile, Ambientale e Territoriale

Corso di Laurea Magistrale in
Ingegneria per l'Ambiente e il Territorio

POLITECNICO
MILANO 1863

Linking physical oceanography, metapopulation dynamics and human pressures. Toward sustainable hake fisheries in the NW Mediterranean Sea

Supervisor:

PROF. PACO MELIÀ

Co-supervisor:

PROF. CARLO PICCARDI

Master Graduation Thesis by:

ANDREA RADICI

Student Id n. 858575

Academic Year 2016-2017

Il libro sacro di cui si conoscono meglio le condizioni in cui è stato scritto è il Corano. Le mediazioni tra la totalità e il libro erano almeno due: Maometto ascoltava la parola di Allah e la dettava a sua volta ai suoi scrivani. Una volta, – raccontano i biografi del Profeta – dettando allo scrivano Abdullah, Maometto lasciò una frase a mezzo. Lo scrivano, istintivamente, gli suggerì la conclusione. Distratto, il Profeta accettò come parola divina quel che aveva detto Abdullah. Questo fatto scandalizzò lo scrivano, che abbandonó il Profeta e perdette la fede.

Sbagliava. L'organizzazione della frase, in definitiva, era una responsabilità che toccava a lui; era lui che doveva fare i conti con la coerenza interna della lingua scritta, con la grammatica e la sintassi, per accogliervi la fluidità d'un pensiero che s'espande fuori d'ogni lingua prima di farsi parola, e d'una particolarmente fluida quale quella di un profeta. La collaborazione dello scirvano era necessaria ad Allah, dal momento che aveva deciso d'esprimersi in un testo scritto. Maometto lo sapeva e lasciava allo scrivano il privilegio di chiudere le frasi; ma Abdullah non aveva coscienza dei poteri di cui era investito. Perdette la fede in Allah perché gli mancava la fede nella scrittura, e in se stesso come operatore della scrittura. [...]

Se a un infedele fosse permesso escogitare delle varianti alle leggende sul Profeta, proporrei questa: Abdullah perde la fede perché nello scrivere sotto dettatura gli sfugge un errore e Maometto, pur avendolo notato, decide di non correggerlo, trovando preferibile la dizione errata. Anche in questo caso, Abdullah avrebbe torto di scandalizzarsi. È sulla pagina, non prima, che la parola, anche quella del raptus profetico, diventa definitiva, cioè scrittura. È solo attraverso la limitatezza del nostro atto dello scrivere che l'immensità del non-scritto diventa leggibile, cioè attraverso le incertezze dell'ortografia, le sviste, i lapsus, gli sbalzi incontrollati della parola e della penna. Altrimenti ciò che è fuori di noi non pretenda di comunicare con la parola, parlata o scritta: mandi per altre vie i suoi messaggi.

— Calvino, *Se una notte d'inverno un viaggiatore*

Esas ambigüedades, redundancias y deficiencias recuerdan las que el doctor Franz Kuhn atribuye a cierta enciclopedia china que se titula *Emporio celestial de conocimientos benévolos*. En sus remotas páginas está escrito que los animales se dividen en: (a) pertenencientes al Emperador, (b) embalsamados, (c) amaestrados, (d) lechones, (e) sirenas, (f) fabulosos, (g) perros sueltos, (h) incluídos en esta clasificación, (i) que se agitan como locos, (j) innumerables, (k) dibujados con un pincel finísimo de pelo de camello, (l) etcétera, (m) que acaban de romper el jarrón, (n) que de lejos parecen moscas.

— Borges, *El idioma analítico de John Wilkins*

The last ever dolphin message was misinterpreted as a surprisingly attempt to do a double-backwards-somersault through a hoop whilst whistling the *Star Spangled Banner*, but in fact the message was: so long, and thanks for all the fish.

— Adams, *Hitchhiker's Guide to the Galaxy*

RINGRAZIAMENTI

Il mio primo ringraziamento non può che andare al professor Melià, che mi ha seguito lungo tutto questo percorso, senza mai far mancare il suo supporto, soprattutto quando le idee erano poche e il morale basso. Ringrazio altresì per la sua disponibilità il professor Piccardi, che è intervenuto soprattutto nel capitolo 7 riguardo all'analisi di rete.

Un grazie va ad Alessandro Ligas, Paolo Sartor e Mario Sbrana del CIBM di Livorno, che mi hanno aiutato a prendere confidenza con la biologia del nasello e con i diversi tipi di pescherecci del mar Tirreno; e parimenti a Isabella Bitetto, Pierluigi Carbonara, Giuseppe Lembo e Maria Teresa Spedicato del COISPA di Bari, che mi hanno fornito numerosi spunti riguardo alla modellistica matematica.

Ringrazio inoltre la professoressa Epifani per i consigli riguardo al test statistico svolto nel capitolo 4, Mokrane Belharet per le nozioni sulle simulazioni lagrangiane dei capitoli 4 e 5, e il professor Mari per gli spunti sulla diffusione degli individui adulti implementata nel capitolo 6.

Inoltre vorrei ringraziare Tobia Rinaldo, collega di tesi per lunghi tratti, così come i dottorandi del gruppo di ecologia del DEIB, e Paolo Giani, perché è una sorgente inesauribile di idee.

Il template su cui sto scrivendo sconsiglia di ringraziare persone che non abbiano partecipato attivamente e, sottinteso, direttamente, al lavoro di ricerca. Tuttavia, non posso trattenermi dal ringraziare la mia famiglia, con mamma e papà in testa, la mia compagna Sabrina, e il mio amico Riccardo (il quale, a dirla tutta, effettivamente ha avuto modo di contribuire a questo testo citando un brano di Borges al momento appropriato) per l'affetto con cui mi hanno accompagnato nella stesura delle seguenti pagine.

Questa tesi è stata concepita nel conesto del Honors Programme "Engineering for Sustainable Development", un programma di formazione del Politecnico di Milano volto a migliorare le competenze interdisciplinari dei futuri ingegneri, aiutandoli a valutare le sfide globali, al fine di operare nel campo dello sviluppo sostenibile.

Il corso di formazione ha compreso anche lo sviluppo di una tesi di master multidisciplinare, che nel mio caso ha incluso aree di ricerca specifiche di ecologia e teoria delle reti.

CONTENTS

LIST OF FIGURES

LIST OF TABLES

ACRONYMS

DCF Data Collection Framework

GNS gillnets

GSA geographic sub area

GSI gonadosomatic index

GTR trammel nets

L50 length of first maturity

LOA length over all

LLS longlines

MEDISEH Mediterranean Sensible Habitats

MEDITS International Bottom Trawl Survey in the Mediterranean

MPAs marine protected areas

NNB Nearest Neighbor bootstrap

OTB otter bottom trawl

PLD pelagic larval duration

S/R Stock recruitment function

SSB spawning stock biomass

SSC small scale fisheries

STECF Scientific, Technical and Economic Committee for Fisheries

TL total length

VMS Vessel Monitoring System

XSA eXtended Survivor Analysis

ABSTRACT

In this work the ecological dynamics of *Merluccius merluccius* in the NW Mediterranean Sea were studied in order to identify candidate areas to be protected to facilitate the long term conservation of the stock and the profitability of fishery. As a first step, oceanographic connections between spawning grounds and nurseries have been studied by means of Lagrangian simulations in order to quantify the extent of the larval exchange between different GSAs in the NW Mediterranean Sea. Having ascertained that, in the majority of cases, less than 1% of the eggs released in a GSA reaches other GSAs, the joint study of the only two GSAs for which the flow was substantial (i.e. the GSAs 9 and 10, Ligurian and Tyrrhenian Sea) has been carried out. Here an indepth evaluation of local-scale connectivity was conducted on a grid formed by cells sized 0.125° (latitude) $\times$ 0.1875° (longitude); the result was summarized in a connectivity matrix. Spawning grounds, to date not mapped, were reconstructed using Lagrangian simulations and suitability maps. In the GSA 9 a metapopulation model was developed, which describes the spatio-temporal dynamics of an age-structured stock subject to the fishing pressure of different fishing vessels. This model was used to simulate the long-term effects of local protections (implemented through fishing closures): areas around Elba island were identified that can significantly increase the spawning stock and the amount of fishing yields with respect to a status quo scenario. Finally, a theorethical network analysis approach was used to characterize cells in terms of centrality indicators; instrenght, betweenness and, partially, information centrality were associated with cells whose closure provides good performance in terms of spawning stock and fishing yield increase.

SOMMARIO

In questo lavoro sono state studiate le dinamiche ecologiche di *Merluccius merluccius* nel mar Mediterraneo nordoccidentale al fine di identificate aree candidate ad essere protette per perseguire la conservazione dello stock e la redditività della pesca sul lungo periodo. In primo luogo sono state studiate le connessioni oceanografiche fra le aree riproduttive (spawning grounds) e le aree di raccolta degli avannotti (nurseries) per mezzo di simulazioni Lagrangiane al fine di quantificare l'entità dello scambio di larve fra diverse GSA del Mediterraneo nordoccidentale. Appurato che, nella maggioranza dei casi, meno dell'1% delle uova rilasciate presso una GSA raggunge altre GSA, si è proceduto allo studio congiunto delle uniche due GSA per cui il flusso è risultato consistente, ovvero le GSA 9 e 10 (Mar Ligure e Tirreno). Qui è stata condotta una valutazione approfondita della connettività a scala locale su una griglia formata da celle di dimensioni 0.125° (latitudine) $\times$ 0.1875° (longitudine); il risultato è stato riassunto in una matrice di connettività. Le aree riproduttive, precedentemente non mappate, sono state ricostruite per mezzo di simulazioni Lagrangiane e mappe di idoneità ambientale. Nella GSA 9 è stato sviluppato un modello di metapopolazione, che descrive le dinamiche spaziotemporali di uno stock strutturato in classi di età sottoposto alla pressione di pesca di diversi pescherecci. Questo modello è stato utilizzato per simulare gli effetti sul lungo termine di protezioni locali (implementate tramite chiusure alla pesca): sono state identificate aree circostanti l'isola d'Elba in grado di aumentare significativamente lo stock di adulti riproduttori e la quantità di pescato rispetto allo status quo. Infine, si è fatto uso della teoria dell'analisi delle reti per caratterizzare le celle in termini di indicatori di centralità; instrenght, betweenness e, in parte, information centrality sono risultate associate a celle la cui protezione fornisce buone prestazioni in termini di aumento di adulti riproduttori e quantità di pescato.

1

INTRODUCTION

Fishing is one of the oldest human activities ever performed on the Mediterranean shores. The birth and the development of ancient societies, such as Mycenaeans and Phoenicians, was based also on the products the sea could give (Carenti, 2012). Although fisheries were born as livelihood activities, they rapidly evolved to become the basis of more advanced ways of production. It is well documented that Phoenicians, in particular, developed the first industry of the production of tyrian purple, which was derived from molluscs *Bolinus brandaris* (Bruin, 1970); its fishery spread all over the Mediterranean Sea, and purple became sign of nobility up to medieval times (Ostrogorski, 1969).

Although the Mediterranean Sea is known to be less productive compared to other european seas (Raffaele, 1888), fishing has been carried out uninterruptedly until today. Nowadays higher demands characterize the exploitation - or, more often, overexploitation - of marine resources, which are threatened also by habitat loss and climate change. According to the Global Biodiversity Outlook 4 (Alkemade et al., 2014), however, the sectors in which efforts put in action to reduce impacts of human activities on biodiversity have been less effective are "avoiding fishing pressure on vulnerable species" and "avoiding overfishing".

Overfishing threatens the conservation of stocks as well as the long term sustainable exploitation of marine resources. It is well known that, according to the Gordon-Schaefer bioeconomic model, conservation and profitability issues acknowledge win-win solutions (Munro, 1979); and, such as many other natural resources, marine resources suffer the so called "tragedy of the commons" in an open access market (Hardin, 1968). As a natural consequence of this, an external regulation by policy makers is needed in order to achieve advantageous solutions for both fish and fishers.

This study focuses on the spatial dynamics of the European hake (*Merluccius merluccius*, L. 1758) stock in the NW Mediterranean Sea, in order to identify candidate locations for the establishment of marine protected areas. During period from 2000 to 2013, *Merluccius merluccius* was the 8^{th} most fished species in Mediterranean sea, and one of the first in terms of discarded. In Italy, it is reported that around 30 percent of specimens caught are discarded, because of the large proportion of juveniles in catches (FAO, 2016). As a result of this pressure, the European hake stock in several areas of the NW Mediterranean Sea is classified as overfished (Ligas and Sartor, 2015).

In order to remedy this unsustainable exploitation, fishery restricted areas are proposed as a tool to allow recovery of threatened fish, especially where juveniles - devoid of economic value, but crucial for the manteinance of the whole stock - and spawners gather. The selection of these areas should take into account larval exchanges between different sites due to oceanic circulation, demography and spatial distribution of fishing effort, in order to understand the dynamic role of different locations.

The present work has been developed in the context of the SafeNet project (`http://www.criobe.pf/recherche/safenet`), a research project funded by the European Commission, which intends to explore a network of MPAs in order to achieve sustainable fisheries in European Union Mediterranean waters. In particular, aim of this thesis is to indicate possible locations for the establishment of marine protected areas, using Lagrangian simulations to investigate the larval connections between different areas, and a metapopulation model that implements the spatio-temporal dynamics of the European hake stock in the Ligurian Sea and Northern Tyrrhenian Sea under the pressure of different fishing segments to simulate the effects of local fishery restrictions in the long term.

As a first step, oceanic connections between different European hake habitats are explored at the basin scale (NW Mediterranean Sea); then, in view of the results obtained, a specific isolated site is analyzed, the Ligurian Sea and the Northern Tyrrhenian Sea, for which detailed time series are available.

More precisely, the thesis is organizes as follows. Chapter 2 introduces the scientific context in which this thesis has been developed: it presents the main knowledge for what concerns *Merluccius merluccius* biology and its fisheries and introduces marine protected areas as a tool to pursue both conservation and profitability issues.

Chapter 3 is dedicated to the technical characteristics of the main material used in this work of thesis.

The following chapters explain both methods and results of each conceptual step of the work, proceeding from a large scale analysis toward the implementation of a metapopulation model at the regional scale.

Chapter 4 explores the entities of the oceanic connections due to larval drift between reproduction sites and nurseries (areas where juveniles aggregate) in the entire NW Mediterranean sea, by means of Lagrangian simulations. The main question asked in this Chapter is: do stocks located far away from each other exchange larvae? If so, are larval fluxes important for the recruitment?

Chapter 5 describes the reconstruction of spawning grounds in the area selected as case study for the analysis carried out in the following chapters. Since Northern Tyrrhenian Sea resulted highly connected with Southern Tyrrhenian Sea, the whole Tyrrhenian Sea is consid-

ered in this step. Spawning grounds are reconstruced from known nurseries via backward Lagrangian simulations. Larval connections between spawning grounds and nurseries are analyzed at a high resolution, and summarized in a connectivity matrix.

In Chapter 6, a metapopulation model is proposed to describe the spatiotemporal dynamics of European hake stock in the northern Tyrrhenian and Ligurian Sea, using the connectivity matrix produced in Chapter 5. This model implements an age structured stock on a spatially explicit grid, trying to model the fishing pressure of different fishing fleets both in time and space.

In Chapter 7 connectivity is analyzed using the instruments provided by network analysis. Centrality indicators are used to identify the locations that most contribute to the connectivity in the study area. Then, the metapopulation model developed in the Chapter 6 is used to assess the consequences of protecting a site in terms of forecasted yields and spawning stock biomass.

Finally, the last Chapter is dedicated to comment the results achieved and propose further improvements to this study.

2 CONTEXT

2.1 STATE OF THE ART

This thesis has been developed in the context of the SafeNet project (http://www.criobe.pf/recherche/safenet). SafeNet aims to identify coherent network(s) of marine protected areas (MPAs) and other area-based fisheries management rules whose emergent properties can help achieve marine conservation while granting the recovery of fish stocks and hence sustainable fisheries in the north-western Mediterranean Sea. European hake is one of the main species taken into consideration.

The SafeNet project inherits data and methods from previous projects. MEDISEH project (Mediterranean Sensible Habitats; Giannoulaki et al., 2013) provides a major literary review regarding the reproduction of the European hake. In the MEDISEH project, maps of spawning grounds (i.e. where mature adults release their eggs) and nurseries (i.e. where the youngest specimens, the recruits, are found in highest abundances) were produced, and breeding periods analyzed.

The main data source used in the MEDISEH project is the MEDITS (International Bottom Trawl Survey in the Mediterranean) scientific surveys project, which was intended to produce information on both benthic and demersal species in term of population distribution as well as demographic structure (http://www.sibm.it/SITO\%20MEDITS/principaleprogramme.htm). In the MEDITS database data about catches were recorded according to a very specific protocol (Bertrand et al., 2017). Surveys have been conducted since 1994; however, many authors complain the uneffectiveness of the nets used in catching large individuals (Giannoulaki et al., 2013). As a result of this, scientific information about spawners is considered to be poor and mainly anecdotal.

LLUCET (Lleonart, 2002) is another major source for MEDISEH reports. In this project several surveys have been performed in the Northern Tyrrhenian Sea, Ligurian Sea and Catalan Sea from 1998 to 2000 in order to collect biological information about recruitment and assess the impact of fisheries.

Additional information on fisheries was provided by the Stockmed project (Fiorentino et al., 2014). Stockmed aimed at the identification of distinct biological units (stocks) for different fish and shellfish species and among different regions. This project provided maps of spatial distribution of the effort of different vessels, the so called

Vessel Monitoring System (VMS) data (EC, 2003; EC, 2008), and maps of potential fishing grounds (Kavadas et al., 2015).

Finally, the STECF (Scientific, Technical and Economic Committee for Fisheries; Cardinale, Damalas, and Chato Osio, 2015) assessment developed an analysis aimed at reconstructing population abundances and other biological parameters (natural mortality, percentage of mature individuals in different age classes, weights, lengths) using a virtual population analysis software, the eXtended Survivor Analysis (XSA) (Darby and Flatman, 1994) in different areas of the Mediterranean Sea. Time series of catches and efforts differentiated per type of vessel (métier) are provided as well.

2.2 THE EUROPEAN HAKE

The European hake (*Merluccius merluccius*, L. 1758) is a demersal species inhabiting the north-eastern Atlantic from Norway to Mauritania and the entire Mediterranean, and along the southern coasts of the Black Sea (Jardas, 1996, Relini, Bertrand, and Zamboni, 1999). In the Mediterranean Sea, this species prefers muddy bottoms, or muddy-sandy (Druon et al., 2015). The bathimetric distribution varies according to the age: juveniles are located almost exclusively on the sea bottom, at depths between 100 and 250 m; older individuals are typical of shallower waters; and finally spawners live between 150 and 350 m; very large specimens can be found also below 500 m (Abella, Serena, and Ria, 2005; Abella et al., 2008; Hidalgo et al., 2008; Lleonart, 2002; Sartor et al., 2015). A general preference for the continental shelf break and the beginning of the shelf slope, between 30 and 700 m depth, can be recognised as a common trait in each life stage (Abella, Serena, and Ria, 2005; Oliver and Massutí, 1994).

2.2.1 *Aspect*

The European hake has a long and cilindrical body (fig. 2.1). The widest part is behind the head. There are two dorsal fins: the first one is short and triangular and the second one is long. The anal fin is similar in shape and size to the second dorsal fin. The ventral fins are placed before the pectoral ones. The caudal fin is cut in a straight line.

2.2.2 *Life cycle*

2.2.2.1 *Early stages*

Like any other fish, eggs of *Merluccius merluccius* are released and fertilized by mature individuals during the spawning season, in very specific locations, called spawning grounds. Reproduction seasons

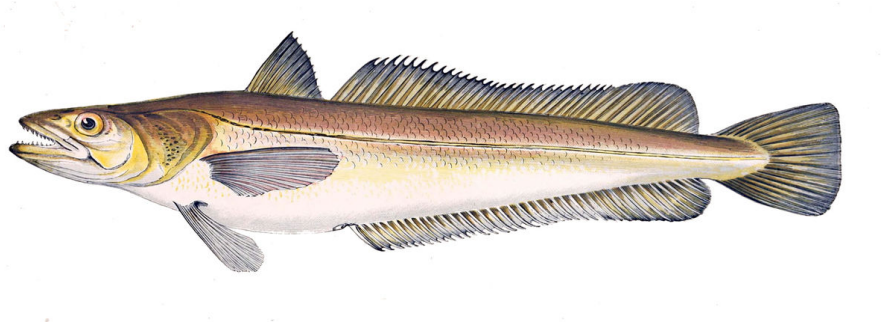

Figure 2.1: *Merluccius merluccius* (from https://it.wikipedia.org/wiki/Merluccius_merluccius)

vary from site to site; very often, several spawning peaks occurs in the same year, seamless (Giannoulaki et al., 2013; Recasens, Chiericoni, and Belcari, 2008). After fertilization, eggs hatch within three days (Raffaele, 1888).

Several attempts to artificially reproduce eggs insemination have been carried out (Coombs and Mitchell, 1982; Bjelland and Skiftesvik, 2006), mainly for acquaculture perspective; all these authors reported difficulties in keeping mature individuals alive after catching, and observed a high mortality of larvae during the experiments. Hatching time has been noticed to be a decrescent function of incubation temperature.

The larval phase, or planktonic life phase, usually coincides with the pelagic larval duration (PLD), which is the period in which the organism has no motion cability, and a passive advection by currents can be assumed. During this life stage, several studies suggested age can be monitored with daily growth increments (rings) in otoliths (Arneri and Morales-Nin, 2000; Belcari, Ligas, and Viva, 2006). This method allows to calculate (or better, to back calculate) hatching date distribution from hauls (Lleonart, 2002).

Larval phase ends with a complete metamorphosis, about a month and a half post hatching. Very different durations of larval phase have been proposed, from less than 40 days (Olivar, Quılez, and Emelianov, 2003) to more than two months (Morales-Nin and Moranta, 2004)[1]. This uncertainty about the effective duration of the larval phase will be dealt with in Chapter 4.

2.2.2.2 *Juveniles: growth and feeding behaviour*

The metamorphosis ending the larval phase, and the consequent settlement in the nurseries, is called recruitment. Recruits are those specimens that have settled on the bottom, becoming available to the fishing gear in well-defined habitats at the end of their larval – pelagic

1 It is curious to note that both autors computed these values from samples hauled in the Catalan Sea.

stage and which remain in these habitats before dispersing or migrating (Giannoulaki et al., 2013).

Since the largest contribution to the recruits abundance of a region is given by eggs released by spawning individuals in the same region, the peak of recruitment matches approximately with the peak of spawning (Abella et al., 2008), delayed of a time span equivalent to the PLD. Recruitment occurs when larvae are 11 to 16 mm total length (TL) (Palomera, Olivar, and Morales-Nin, 2005). In the first stages of this life phase, hakes have a growth from 1 to 1.5 cm $month^{-1}$ (Arneri and Morales-Nin, 2000; Lleonart, 2002; Druon et al., 2015).

It has been noticed that, in the Catalan Sea, individuals below 4.5 TL usually feed on benthonic preys, mainly crustacean, such as Euphausiacea (krill) and Mysidacea (shrimps), while larger individuals display nocturnal migration toward the water column and feed equally on both crustaceans and fish, such as *Gadiculus argenteus* or *Maurolicus muelleri* (Bozzano, Sardà, and Ríos, 2005).

Hakes feeding on other fish seem to differentiate their prey according to the location. In the Adriatic Sea, individuals larger than 16 cm (which is the standard length at the end of the first year[2]) usually feed on *Sardina pilchardus*, *Sprattus sprattus* and *Engraulis encrasicolus*, while in the Cantabrian Sea the most frequently prayed species are *Micromesistius poutassou* and *Trachurus trachurus* (Velasco and Olaso, 1998). Cannibalism, although recorded, is sporadic, and typical of large specimens (Bjelland and Skiftesvik, 2006; Bozzano, Sardà, and Ríos, 2005).

In the Tyrrhenian Sea a migration at the end of the first year of life is observed toward shallower waters, from depth of 120 - 200 m to 70 - 100 m (Bartolino et al., 2008). It has been supposed that this displacement could be linked to a shift in the diet habits.

2.2.2.3 *Mature individuals*

As reported in STECF assessments (Cardinale, Damalas, and Chato Osio, 2015), the majority of hakes becomes fertile during the third year of life. However, the most common tool used to identify mature individuals is the length of first maturity (L_{50}), i.e. the length at which half of the (female) sampled population becomes fertile. This value varies from region to region, but lengths from 30 to 37 cm are widely accepted in the NW Mediterranean Sea (Giannoulaki et al., 2013).

It is known that large individuals are able to migrate across different regions, since surveys (such as MEDITS) have identified spec-

2 This length varies from region to region. Other authors suggest higher values, such as 18 cm (Giannoulaki et al., 2013); italian law Reg. EC 1626/1994, aiming at protect specimens younger than one year, set this value at 20 cm. These differentiations usually arise when there is a mismatch between scientific surveys and reproduction peaks.

imens far from nurseries and fishing grounds, but this behaviour is poorly documented from a quantitative perspective.

Merluccius merluccius can grow up to 130 cm TL, living up to 20 years, but catches are mainly composed of individuals shorter than 60 cm TL (Jardas, 1996).

2.3 HAKE FISHERIES IN THE MEDITERRANEAN SEA

Fisheries in the Mediterranean Sea are usually classified according to the métier (i.e. vessels equiped with a certain fishing gear). This classification underlies different target species, different vessel lengths - or better, length over all (LOA) - and different scopes (artisanal/recreational or industral/commercial fishing). A more specific way of grouping can differentiate between fleet segments (an example can be Russo et al., 2017), discriminating between lengths, targeted species and ports, too.

European hake is fished in each geographic sub area (GSA) involved in the SafeNet project, with the only exception of Corsica island (GSA 8), where catches are sporadic.

The following classification is reworked from STECF Expert Working Group on landing obligation (Cardinale, Damalas, and Chato Osio, 2015) and SafeNet deliverable 2.5 about socioeconomic indicators (Sartor et al., 2015), which in turn analyzed the Data Collection Framework (DCF) at GSA level (see figure 3.1). Only fisheries landing hakes are considered.

2.3.1 *Longlines*

Longline fishing uses longlines (LLS)[3], long and sturdy lines, called main lines, with baited hooks attached at intervals by means of branch lines called snoods (braccioli). Main lines can be selected to reach depths in the order of some hundreds of meters, while snoods can vary from 1 to 100 m length depending on the mainline type (fig. 2.2). Usually small scale vessels, from 6 to 12 m LOA, are equipped with this gear.

In GSA 6 (Catalan Sea) hake is by far the first species in landings, and one among the first in the GSA 7 (Gulf of Lion).

Because of its selectivity, it is supposed to be a potential tool to reduce fishing mortality on recruits. However, this gear is prone to incidental catching against non-fish species, such as seabirds, turtles and dolphins.

3 Italian: palamito

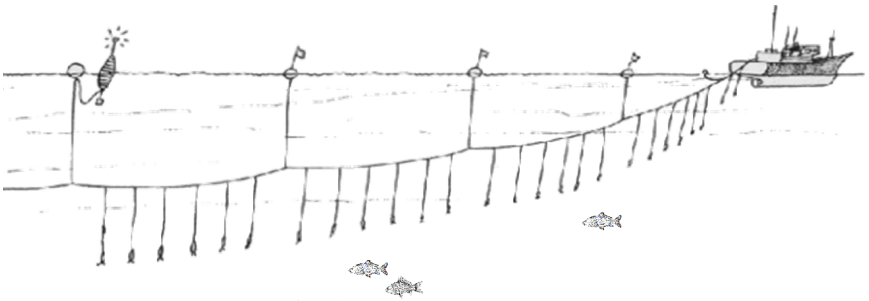

Figure 2.2: Longlines (from http://safinacenter.org/2015/08/fishing-gear-101-longlines-the-snaggers/)

2.3.2 *Gillnets*

Gillnetting is based on gillnets (GNS)[4]. These nets are made up of vertical panels of netting normally set in a straight line. Fish may be caught in several ways, but most often they are gilled, or however held by a protrusions (teeth, spines) or by the entire body. A fish swims into a net and passes only part way through the mesh. When it struggles to free itself, the twine slips behind the gill cover and prevents escape (fig. 2.3). Usually vessels from 6 to 18 m LOA are equipped with this gear.

In GSA 9 (Ligurian and Northern Tyrrhenian Sea) this gear is mainly used to fish hake[5], which results to be the second targeted fish by gillnets in GSA 7.

Gillnets are supposed to have a high degree of size selectivity because of its efficient mesh size regulation.

2.3.3 *Trammel nets*

Similar to gillnet, trammel nets (GTR)[6] are made up of three layers of netting. Two outer layers of large mesh overlay a sheet of fine small mesh between them. The inner layer of small mesh netting is hung slacker that the outer two nets; this creates plenty of slack netting in which the fish swim into and get tangled in pockets of netting between the two outer layers (fig. 2.4). Vessels from 6 to 12 m LOA are mainly equipped with trammel nets, with the only exception of GSA 7, where the only fleet segment is 12 to 18 m.

It is rare to capture a hake with this gear, which usually targets other species, such as *Mullus barbatus* and *Mullus surmuletus*. Only in the GSA 8 (Corsica) hake landings by this métier are larger than zero.

This method has a poorer selectivity compared to gillnets.

4 Italian: rete da posta
5 In Tuscany, vessels equipped with this gear are also called “nasellare”
6 Italian: tramaglio

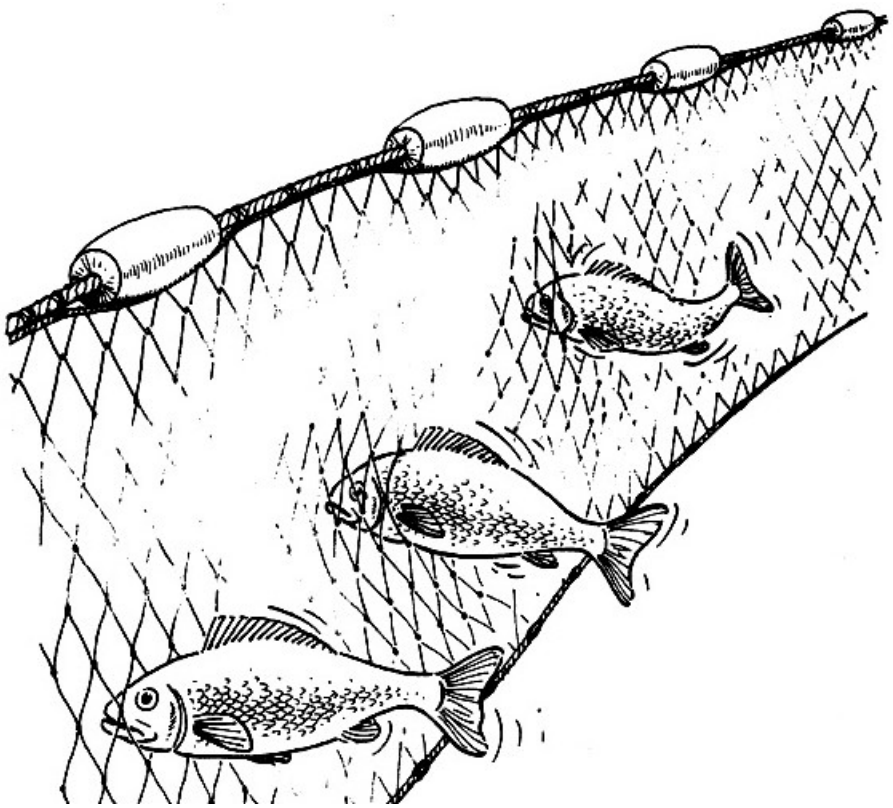

Figure 2.3: Gillnets (from http://www.fao.org/docrep/003/x6935e/x6935e00.htm)

2.3.4 *Otter bottom trawls*

Trawling, or otter bottom trawl (OTB)[7], is by far the clearest example of industrial fishing. It can be carried out by one trawler or by two trawlers fishing cooperatively. A large net is kept open in horizontal and vertical dimensions; while it is dragged, the body of the net guides the fishes inwards, where they are collected in a "cod-end" of a suitable mesh size (fig. 2.5). Large sized vessels are used as trawlers. Usually, this method is further splitted, depending on the depth of the net:

2.3.4.1 *OTB targeting demersal species*

This fleet segment gives the highest hake landings in the analyzed GSAs, with the exception of GSA 8. These vessels are the shortest among trawlers, being usually below 24 m long. They usually fish in the shallowest waters.

7 Italian: pesca a strascico

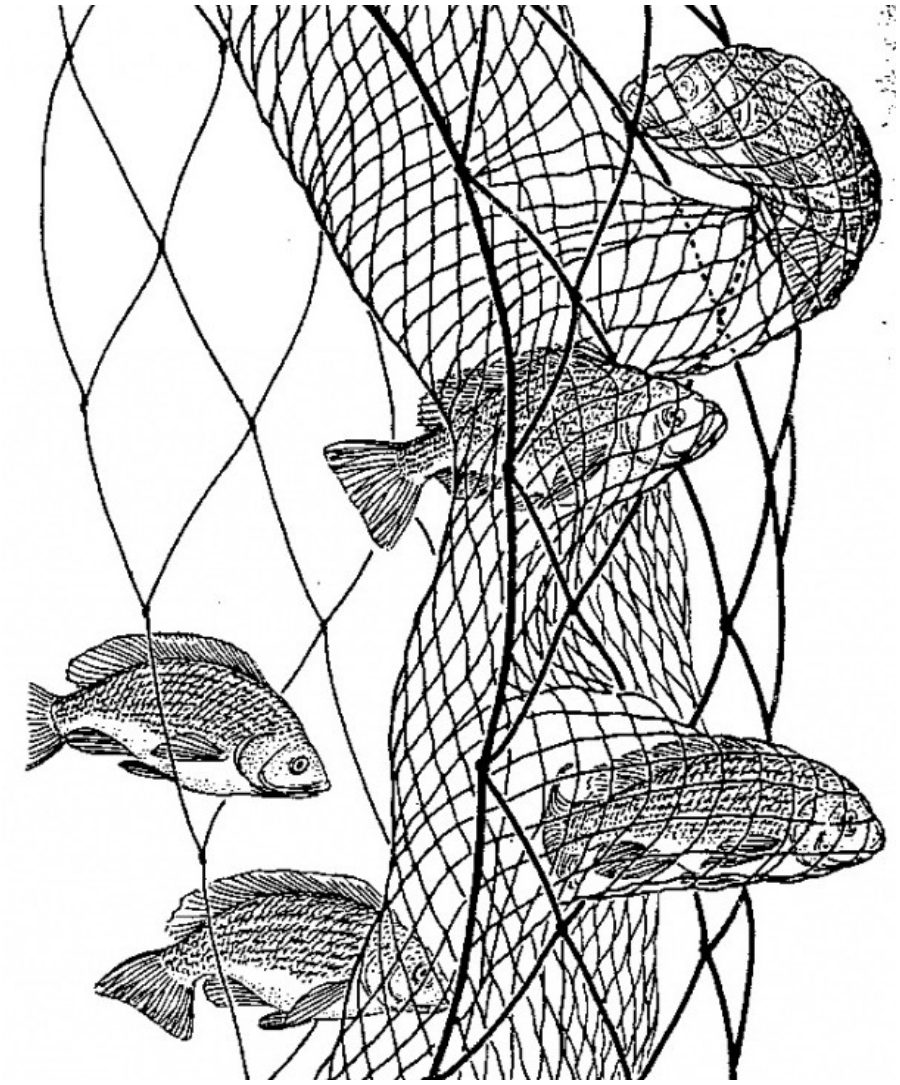

Figure 2.4: Trammel nets (from http://www.memphisnet.net/trammelnets)

2.3.4.2 *OTB targeting deep water species*

Aristeus antennatus is the main and only target of this trawling. Hake catches are quite occasional, being the cod-end depth below 500 m underwater; nevertheless, the largest and oldest hakes are fished this way. More than half of this fleet segment is composed by vessels longer than 24 m.

2.3.4.3 *OTB targeting mixed demersal and deep water species*

Aristeus antennatus is again the main species targeted by this fleet segment. Its catches are comparable in landings to those of other species, such as hake or *Micromesistius poutassou*. Vessels belonging to this fleet segment are usually longer than 24 m.

This gear has the poorest selectivity: very often individuals below the minimum allowed size (20 cm) are catched and discarded.

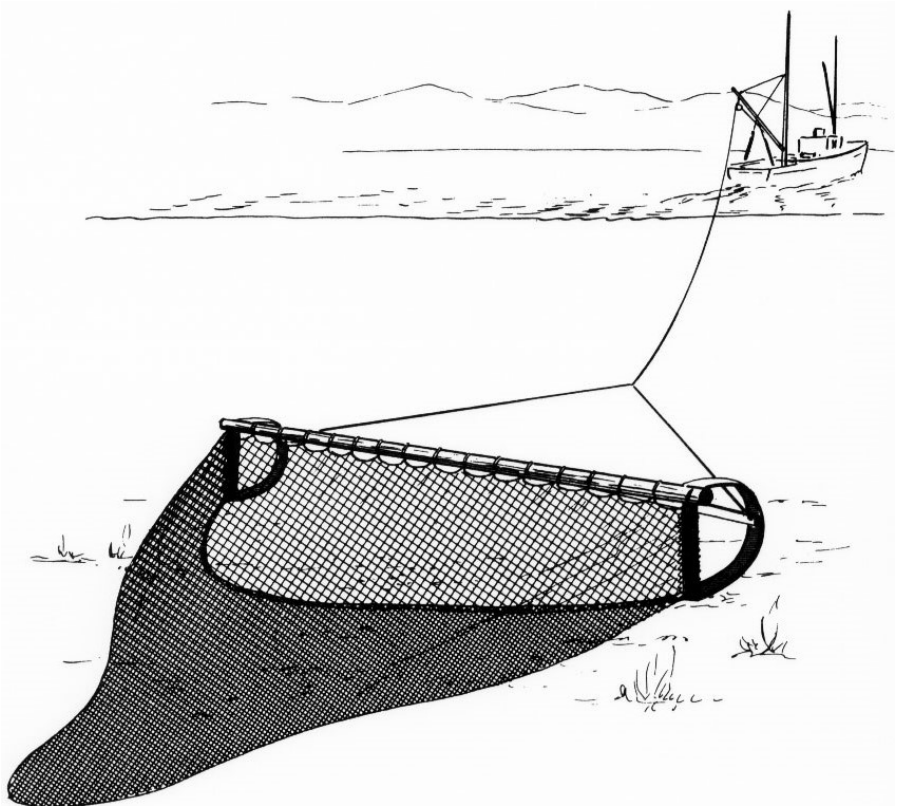

Figure 2.5: Bottom otter trawl (from http://www.gulfofmaine-census.org/education/research-technology/sampling-tools-for-physical-capture/)

2.4 MARINE PROTECTED AREAS

In order to protect endangered species and allow recovery of overfished stocks, marine protected areas are established. MPAs do not follow a unique management: some provide only temporary closures, while others allow only specific kinds of fisheries, usually for recreational uses (Carbonara et al., 2015). The recognition status differs from site to site, as the adopted measures for the violators of the regulation.

Very often, MPAs are established along coastlines to protect costal species. Those MPAs are usually the most restrictive, not allowing any kind of fishing, especially commercial fishing. The Tuscany Archipelago can be considered as an example, since no activity is allowed within a specific distance from the coast.

On the other hand, MPAs established far from the coasts more easily focus the protection on specific targets. For instance, the brown area covering large part of the Ligurian Sea in figure 2.6, the Pelagos Sanctuary, protects marine mammals only (all year around).

Exceptions are given to this general pattern. The fishing restricted area of Continental slope of the Eastern Gulf of Lions aims at protect-

ing also nurseries of *Merluccius merluccius*, and do not allow any kind of demersal fishing.

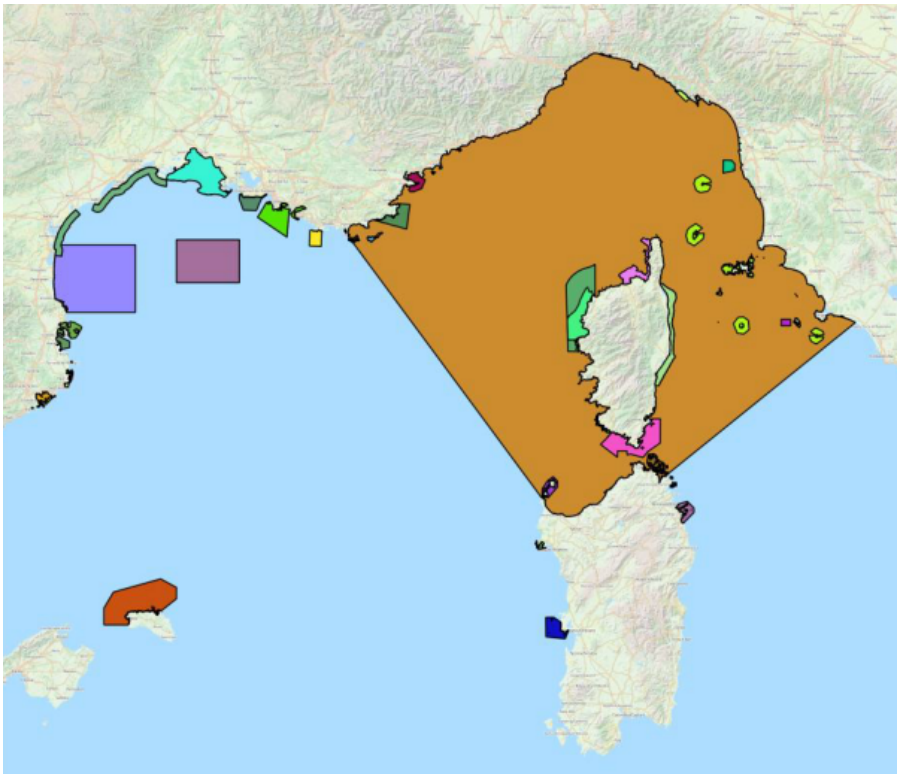

Figure 2.6: Marine protected areas in the GSAs interested by SafeNet project (Ligas and Sartor, 2015).

Marine protected areas are recognised to be an effective tool to achieve conservation of species threatened by overfishing. Moreover, a policy aimed at establishing protected areas in strategic sites could help in recovering the stock where other methods showed ineffectiveness, such as mesh size regulations or catches limitations.

3 MATERIALS

In this Chapter, tools used in the present work are listed and their characteristics explained.

3.1 CURRENTS FIELDS

In order to analyze and quantify the larval drift between different European hake habitat in the NW Mediterranean Sea, Lagrangian simulations were performed. This connectivity assessment was possible using the outputs of Copernicus - Marine Environment Monitoring Service project (http://marine.copernicus.eu/). This database provides a daily motion field for years from 1985 to 2015, with a spatial resolution of 0.0625° both in latitude and in longitude (≈ 8 km), describing currents in the entire Mediterranean Sea, and partially the Black Sea. The vertical resolution of currents includes 72 depths, at increasing intervals, from 0 to about 5'000 m.

In the simulations, the time span was reduced to ten years, from 2004 to 2013, which represent the balance between homogeneity of the time series (the motion field is always referred to 8 a.m.) and proximity to present.

3.2 NURSERIES AND SPAWNING GROUNDS

Within the MEDISEH project, several shapefiles have been produced, corresponding to nurseries and spawning grounds in the Mediterranean Sea (Giannoulaki et al., 2013). Unfortunately, this work covers only GSAs (figure 3.1) neighbouring the european coasts. In this case, spawning ground of the GSAs 5, 7 and 11 (fig. 3.3), and nurseries of the GSAs 5, 6, 7, 9, 10, and 11 (fig. 3.2) have been identified in the western Mediterranean Sea (see table 3.1).

In the MEDISEH report, European hake's nurseries and spawning grounds are ranked into 5 classes, according to their interannual persistence (tab. 3.2). These maps are obtained from presence data collected in the MEDITS project. Several models, belonging to the families of generalized additive mixed models (GAMM) and zero inflated generalized additive models (ZIGAM) were use to include a numer of environmental covariates (latitude, longitude, year, depth, bottom stepness, distance from the coast) and thus identify the most likely sites where hakes reproduce and where recruits settle on the bottom (Colloca et al., 2015).

GSA id	GSA name	spawning grounds	nurseries
5	Balearic Islands	yes	yes
6	Catalan Sea	no	yes
7	Gulf of Lion	yes	yes
8	Corsica Island	no	no
9	Ligurian and Northern Tyrrhenian Sea	no	yes
10	Central and Southern Tyrrhenian Sea	no	yes
11	Sardinia Island	yes	yes

Table 3.1: Nurseries and spawning grounds shapefiles provided by MEDISEH project.

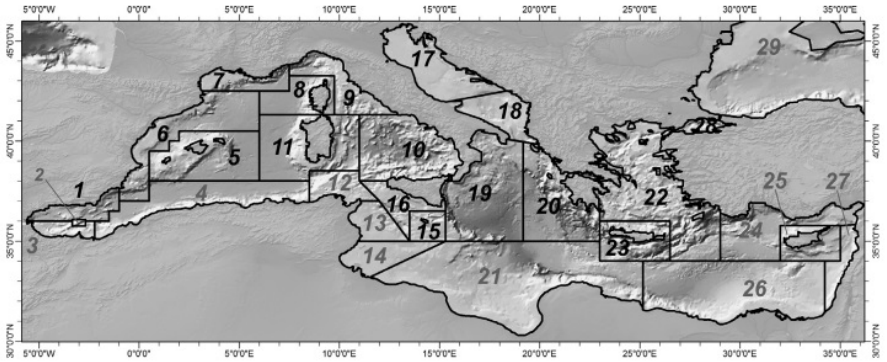

Figure 3.1: GSAs in the Mediterranean Sea (Druon et al., 2015). GSAs covered by the MEDITS project are labelled in bold.

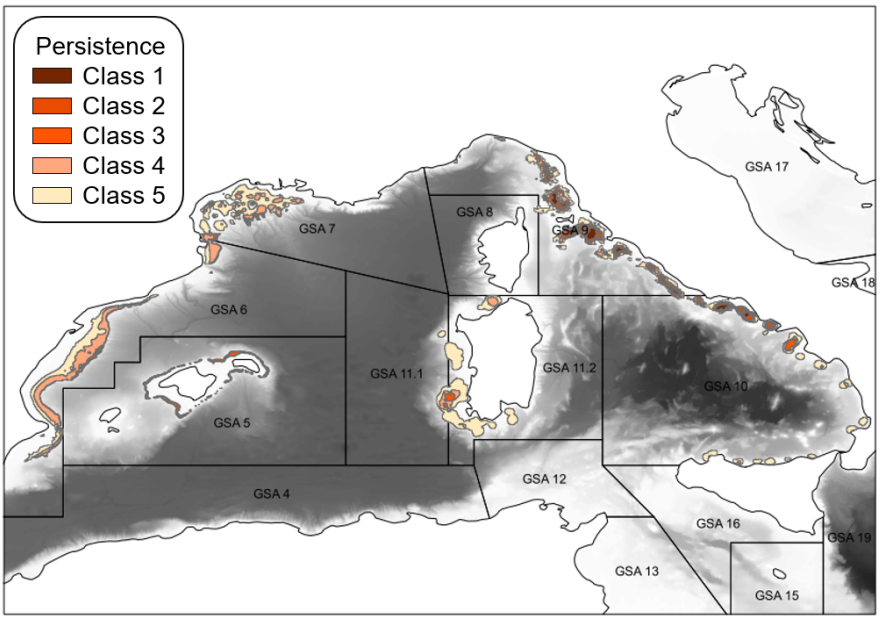

Figure 3.2: Nurseries identified in the western Mediterranean: Balearic Islands (GSA 5), Iberian Sea (GSA 6), Gulf of Lion (GSA 7), Ligurian Sea with the Northern Tyrrhenian Sea (GSA 9), the southern Tyrrhenian Sea (GSA 10), and Sardinia (GSA 11). Higher temporal persistence is identified by darker colours.

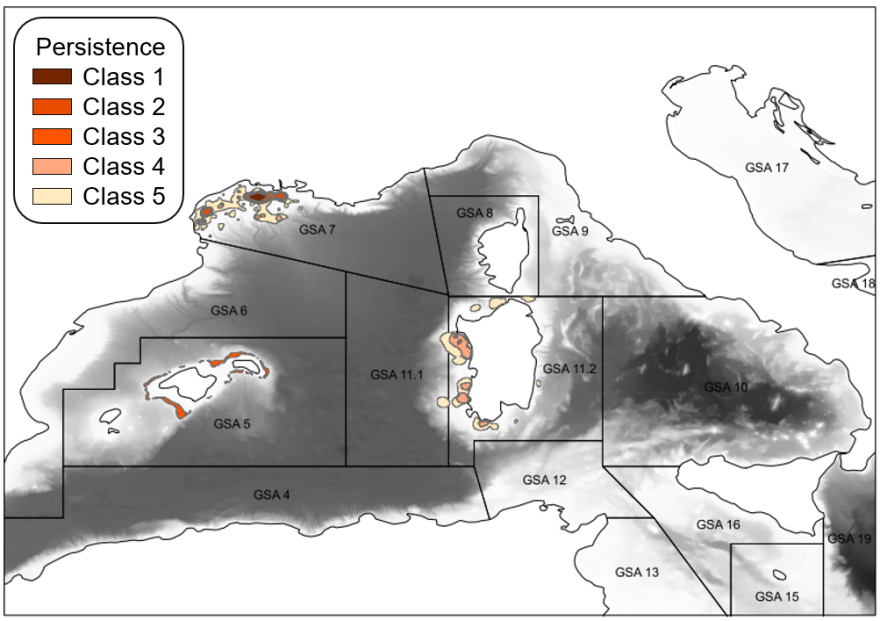

Figure 3.3: Spawning grounds identified in the western Mediterranean: Balearic Islands (GSA 5), Gulf of Lion (GSA 7), Sardinia (GSA 11). Higher temporal persistence is identified by darker colours.

Persistence class	lower boundary	higher boundary	mean level
5	0.05	0.2	0.125
4	0.2	0.4	0.3
3	0.4	0.6	0.5
2	0.6	0.8	0.7
1	0.8	1	0.9

Table 3.2: Persistence classes of nurseries and spawning grounds.

3.3 PRESENCE DATA

MEDITS surveys have collected catches data since 1994 (http://www.sibm.it/SITO\%20MEDITS/principaleprogramme.htm). An otter bottom trawl is used to collect samplings during surveys, which are usually performed in summer. For each specimen, sex, species and age class is noted according to a very specific protocol (Bertrand et al., 2017); depth, latitude and longitude of the haul are recorded too. Unfortunately, many authors complain about the uneffectiveness of the nets used in catching large individuals (Giannoulaki et al., 2013). As a result of this, scientific information about spawners is poor and anecdotal, and many spawning grounds have not been mapped in the MEDISEH project (tab. 3.1).

3.4 BATHYMETRY

Bathymetry in the Mediterranean Sea is an output of the Emodnet project (http://www.emodnet-bathymetry.eu/). The resolution of the bathimetric maps is 0° 0′ 7.5″ ($\approx$ 30 m).

This grid was interpolated to calculate high resolution depths and identify potential spawning grounds in Chapter 5.

3.5 BIOLOGICAL TRAITS, ABUNDANCES AND EFFORT TRENDS

STECF assessment represents the main source of information (Cardinale, Damalas, and Chato Osio, 2015). For what concerns this work, this report provides assessments of "trends in historic and recent stock parameters for the longest time series possible available up to and including 2014". About GSA 9, the following information is provided:

1. Abundances of seven age classes, from 0 to 6+, from 2006 to 2014;
2. Fishing mortality for each class and each year;
3. Recruits and spawning stock biomass (SSB) abundances at each year;
4. Natural mortality for each age class, estimated using PROD-BIOM software (Abella, Serena, and Caddy, 1998);
5. Proportion of mature individuals at each age class;
6. Average weight at each age class;
7. Allometric relation and body growth curve parameters (Von Bertalanffy, 1938).

In order to estimate the first three parameters, a virtual population analysis, the eXtended Survivor Analysis (XSA, Darby and Flatman, 1994), was performed. Inputs to XSA are composed by catches, densities, weights and natural mortalities for each age class.

3.6 FISHING GROUNDS

Fishing grounds are defined as those locations in which fishing effort is concentrated. Two ways of measuring spatial distribution of effort can be explored:

1. For those vessels with LOA > 15 m, Vessel Monitoring Systems data are partially available. The VMS was introduced by the European Union for remote control of fishing vessels. Positions, speed and prow heading are recorded by an automatic transmitting station (the so-called blue box), and periodically sent via satellite transmission (EC, 2003; EC, 2008). Unfortunately, blue boxes are mandatory for large scale fisheries only, tipically trawlers; data about small scale fisheries, such as longlines, gillnets and trammel nets, which acccount for the 43% of total hake landings in GSA 9 in 2006 - 2014 (Cardinale, Damalas, and Chato Osio, 2015) would be neglected. A secondary puzzle is represented by the interpretation of VMS data, since it is not possible to infer directly the activity of fishing from the presence of a vessel; however, several methods have been proposed to clean VMS data (Russo et al., 2011);

2. In order to overcome the lack of information about vessels with LOA < 15 m, Kavadas et al. (2015) developed a Multi-Criteria Decision Analysis tool (MCAT) to extract fishing footprints in eastern Ionian Sea, aimed especially at dealing with small scale fisheries, accounting for 95% of the greek fleet. This method computes spatial indices as the fuzzy product of a fishery suitability index and an activity index. The fishery suitability index is the result of an Analytic Hyerarchy Process (AHP), which combines different criteria, such as bathymetry, distance from the coast, legislation, primary production parameters, weighted and linearly combined at the resolution of the data. The activity index spatially interpolates on the sea surface an indicator of fishing effort computed for each port/fleet. This indicator, VAI_p, is explained by equation 3.1:

$$VAI_p = \sum_{i=1}^{N_p} L_i GT_i \tag{3.1}$$

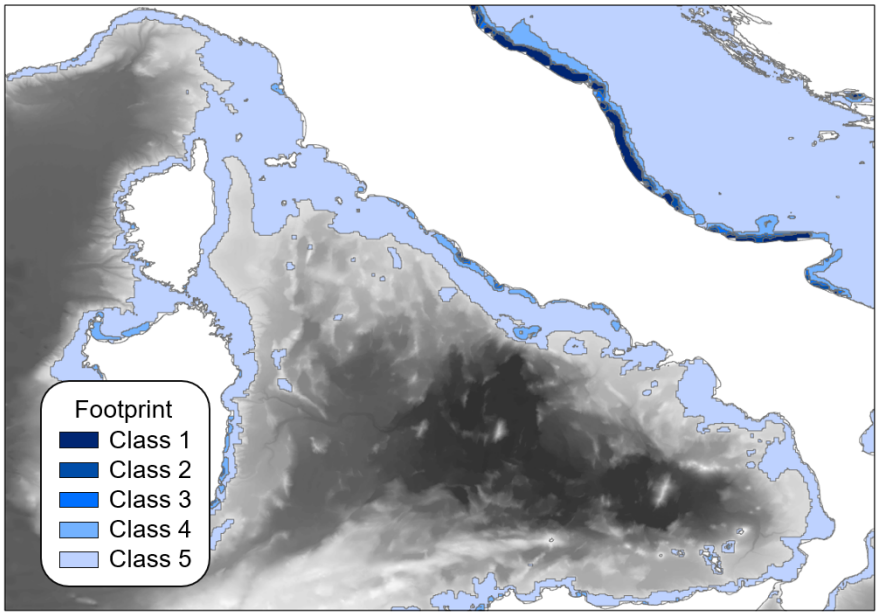

Figure 3.4: Potential fishing grounds identified for small scale fisheries from 0 to 12 m LOA (SSC 0-12). Higher indices are identified by darker colours.

Where p identifies the port, N_p i the number of vessels in port p, i identifies the vessel, L_i is the i—vessel length in port p, GT_i its gross tonnage (see Kavadas et al., 2015 for details).

The same procedure was used in the Stockmed project (Fiorentino et al., 2014) to map the fishing effort in all the European GSAs, differentiating between métier and LOA. Concerning hake fisheries, two métiers - otter bottom trawl, (OTB), and small scale fisheries (SSC), which groups longlines, gillnets, trammel nets - and two lengths (0 m - 12 m; 12 m - 24 m) are available (fig. 3.4, 3.5, 3.6, 3.7).

These maps have been used in order to spatially weight the fishing effort of these four fleet segments in Chapter 6.

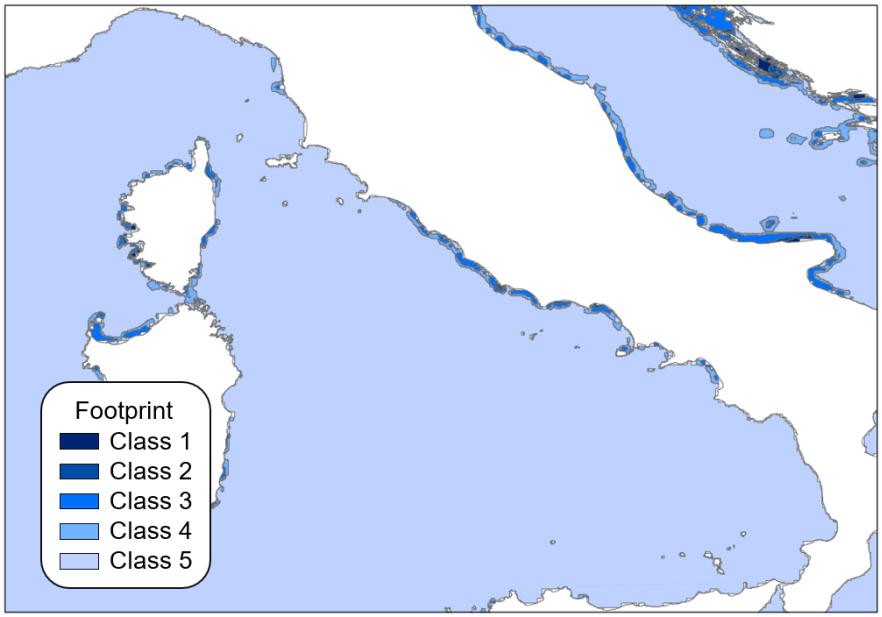

Figure 3.5: Potential fishing grounds identified for small scale fisheries from 12 to 24 m LOA (SSC 12-24). Higher indices are identified by darker colours.

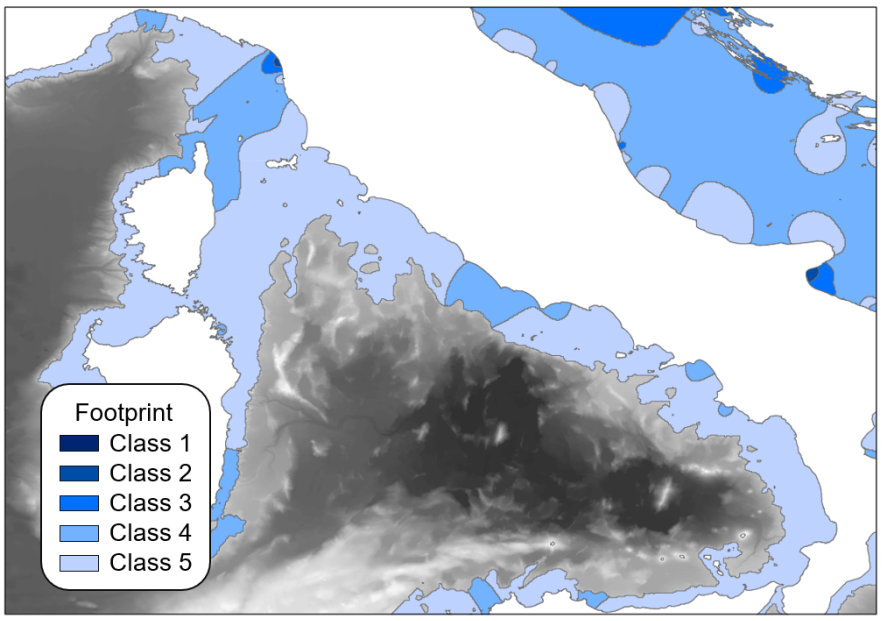

Figure 3.6: Potential fishing grounds identified for otter bottom trawlers from 0 to 12 m LOA (OTB 0-12). Higher indices are identified by darker colours.

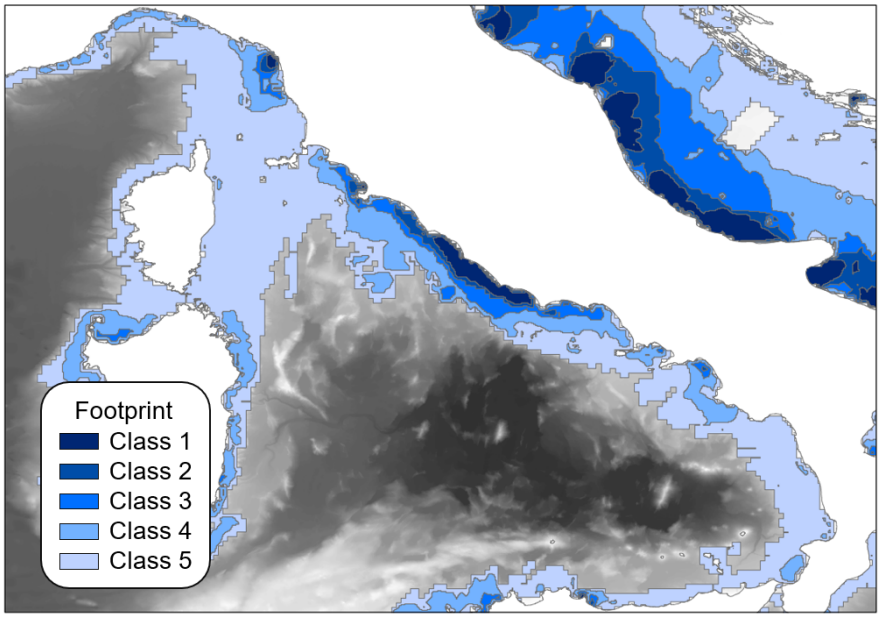

Figure 3.7: Potential fishing grounds identified for otter bottom trawlers from 12 to 24 m LOA (OTB 12-24). Higher indices are identified by darker colours.

4

CONNECTIVITY ASSESSMENT IN THE NW MEDITERRANEAN SEA

The aim of this Chapter is to investigate the connectivity in the NW Mediterranean Sea. In particular, the focus is placed on the connections between spawning grounds, i.e. the areas where fertile adults release eggs, and nurseries, i.e. the areas in which the larvae, having already developed sufficient motion capacity, terminate their planktonic phase and settle in the sea bottom, thus becoming recruits.

The extent by which these connections actually affect recruitment in different GSAs will justify (or not) the study of an isolated GSA.

4.1 METHODS

Connectivity among patches of suitable habitat has been assessed by means of Lagrangian simulations. Previous work suggested that this phenomenon could play a relevant role in the dynamics of this species (Fiorentino et al., 2014; Oliver and Massutí, 1994), while other works pointed out that larval retention could have important implications on the management and conservation of marine resources (Melià et al., 2016).

Hake eggs and larvae have been modelled as Lagrangian particles released in the water column from spcific locations and left free to float, passively carried by the current. These specific locations should correspond to the spawning grounds; unfortunately, as anticipated in the previous Chapter, in many GSAs only nurseries have been mapped (Giannoulaki et al., 2013).

In order to deal with this lack of data, different simulations were carried out:

1. From the spawning grounds, forward: type-I;
2. From the nurseries, forward: type-II;
3. From the nurseries, backwards: type-III.

Type-I simulations were carried out in the GSAs in which both spawning grounds and nurseries have been mapped, i.e. GSAs 5, 7, and 11, and intended to investigate the fate of the eggs released in the known spawing grounds during breeding periods (i.e. the fraction of eggs arrived in each nursery).

Type-II simulations were carried out for all GSAs in the NW Mediterranean, with particular attention to the same GSAs 5, 7 and 11, replacing the corresponding spawning grounds with the nurseries. The

rationale of this substitution is to verify if there is a significant difference between nurseries and spawning grounds in terms of connectivity - that is, if it is possible to make up for the lack of information on many spawning grounds using nurseries as a surrogate. A statistical test was performed to verify the goodness of this hypothesis.

Finally, type-III symulations were carried out to evaluate the contribution of the different spawning grounds to the nursery recruitment from which the simulations were started.

GSAs considered in this section are 5 (Balearic island), 6 (Catalan Sea), 7 (Gulf of Lion), 9 (Ligurian and Northern Tyrrhenian Sea), 10 (Central and Southern Tyrrhenian Sea), 11 (Sardinia). No spawning grounds or nurseries have been mapped in GSA 8 (Corsica) (see table 3.1).

4.1.1 *Release settings*

Each European hake egg/larva is represented by a Lagrangian particle in the space. In each simulation, conducted separately for each GSA, 100'000 particles were released every year, from 2004 to 2013. Three coordinates, latitude, longitude and depth (or y, x and z) define the position of each particle in the space at each time step.

4.1.1.1 *Horizontal distribution*

Shapefiles of spawning grounds were used to model the particles starting positions of the particles. The particles density in each polygon was set to be proportional to the mean persistence of that polygon (tab. 3.2).

In this procedure, it is implied that mean spatial density and temporal persistence can be superimposed. This means that a higher interannual persistence of recruits (or spawners) identified during MEDITS samplings (Bertrand et al., 2017) in a certain location can be interpreted as a higher mean density of recruits (or spawners) in that location. This hypothesis was assumed in order to specify a reasonable criterion for setting the horizontal distribution of releases.

Once fixed the density of releases, particles have been extracted uniformly in each shapefile polygon.

4.1.1.2 *Vertical distribution*

The determination of the vertical distributions of the larval release is the result of a compromise between different needs:

1. The released particles should be present at the depths at which the larvae are usually found in large quantities during surveys. Olivar, Quılez, and Emelianov (2003) suggest a range between 50 m and 150 m, referring to the past literature, and instead reports depths between 100 m and the shelf break (250-300

m) in the measurements in the GSA 6. It has to be said that many authors complain about the difficulties in finding hake larvae/egges in field surveys (Sabates, 1990);

2. Some of the spawning grounds and nurseries identified in the MEDISEH project (Giannoulaki et al., 2013) are located only a few tens of meters under the level of the sea. It is evident that, in these areas, larvae should be released above the bathymetric level, even if this partially contradicts literature information.

As a result, the depth of each particle has been randomly extracted from a uniform distribution between 100 - 300 depth, with depth correction where necessary. As a result of this correction, the vertical distribution of releases peaks in the depth range 50 - 250 m (fig. 4.1).

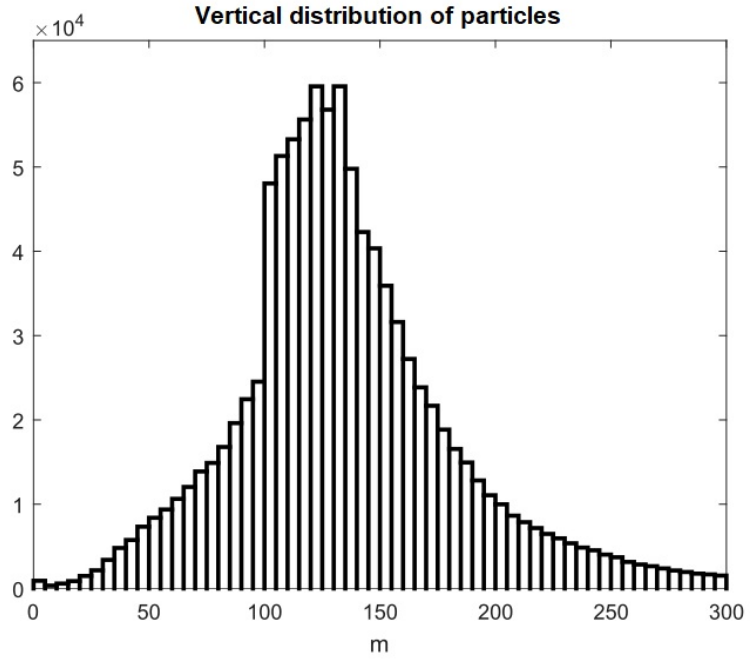

Figure 4.1: Vertical distribution of particles released during recruitment in GSAs 9 and 10. As a result of the correction due to the bathymetry, the profile describes a mode between 100 and 200 m depth.

4.1.2 *Pelagic larval duration*

Several authors have proposed different values of the PLD, even in the same GSA. A summary is given by table 4.1. Values range from a minum of $\approx$ 40 days up to a maximum of $\approx$ 70 days, with the only exception of the maximum values given by Morales-Nin and Moranta (2004) observations in the Catalan Sea.

In order to represent this variability, PLD was modelled as a Gaussian random variable, with mean $\mu = 55$ days and a standard devia-

tion of $\sigma = 5$ days, for every GSA. This approach allows taking into account the natural uncertainty given by the biological process, making the only assumption that larval phase is more likely to complete around the mean duration rather than far from it.

GSA	average (d)	interval (d)	author
5	47.6	41.0 - 57.0	Hidalgo et al., 2009
6	-	more than 30	Olivar, Quılez, and Emelianov, 2003
6	59.5	47 - 87	Morales-Nin and Moranta, 2004
6	63.2	40 - 93	Morales-Nin and Moranta, 2004
6	67.1	50 - 87	Morales-Nin and Moranta, 2004
6	62.5	40 - 94	Morales-Nin and Moranta, 2004
6	-	40 - 58	Palomera, Olivar, and Morales-Nin, 2005
7	43.9	-	Morales-Nin and Aldebert, 1997
9	52	39 - 71	Belcari, Ligas, and Viva, 2006
9	57.5	45 - 71	Ligas et al., 2003
17	40	-	Arneri and Morales-Nin, 2000
-	-	45 - 60	Druon et al., 2015

Table 4.1: Summary of proposed or currently adopted values of PLD

4.1.3 *Temporal distribution*

Eggs (or larvae) are released in well specific places and times. The assignment of a time coordinate of recruitment or spawning to each particle of the simulation is an operation that takes into account first of all the scientific literature. This is supposed to suggest a pattern of recruitment and spawning to be modelled and repeated.

4.1.3.1 *Literature review*

The most specific indications about spawning and recruitment periods are the following:

1. Several authors report that the spawning and recruitment seasons of European hake are very long. Recasens, Chiericoni, and Belcari (2008) report that at any time of the year, at least in the GSA 9, it is possible to capture a recruit or a spawner. Similar considerations apply to almost all investigated GSAs;

2. Abella, Serena, and Ria (2005) suggest that at each spawning peak corresponds a recruitment peak, which is temporarily shifted by about one PLD;

3. Considering spawning in the GSA 5:

    a) In the MEDISEH project (Giannoulaki et al., 2013) a long period of spawning between autumn and winter is reported,

highlighting the presence of fertile individuals throughout all the year;

b) Massutí et al. (2008) report only an autumnal spawning;

4. The recruitment in the GSA 5, on the other hand, occurs between February and June;

5. About spawning in the GSA 6:
   a) Recasens, Chiericoni, and Belcari (2008) suggest that spawning takes place between August and December;
   b) Olivar, Quılez, and Emelianov (2003) anticipate the beginning of the reproduction season in June;

6. Regarding recruitment in the GSA 6, the MEDISEH project (Giannoulaki et al., 2013) indicates that it is distributed over two peaks, one between spring and summer, the other between the end of summer and the beginning of winter;

7. Morales-Nin and Aldebert (1997) argue that spawning in the GSA 7 is distributed throughout the year, and that there are two peaks, one between November and December and another around March;

8. The same authors indicate two main periods for recruitment, June-July and October-December;

9. With regard to spawning in the GSA 9:
   a) MEDISEH reports (Giannoulaki et al., 2013) and the Subtask 3.2 of the LLUCET project (Lleonart, 2002) argue that it takes place mainly between January or February and May, with peaks in February and May;
   b) The sub-task 2.3 of the LLUCET project (Lleonart, 2002) shows a very slight peak of spawning around September - October, and a very strong spawning activity between February and May, considering however one year of samplings;

10. Regarding recruitment in GSA 9:
    a) According to the MEDISEH project (Giannoulaki et al., 2013), there are two peaks, one in spring - summer, and a secondary and more relaxed one in autumn - winter;
    b) Abella et al. (2008) agree to report two peaks, one evident in spring and a secundary one in late autumn;
    c) Morales-Nin and Aldebert (1997) report a peak in spring and one in autumn;

11. With regard to the GSA 10, on recruitment, the MEDISEH project (Giannoulaki et al., 2013) reports:

   a) A spring-summer peak in the northern portion (roughly from Salerno up);
   b) An autumn peak in the southern portion;

12. As for the spawning in the GSA 10, Carbonara (unpublished) identified two periods (without assigning them to particular areas), a peak between January and March and another between August and September;

13. About spawning in the GSA 11:
   a) MEDISEH reports a spawning activity all year round, with two peaks, respectively in summer and in winter;
   b) Other sources highlight only a primary peak between December and February (Carbonara, unpublished);

14. No information has been found in literature about recruitment in the GSA 11.

It is worth pointing out that, while for recruitment the period is univocally identified by the sudden appearance of extremely small individuals ($\approx$ 2.5 cm), or recruits, at least two ways are proposed in the literature to identify spawning activity:

1. The first consists in evaluating the stage of fertility of the adult specimens, and in particular by gonadosomatic index (GSI), i.e the ratio between the weight of the gonads and the total weight without bowel. This method has been used by Recasens, Chiericoni, and Belcari (2008) and in sub-task 3.2 of the LLUCET project Lleonart (2002);

2. The second main method consists in identifying the hatchdate, i.e. the hatching date of the eggs, by subtracting the daily increments on the otoliths of the larvae or recruits caught to the haul's date. From 2 to 3 days of hatching should be removed to identify the spawning. This second method has been used in subtask 2.3 of the LLUCET report (Lleonart, 2002). Unfortunately, it has the major shortcoming of not taking into account fluctuations in larval and juvenile mortality during the year (Campana and Jones, 1992).

Some information is partly contradictory; how can the lower peak in recruitment of the GSA 9 be explained, if the sources are in disagreement in identifying a late peak of spawning? Many other information, however, are reassuring; for example, the recruitment of the northern part of the GSA 10 seems to coincide with the most evident one of the GSA 9, with which it borders without there being evident ecological obstacles.

Finally, it seems reasonable to hypothesize that information about recruitment in GSA 10 could be geo-referenced: the peak of spawning between January and March could correspond to the peak of late spring northern recruitment, and the peak between August and September could be followed by the southern autumn peak.

To solve the contradiction over the spawning of the GSA 9, data from Recasens, Chiericoni, and Belcari (2008) article were directly consulted. As it can be seen in figure 4.2, actually in the months between October and November there is a percentage of spawners slightly higher (15-20% of the total) than what could be found in December, January or in summer (5-15%), although lower than spring peaks (50%).

This could legitimize the hypothesis that a secondary maximum of spawning, even if neglected by the author, is plausible around October, which would explain a recruitment peak in December, as reported in the literature. This would also be consistent with the calculation of the hatching date from LLUCET project, which identified a maximum between September and October (fig. 4.3).

Moreover this latter image helps to value the extent of seasonal variations, at least in a multimodal distribution, where the spring peaks (here, to be honest, one only spring peak) count for a percentage higher than 20% of annual spawning, the secondary peak less than 10%, and the rest is spread over the whole year.

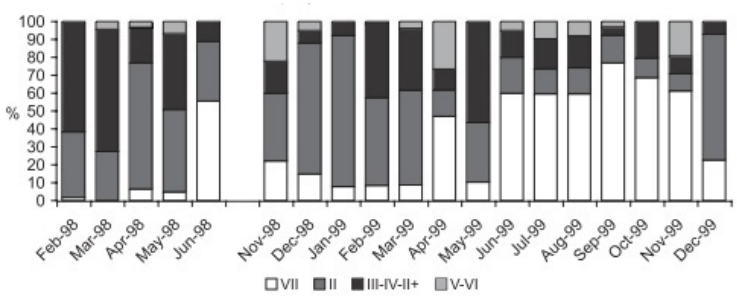

Figure 4.2: Age structure of hake fish caught off the coast of Tuscany (from Recasens, Chiericoni, and Belcari, 2008). Classes III, IV and II + represent spawners, pre spawners and partial spawners.

4.1.3.2 *Modelling the temporal distribution*

The instrument that was considered appropriate for modeling the temporal distribution of particles is the Gaussian random variable. This variable allows qualitatively to represent phenomena in which a value is thickened around the mean, with symmetrical tails. Moreover, it can easily be added to another normal random variable, (in this case, the PLD), obtaining a new normal random variable.

In the literature it is customary to use the uniform random variable in the case in which only the domain within a phenomenon occurs

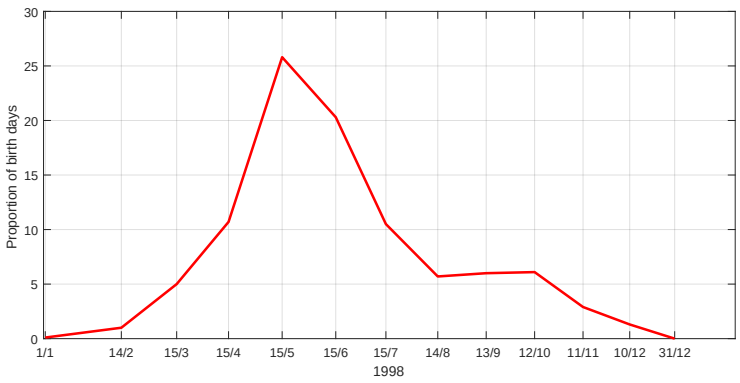

Figure 4.3: Frequency distribution of the backcalculated birth days of the recruits fished in the four surveys of the LLUCET project (Lleonart, 2002), between '98 and '99 off the tuscanian coasts.

(in this case, the spawning or recruitment period) is known. However, it seemed that the uniform variable did not fit in this context, either because it looks very unlikely that a natural phenomenon starts with a discontinuity at the beginning of a month, or because the presence of a distribution with two tails allows to suitably weight the periods with respect to which the sources are discordant, such as the spawning in January for the GSA 9. Finally, a uniform variable would not be suitably added to a normal variable (the PLD).

In this case, a Gaussian variable was used, so that the spawning or recruitment period indicated in the literature is in the range $(\mu - 2\sigma; \mu + 2\sigma)$, which covers about 95% of the probability.

The idea is to create one or more random variables for each peak of spawning, which corresponds to a random recruitment variable. This, due to the propagation of variance in the linear combination of normal variables, will result more flattened:

$$N(\mu_S; \sigma_S) + N(\mu_{PLD}; \sigma_{PLD}) \sim N(\mu_R; \sigma_R) \tag{4.1}$$

$$\mu_R = \mu_S + \mu_{PLD} \tag{4.2}$$

$$\sigma_R = \sqrt{\sigma_S^2 + \sigma_{PLD}^2} \tag{4.3}$$

Where S = spawining, PLD is the pelagic larval duration, and R = recruitment.

When multimodals spawnings or recruitments occurs, different weights were assigned to them, in order to clearly highlight the difference between primary and secondary peaks. As a rule of thumb, 70% of the particles were assigned to the former, while 10% to the latter. Furthermore, a portion of particles (20%) in each simulation is uniformly

distributed throughout the year. This is due to the fact that it is always possible to find a spawner or a recruit at any time of the year.

4.1.3.3 *An example: spawning and recruitment in the GSA 9*

For the GSA 9, spawning was modelled with a trimodal distribution. A prolonged and strong spawning between January and May is known, with peaks in February and May, and another corresponding to a secondary recruitment around December.

Two normal variables were placed at two peaks, one in the middle of February (14 February, day 45), with a standard deviation that allows to cover also January (σ = 22.5 d), and one in the first half of May (5 May = 125 d), with a lower standard deviation (σ = 12.5 d), to ensure that it can be connected to the 14 February maximum, without significantly increasing spawning in June.

By the law of the linear combination, these two peaks produce two other peaks (of recruitment) transposed by a PLD, with an appropriately increased standard deviation:

$$\mu_{R.1} = 45\text{d} + 55\text{d} = 100\text{d} \tag{4.4}$$

$$\sigma_{R,1} = \sqrt{(22.5\text{d})^2 + (5\text{d})^2} \approx 23\text{d} \tag{4.5}$$

$$\mu_{R.2} = 125\text{d} + 55\text{d} = 180\text{d} \tag{4.6}$$

$$\sigma_{R,2} = \sqrt{12.5\text{d}^2 + 5\text{d}^2} \approx 13.5\text{d} \tag{4.7}$$

The autumnal spawning period was obtained assuming previously a value of μ and σ for the late autumn recruitment, of which there are more testimonials. It was placed on 5 December (339 d), with a standard deviation a little higher than that correspondig to the peak of May, 15 days. In this way, reversing equations 4.2 and 4.3, the peak of spawning results on 11 October (284 d), with a slightly smaller deviation (14.1 d). Some hatchdates were placed in September and November.

Finally, a portion of particles equal to 70% was assigned to the spring spawning, equally subdivided between the first and second peak, and one equal to 10% to the autumnal peak; the remaining 20% was spread uniformly throughout the year.

In tables 4.2 and 4.3 all the parameters are summarized for modelling spawning and recruitment periods in all the GSAs, following

the same procedure hence shown. For those situation in which spawning and recruitment are completely decupled, it was preferred to keep the incongruity rather than contradict scientific literature, such as in the case of GSAs 5 and 7.

GSA	time span	μ (days)	σ (days)	weight
5	autumn - winter	348 (14th December)	26.25	0.8
6 (1)	August - December	289 (16th October)	38	0.7
6 (2)	June	166 (15th June)	7.5	0.1
7	late autumn - winter	15 (15th January)	37.5	0.8
9 (1a)	(Jan.) February - May	45 (14th February)	22.5	0.35
9 (1b)	(Jan.) February - May	125 (5th May)	12.5	0.35
9 (2)	(Sept) October (Nov.)	284 (11th October)	14.1	0.1
10 North	January - March	45 (14th February)	22.5	0.8
10 South	August - September.	243 (31st August)	15	0.8
11 (1)	winter	14 (14th January)	22.5	0.7
11 (2)	summer	218 (6th August)	22.5	0.1

Table 4.2: Summary of spawning modeling. In each simulation, 20% of the released particles is distributed uniformly during the year.

GSA	time span	μ (days)	σ (days)	weight
5	feb. - jun.	107 (17th April)	37.25	0.8
6 (1)	late autumn	344 (10th December)	38.3	0.7
6 (2)	August	221 (9th August)	9	0.1
7 (1)	early summer	182 (1st July)	15	0.4
7 (2)	autumn	320 (16th November)	22.75	0.4
9 (1a)	spring	100 (10th aprile)	23)	0.35
9 (1b)	spring - summer	180 (30th June)	13.5	0.35
9 (2)	late autumn	339 (5th December)	15	0.1
10 North	(late?) spring	100 (10th April)	23	0.8
10 South	autumn	298 (25th October)	15.8	0.8
11 (1)	winter - spring	69 (10th March)	23	0.7
11 (2)	summer - autumn	273 (30th September)	23	0.1

Table 4.3: Summary of recruitment modeling. In each simulation, 20% of the released particles is distributed uniformly during the year.

4.1.4 *Current fields cleaning*

Current velocity fields are defined by a tridimensional matrix in the space. Obviously, velocity is not defined under the sea bottom and on the mainland, where the matrix contains not-a-numbers. However,

this does not prevent particles from falling out of this domain, mainly because of the coarse resolution of the current fields (which does not fully cover the areas closest to the shore) and wrong setting of the starting position. This would result in an error in the calculation of the spatially interpolated velocity vectors.

In order to avoid this problem, current velocity was set to zero in grid points containing a not-a-number value but being nearest neighbours of valid grid points. In this way, velocity fields near coasts were interpolated up to the domain boundaries allowing a more realistic description of particle behaviour close to the coastline.

4.1.5 *Trajectories integration*

At each time step, a particle is immersed in the current field. Velocity vectors are assigned by linear interpolation of the current matrix. Once released, a particle is kept at the same depth for the whole duration of the simulation (i.e. $v_z(x, y, z, t) = 0, \forall x, y, z, t$), since the vertical component of velocity fields is negligible with respect to the horizontal one, and the precision with which it is estimated is much lower.

Temporal integration of the trajectories is performed with a three hour time step. At each time step, particles positions are upgraded using a forward Euler method.

4.1.5.1 *Forward simulations integration*

In these simulations, particles are released from the spawning grounds or from the nurseries (type-I and type-II respectively) during the spawning periods, and proceed forward for a time span equal to the PLD. The components $v_x(x, y, z, t)$ and $v_y(x, y, z, t)$ are obtained by linear interpolation of the motion field (eq. 4.8 and 4.9)[1]:

$$x_i(t+1) = x_i(t) + v_x(x_i(t), y_i(t), z_i, t)dt \tag{4.8}$$

$$y_i(t+1) = y_i(t) + v_y(x_i(t), y_i(t), z_i, t)dt \tag{4.9}$$

4.1.5.2 *Backward simulations integration*

In the case of type-III, particles are released from the nurseries during the recruitment periods, and move backwards for a time span equal to the PLD. The previous formulas for integration change, and become:

$$x_i(t-1) = x_i(t) - v_x(x_i(t), y_i(t), z_i, t)dt \tag{4.10}$$

1 Note that the term z, as explained in the previous paragraph, does not appear on the left in the equations, nor it depends on time

$$y_i(t-1) = y_i(t) - v_x(y_i(t), y_i(t), z_i, t)dt \tag{4.11}$$

It can be immediately noticed that the equations 4.10 and 4.11 do not allow to perfectly reproduce contrariwise trajectories. To get the perfect coincidence, the motion field of the next (unknown) position should be applied, reversing equations 4.8 and 4.9 and replacing t with $t-1$:

$$x_i(t-1) = x_i(t) - v_x(x_i(t-1), y_i(t-1), z_i, t)dt \tag{4.12}$$

$$y_i(t-1) = y_i(t) - v_y(x_i(t-1), y_i(t-1), z_i, t)dt \tag{4.13}$$

However, as a fist approximation, it can be assumed that the error of applying equations 4.10 and 4.11 instead of 4.12 and 4.13 respectively can be neglected, since the order of magnitude of each step is usually well below the resolution of the velocity field.

4.1.6 *Comparison between type-I and type-II simulation*

A statistical test was performed to assess whether or not there are significant differences between type-I and type-II simulations, i.e. whether dispersal patterns from the spawning grounds are significantly different from those of from the respective nurseries.

The statistical test adopted is the test of the equality of two multinomial distributions (as performed in Mood, 1974). It compares two random samples that are supposed to be extracted from the same multinomial distribution.

The statistic Q_{2k}, which under the hypothesis of equality follows the Chi-square distribution, is proportional to the square of the difference between the absolute expected frequencies and the absolute observed frequencies of some events; the higher this is the less equality of distributions is likely.

As a first step, the NW Mediterranean domain was divided into cells with a size of 0.315° of latitude $\times$0.315° of longitude, i.e. about one order of magnitude less than the extension of nurseries and spawning grounds. Then the number of particles released in each simulation falling into each cell i, j at the end of the Lagrangian simulation was counted; these (absolute) frequencies represent the realizations of the multinomial distribution. The grid is shown in figure 4.4.

This procedure was repeated for both type-I and type-II simulations, for GSAs 5, 7 and 11 separately, i.e. those GSAs in which both spawning grounds and nurseries were mapped in th MEDISEH project

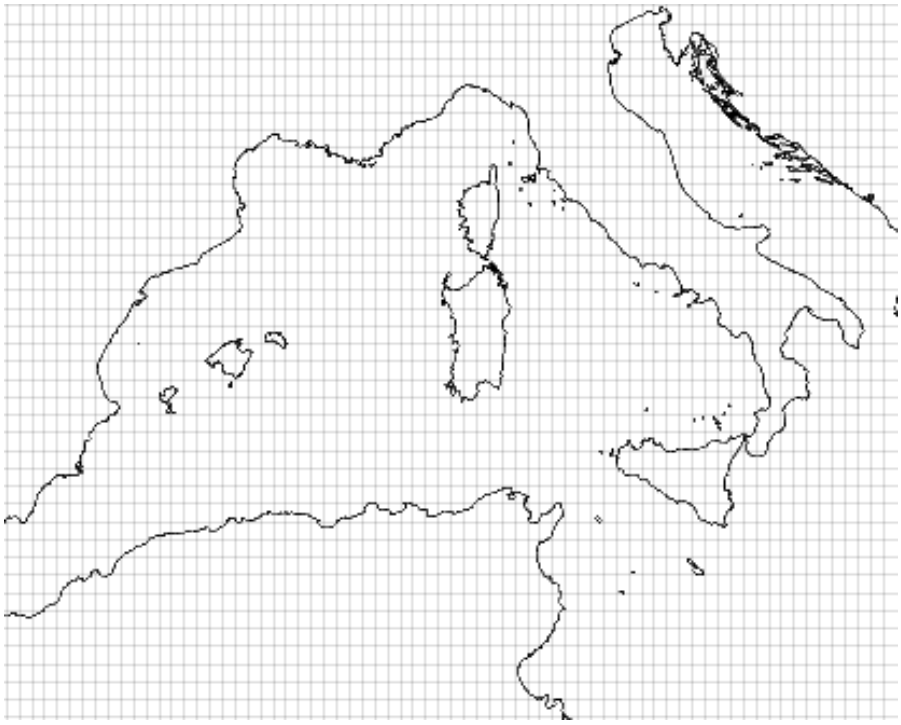

Figure 4.4: Statistical test grid.

(Giannoulaki et al., 2013). Under the null hypothesis, each of these two samples is supposed to produce a Chi-square statistic with $g = max(i)max(j) - 1$ degrees of freedom. In this case, the grid produced has 80 rows and 41 columns, hence g = 3279 degrees of freedom.

The overall statistic is given by the equation 4.14:

$$Q_{2k} = \sum_{k=I}^{II} \sum_{i,j} \frac{(n_{i,j,k} - \sum_{i,j} N_k p_{i,j})^2}{\sum_{i,j} N_k p_{i,j}} \tag{4.14}$$

Where N_k defines the number of particles released in the simulation k (I or II) from a certain GSA, $n_{i,j,k}$ the number of particles released in the simulation k falling in the cell labelled with i, j, and $p_{i,j}$ is the theoretical probability of a particle to fall in a certain cell.

The values of $p_{i,j}$ can be easily estimated starting from the absolute frequencies of both samples. The maximum likelihood estimators are given by the equation 4.15:

$$p_{i,j} = \frac{N_{i,j,k=I} + N_{i,j,k=II}}{\sum_{i,j}(N_{i,j,k=I} + N_{i,j,k=II})} \tag{4.15}$$

4.2 RESULTS

4.2.1 *Type-I simulations*

In the first type of simulations, as previously mentioned, particles were released from spawning grounds during periods of increased reproduction activity, and dispersal was investigated.

Table 4.4 shows the relative frequencies of the arrivals in the various known nurseries. The sum of each row corresponds to one million (100.000 releases per year, for 10 years).

From \to	GSA 5	GSA 6	GSA 7	GSA 9	GSA 10	GSA 11	lost
GSA 5 s.g.	**20.57%**	0.04%	<0.01%	0%	0%	<0.01%	79.39%
GSA 7 s.g.	0.04%	0.45%	**44.54%**	0%	0%	0%	54.96%
GSA 11 s.g.	0%	0%	0%	<0.01%	<0.01%	**23.18%**	76.83%

Table 4.4: The table shows the frequencies of the arrivals to the nurseries in the first row, starting from the spawning grounds in the first column. Retention (i.e. the fraction of particles arriving in the GSA of origin) is highlighted in bold.

The highest percentages (55% - 80%) are observed in the last column, which represents the particles that are lost in the open sea. Among the larvae that managed to reach a favorable habitat, the vast majority remains in the GSA of origin (21% - 45%). Furthermore, retention seems to grow with the size of the nearest (mainland) obstacle: it is smaller in the Balearics, which are completely surrounded by open sea; slightly larger in Sardinia, which has a longer coastline; even higher in the Gulf of Lion, which by nature embraces the spawning grounds of GSA 7 for more than half of the horizon.

The high retention rate could also be the effect of the interpolation method of the field of motion, which places zero velocity on the mainland, slowing the particles near the coast. However, a test was conducted to verify that all particles changed their position during simulations, and it resulted positive.

Finally, the percentage of particles travelling from one GSA to another is extremely low; only between GSAs 7 and 6 there seems to be a relevant flow, from France to Spain, of one point every 200.

4.2.2 *Type-II simulations*

The simulations were repeated starting from the nurseries instead of the spawning grounds. The summary is shown in table 4.5.

Also in this case, in which the nurseries are thought to play the part of the spawning grounds, the highest percentages, although slightly lower (42% - 72%) are observed in the last column. It is also confirmed the tendency of particles to remain within the GSA of origin (22%

From \to	GSA 5	GSA 6	GSA 7	GSA 9	GSA 10	GSA 11	lost
GSA 5 n.	**21.55%**	0.04%	<0.01%	0%	0%	<0.01%	78.40%
GSA 6 n.	*0.09%*	**54.97%**	*0%*	*0%*	*0%*	*0%*	*44.94%*
GSA 7 n.	0.21%	0.30%	**44.65%**	0%	0%	0%	54.84%
GSA 9 n.	*0%*	*0%*	*<0.01%*	**58.24%**	*0.01%*	*0%*	*41.75%*
GSA 10 n.	*0%*	*0%*	*0%*	*2.67%*	**64.29%**	*0%*	*33.05%*
GSA 11 n.	0%	0%	0%	0%	<0.01%	**47.00%**	53.00%

Table 4.5: The table shows the frequencies of the arrivals to the nurseries in the first row, starting from the nurseries in the first column. Retention (i.e. the fraction of particles arriving in the GSA of origin) is highlighted in bold. In italics the GSAs without spawning grounds.

- 64%). The phenomenon hypothesized in the previous simulations, according to which more coastline was combined to greater retention, is now only true in a statistical sense, because the retention of GSA 7 is lower than that of GSA 11.

Finally, a more substantial stream of particles appears (1 point every 35 - 40) between different GSAs, in particular between GSA 10 (Southern Tyrrhenian Sea) and 9 (Northern Tyrrhenian Sea and Ligurian Sea). It is not surprising that this flow is the highest, because these GSAs are physically contiguous, without ecological obstacles to separate them.

In this table, advection pattern carrying larvae from east to west, parallel to the coastline (GSAs 10 - 9 - 7 - 6) can be identified. This pattern is attributable to various currents - East Corsica Current, Ligurian Current (Abella et al., 2008), Western Winter Intermediate Waters (Hidalgo et al., 2008) - which belong to the same main cell of the western Mediterranean, charachterized by a counterclockwise circulation (Millot, 1999). Islands (GSA 5, 1, 11) contribute to create smaller circulation cells which do not produce an equally traceable transport pattern.

4.2.3 *Statistical test between type-I and type-II simulations*

The calculation of the statistics is summarized in table 4.6. P-values, calculated with the approximation given by the function of Microsoft Office Excel, were from 0. This means that the hypothesis of equality of dispersal should in principle be rejected, and that therefore nurseries can not be strictly used as surrogate of spawning grounds. The maximum value of the acceptable statistic, to have a p-value of at least 0.05, is $Q_{2k} = 3413.3$.

GSA	statistic Q	p-value
5	20'922.4	0
7	239'010.2	0
11	488'988.6	0

Table 4.6: Chi-Square test summary, with g = 3279 degrees of freedom

4.2.3.1 *Comparison between type-I and type-II simulations*

In figure 4.5 (releases from GSA 5) a very similar dispersal pattern can be observed between the two simulations. What is evident is the communication with the African coasts, excluded from MEDITS and MEDISEH projects. It remains to be determined whether or not along the Algerian coasts there are nurseries able to host the larvae.

Even the Gulf of Lion (figure 4.6) generates a similar distribution between the two simulations, although in this case some differences appear (the yellow patch seems wider in the case below, for example west of the Balearics).

Finally, as in the previous case, the dispersal of larvae released from Sardinia (figure 4.7) appears wider in the case of type-II simulations; moreover, as for the GSA 5, a contribution to the nurseries of the GSA 12 (Gulf of Tunis), whose existence is reported in the literature (Bouhlal and Ktari, 1975), is evident. On closer inspection, it can also be noted that the areas of greatest presence (orange colour) in the image below are more thickened in the nurseries, namely that the simulation of type-II shows greater retention. To confirm this, tables 4.4 and 4.5 actually show an increase in the number of particles reaching (or remaining in) GSA 11 nurseries from 23.1% to 47.0% of the total.

4.2.4 *Type-III simulations*

Summary table 4.7, showing the relative frequencies of arrivals in various spawning grounds of particels released from nurseries and submitted to backward Lagrangian simulations, can be considered generally consistent with table 4.5. Where a connection was found between the spawning ground of the GSA i and the nursery of the GSA j in type-I simulations, this was also found backwards, from the nursery j to the spawning ground i, with the exceptions of some connections concerning the GSA 11:

1. Particles released from the spawning grounds of the GSA 5 reach the nurseries of the GSA 11, but the backwards simulations do not reach the GSA 5;

2. The same occurs between the spawning grounds of the GSA 11 and the GSA 10;

3. Particles released in spawning grounds in GSA 7 do not reach the GSA 11 nurseries; on the contrary, type-III simulations reach GSA 7;

However, these three exceptions account for <0.01% of the simulated particles.

From \to	GSA 5	GSA 7	GSA 11	lost
GSA 5 n.	**27.51%**	0.04 %	0	72.45%
GSA 6 n.	0.03%	0.03%	0	99.93%
GSA 7 n.	<0.01%	**26.50%**	0	73.50%
GSA 9 n.	0	0	<0.01%	>99.99%
GSA 10 n.	0	0	0	100%
GSA 11 n.	0	<0.01%	**20.77%**	79.23%

Table 4.7: The table shows the relative frequencies of arrivals to spawning grounds in the first row, proceeding backwards from the nurseries in the first column. Retention cases in bold.

4.2.5 *Comments about larval connections in the NW Mediterranean Sea*

The existence of connections between different GSAs through larval dispersal has been assessed. However, these connections have been proven to weakly influence recruitment: the largest part of released eggs is lost in the sea, or remains in the GSA of origin.

A order of magnitude could be associated to larval connections between different GSAs. For instance, considering larval drift from GSA 7 to GSA 6, the highest between those correctely estimated between spawning grounds and nurseries (0.45%). Time series provided by STECF project (Cardinale, Damalas, and Chato Osio, 2015) assign a mean value of 47.5×10^6 recruits between 1998 and 2014 in GSA 7. At first approximation, this value can be considered as depending only from spawning the Gulf of Lion; the number of released eggs is obtained by dividing the number of recruits with the proportion of retained specified by table 4.4 (eq. 4.16):

$$47.5 \times 10^6 recruits/0.445 = 10.71 \times 10^7 eggs \tag{4.16}$$

The total number of eggs leaving GSA 7 and approaching GSA 6 is obtained by multiplying the numebr of eggs released from GSA 7 for the connectivity coefficient specified in the same table 4.4 (eq. 4.16):

$$10.71 \times 10^7 eggs \times 0.0045 = 48.0 \times 10^4 recruits \tag{4.17}$$

Compared to the mean abundance of recruits in the Catalan Coast in years 2005 - 2014 (16.39×10^7, from Cardinale, Damalas, and Chato Osio, 2015), this connection represents only the 0.29% of the total number of recruits. This value could play an important role in determining genetic shuffling, but it does not provide a relevant source of support for the hake stock in GSA 6.

Only one value seems to rise over the others: the connectivity between GSA 9 and GSA 10. This high level of connectivity suggests that these two areas should be studied together - although the 2.67% value has been improperly estimated starting from the nurseries of the GSA 10 and not from (not, to date, modeled) spawning grounds of the same region.

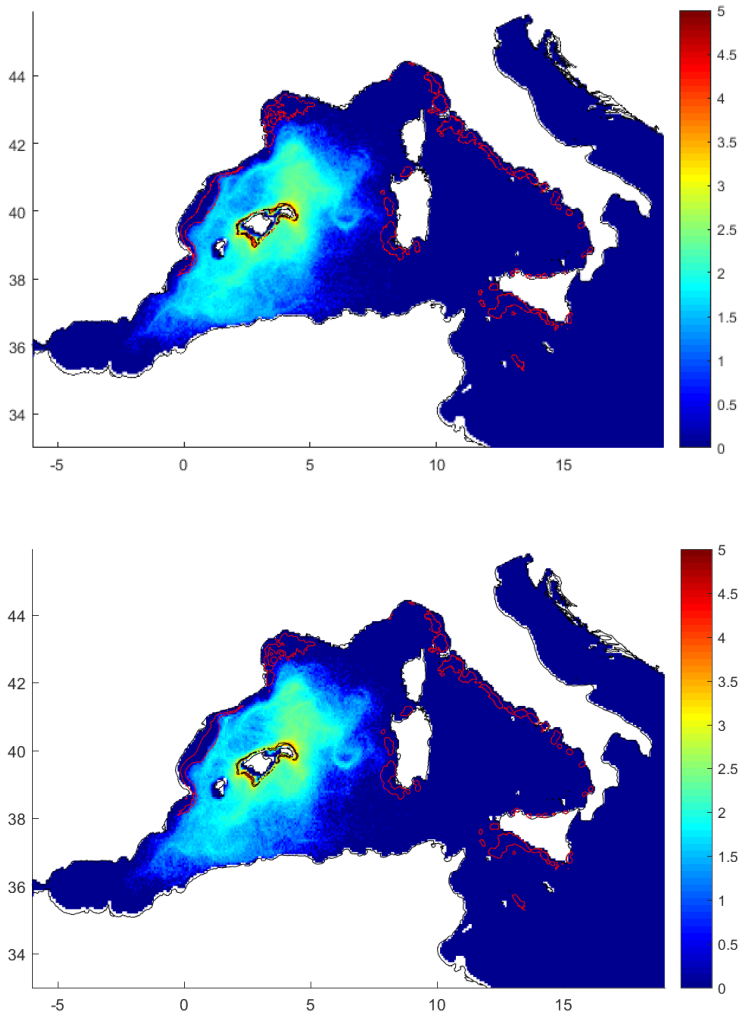

Figure 4.5: Distribution of particles in simulations starting from GSA 5 (Balearic Islands). Above the simulation of type-I (from spawning grounds), below the simulation of type-II (from nurseries). In black the starting polygon, in red the possible nurseries for settlement. The density scale is logarithmic: a red colour indicates the presence of 10^5 particles per unit area.

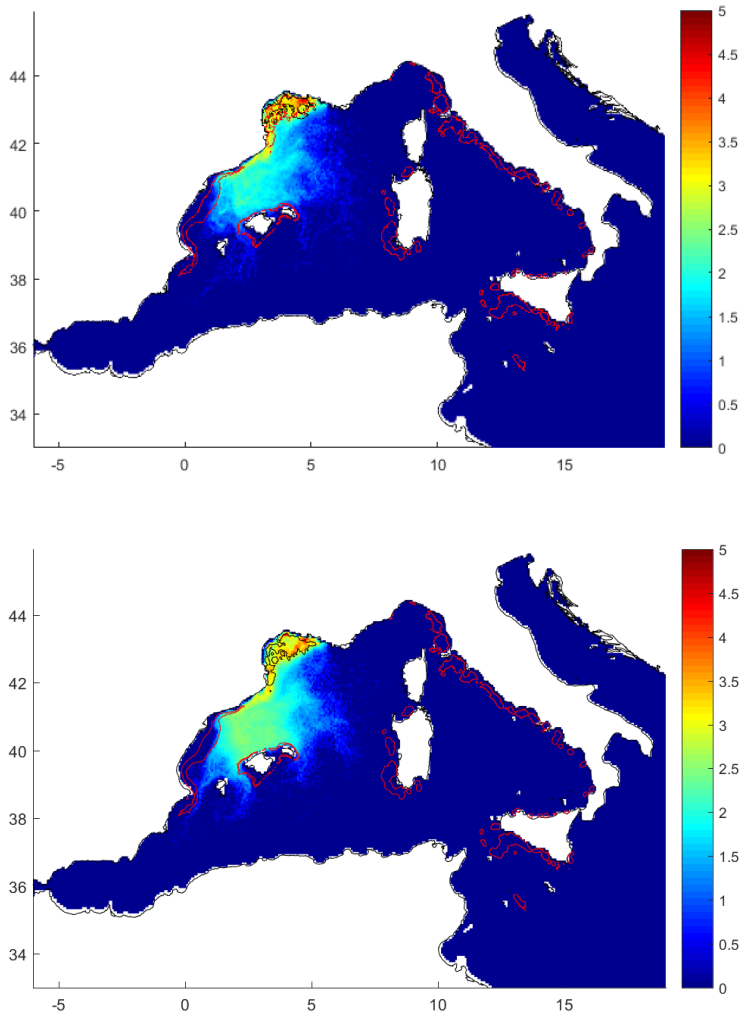

Figure 4.6: Distribution of particles in simulations starting from GSA 7 (Gulf of Lion). Above the simulation of type-I (from spawning grounds), below the simulation of type-II (from nurseries). In black the starting polygon, in red the possible nurseries for settlement. The density scale is logarithmic: a red colour indicates the presence of 10^5 particles per unit area.

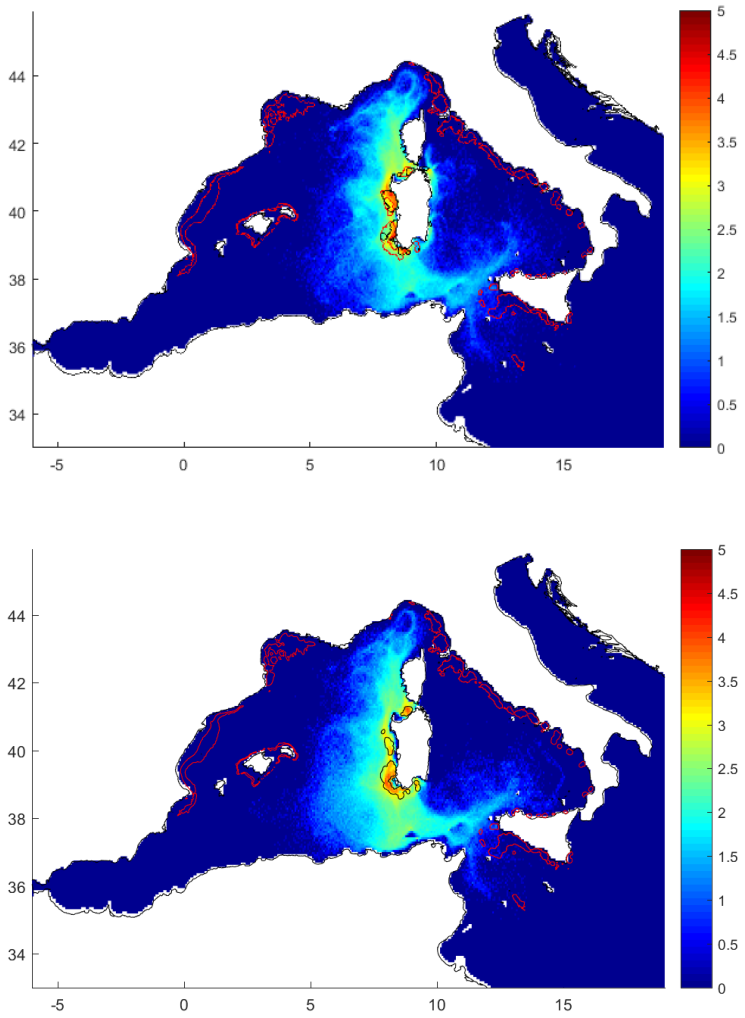

Figure 4.7: Distribution of particles in simulations starting from GSA 11 (Sardinia). Above the simulation of type-I (from spawning grounds), below the simulation of type-II (from nurseries). In black the starting polygon, in red the possible nurseries for settlement. The density scale is logarithmic: a red colour indicates the presence of 10^5 particles per unit area.

5 CONNECTIVITY ASSESSMENT IN GSAS 9 AND 10

In view of the results of Chapter 4, GSAs in the NW Mediterranean Sea can be assumed to be almost isolated from a larval connection point of view, the only two exception being GSAs 9 and 10; in order to study the stock dynamics in the Ligurian Sea and in the Northern Thyrrenian Sea, the larval flux from GSA 10 toward GSA 9 can not be actually neglected.

As a consequence, in this Chapter the focus is pointed at the joint reconstruction of the missing spawning grounds in GSAs 9 and 10, and produce a tool able to represent larval drift between the spawning grounds and the nurseries of GSAs 9 and 10 with a high resolution.

5.1 METHODS

5.1.1 *Spawning grounds reconstruction*

To remedy the lack of data on the presence of spawning grounds in the GSAs 9 and 10, in this section a new method based on Lagrangian simulation is illustrated.

Inspiration was taken by type-III simulations. At least in a naive way, all the recruits settled in the nurseries should have been released in a spawning ground. Assuming that retention is predominant over contributions from other areas, the nursery of a certain GSA is fed only from the spawning grounds of the same GSA. This assumption is realistic, as it has been shown in Chapter 4, provided that there are evident ecological obstacles between other reproduction areas. The latter condition means that GSAs 9 and 10 have to be studied together.

This method uses backward Lagrangian simulations in order to obtain a pattern of potential release particles and applies a suitability criterion to identify those areas which are (more likely) effective spawning areas. The following procedure was adopted:

1. A high number of particles was released in the nurseries of GSA 9 and 10 (fig. 5.1);
2. Backwards Lagrangian simulations were performed, like those of type III explained in Chapter 4. Final positions (latitude, longitude and depth) were recorded;
3. A boolean suitability criterion was adoped to select only particles in a favourable habitat;
4. The domain was divided into sufficiently small cells ($\approx 1\ km^2$);

5. Densities of remaining particles were calculated in each cell, and compared to those equivalent to MEDISEH persistence classes (table 5.1);

6. Shapefile of spawning grounds were reconstructed selecting only cells satisfing this minimum density threshold.

Since a higher accuracy is required to reconstruct spawning grounds (compared with simply assessing connectivity across a wide geographic basin), 1'000'000 particles were released from nurseries in GSAs 9 and 10. The domain has been divided into cells of 0.0089° of latitude × 0.0125° of longitude; each cell covers roughly 1 km^2.

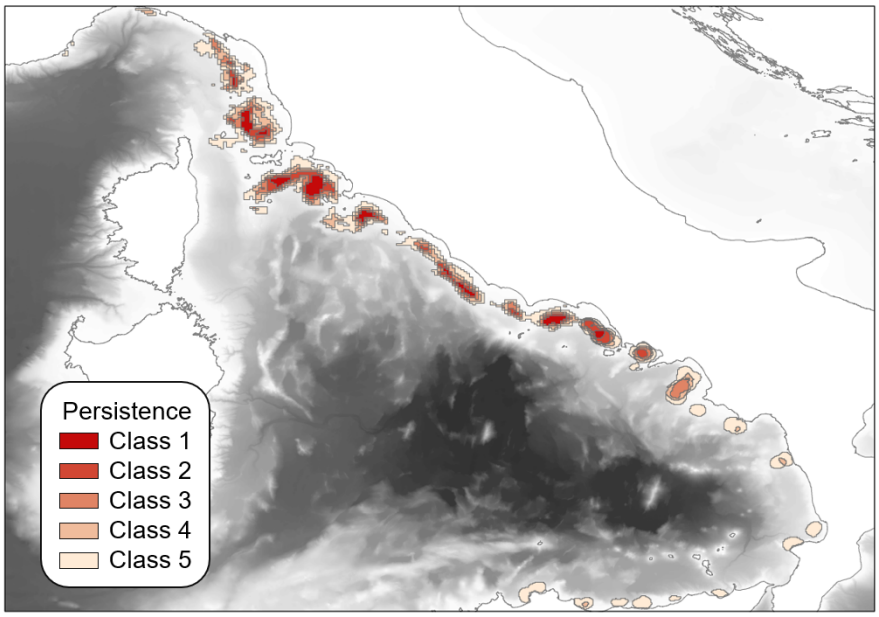

Figure 5.1: Nurseries in GSAs 9 and 10 with different persistence classes (form Giannoulaki et al., 2013)

5.1.1.1 *Suitability criterion: bathymetry*

In order to define a preferential interval of depth from which eggs can be released, MEDITS data on the location of spawners and post spawners (class 3 and 4 according to Bertrand et al., 2017) were scrutinized. Only 272 female specimens have been caught during 21 year of trawling surveys (1994 - 2014), 189 in the GSA 9 and 83 in the GSA 10. This low number of catches should be attributed to the fishing gear used to perform such surveys, the otter bottom trawl (Giannoulaki et al., 2013; Russo et al., 2017). The observed ineffectiveness in catching large individuals is most likely due to the the good swimming skill characterising large hakes, coupled with an unsufficiently wide opening of the net.

MEDITS database reports the hauling depth for each specimen. This allows to build a histogram showing the frequency distribution

of catches, expressed in terms of spatial densities, (fig. 5.2) over different depths. This distribution seems to suggest a uniform distribution of spawners in the vertical dimension, with a slight preference for shallow waters (50 - 200 m). This may be explained by hypothesizing that only young spawners - living in shallower waters - were easily detected, while older - and larger individuals, living deeper in the sea - were harder to capture.

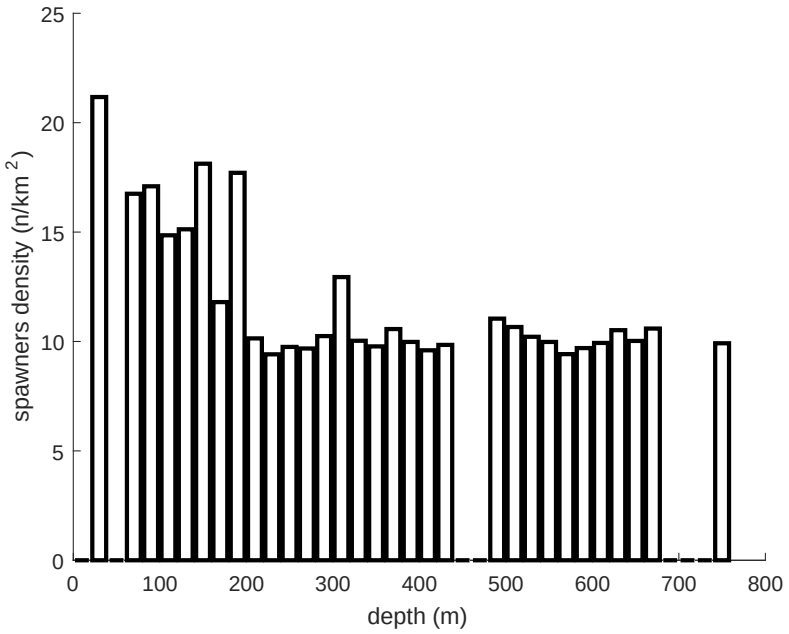

Figure 5.2: Distribution of relative frequencies of spawners at different depths.

In addition, a cumulated histogram was produced (fig. 5.3), in order to determine the two isobathes identifying the depth range in which most spawners are found. Depths corresponding to the 10th and 90th quantile were selected, equal to 70 m and 620 m respectively.

For each simulated particle, the corresponding bathimetric depth was associated using data produced by Emodenet project (`http://www.emodnet-bathymetry.eu/`). Particels whose bathymetric depth was lower than 70 m or larger than 670 were deleted.

5.1.1.2 *Density threshold definition*

Successful particles were used to reconstruct the distribution of spawning grounds. The Ligurian and Tyrrhenian Sea were subdivided with a high resolution grid ($0.0089° \times 0.0125°$, ≈ 1 km^2) and each particle was associated with a cell of the grid.

In order to identify the minimum number of particles that should reach a cell in order to consider it as a "spawning cell", inspira-

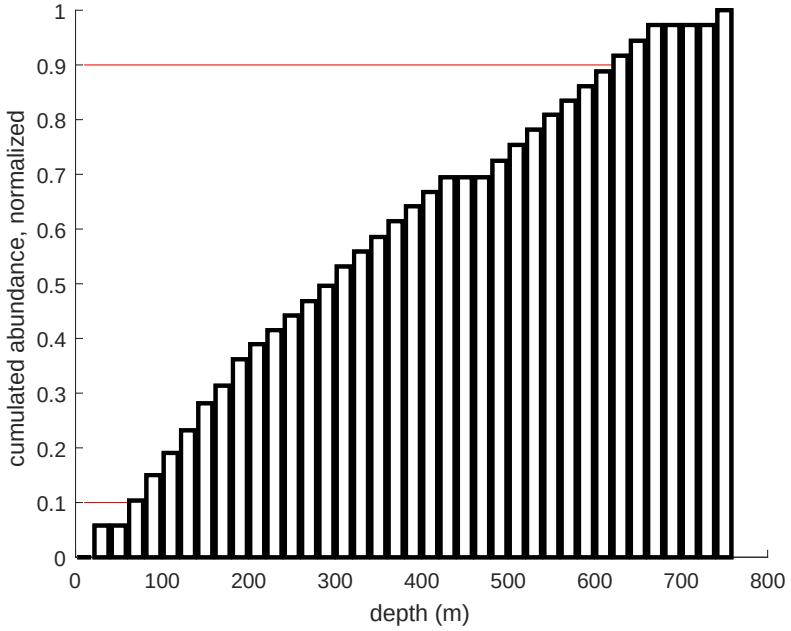

Figure 5.3: Cumulative distribution of relative frequencies of spawners at different depths. Red lines represent the 0.1 quantile and the 0.9 quantile.

tion was taken from MEDISEH persistence classes (Giannoulaki et al., 2013). Once again, the conceptual superimposition between mean spatial density and temporal persistence was appealed. First of all, the density of particles released in each nursery, characterized by a specific class of temporal persistence, was calculated. Thus, the average number of releases was obtained, multiplying the density by the amplitude of a cell and the time span of the whole simulation (10 years). For example, if 500 particles were released in a 20 km^2 nursery, characterized by the temporal persistence class 5 (i.e. the lowest), this means that the density of releases in nurseries characterized by that level of temporal persistence is 25 $particles/km^2$, and that, in 10 years, 250 particles have actually been released. As a consequence, a "spawning cell", to be classified within level 5, must contain at least 250 particles, which means that 250 $particles/cell$ is the threshold.

The thresholds are summarized in table 5.1.

5.1.2 *Larval conncectivity assessment in GSAs 9 and 10*

After reconstructing the spawning grounds, these were used to assess larval connectivity in the Ligurian-Tyrrhenian basin.

To this end, both nurseries and spawning grounds were divided into a relative coarse grid, each cell being 0.125° latitude $\times$0.1875° longitude, $\approx$ 215 km^2 (fig. 5.4). This subdivision was selected to allow a balance between sufficiently good spatial resolution and easy

Peristence class	% minimum persistence	threshold (particles/cell)
5	0.05	110.1
4	0.2	440.5
3	0.4	881.0
2	0.6	1321.5
1	0.8	1761.9

Table 5.1: Equivalence between persistence classes and particles densities.

handling of spatial representation. A total of 194 cells contained either a nursery or a spawning ground or both (in most of the cases), 124 in GSA 9 and 70 in GSA 10.

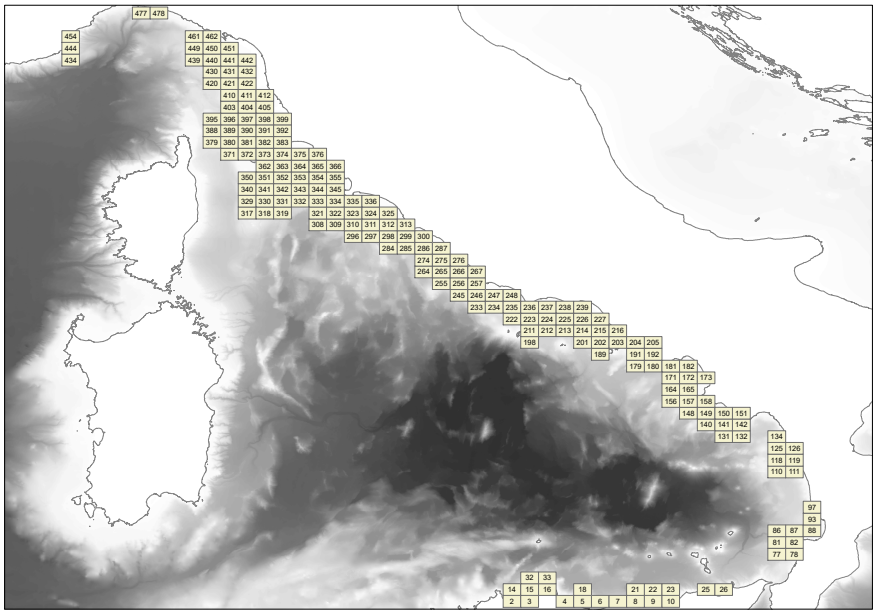

Figure 5.4: Grid used to assess larval dispersal between different areas.

Forward Lagrangian simulations were repeated for the usual time span from 2004 to 2013, with 1'000'000 particles being released in each simulations. Two matrices were produced as output of this simulations.

1. In the first, each element $a_{i,j}$ of the matrix M_a contained the total number of particles that left a spawning ground in cell i and reached a nursery in cell j;

2. In the second matrix M_p, each element $p_{i,j}$ contained the proportion of particles having left a nursey in cell i and having reached a spawning ground in cell j over all the particles released in cell i; or better (eq. 5.1):

$$p_{i,j} = \frac{a_{i,j}}{N_i} \tag{5.1}$$

Where N_i is the number of eggs released in cell i, and:

$$\sum_{j=1}^{194} a_{i,j} \leqslant N_i \tag{5.2}$$

Since some particles may not have reached a nursery at the end of their larval duration.

5.2 RESULTS

5.2.1 *Spawning grounds*

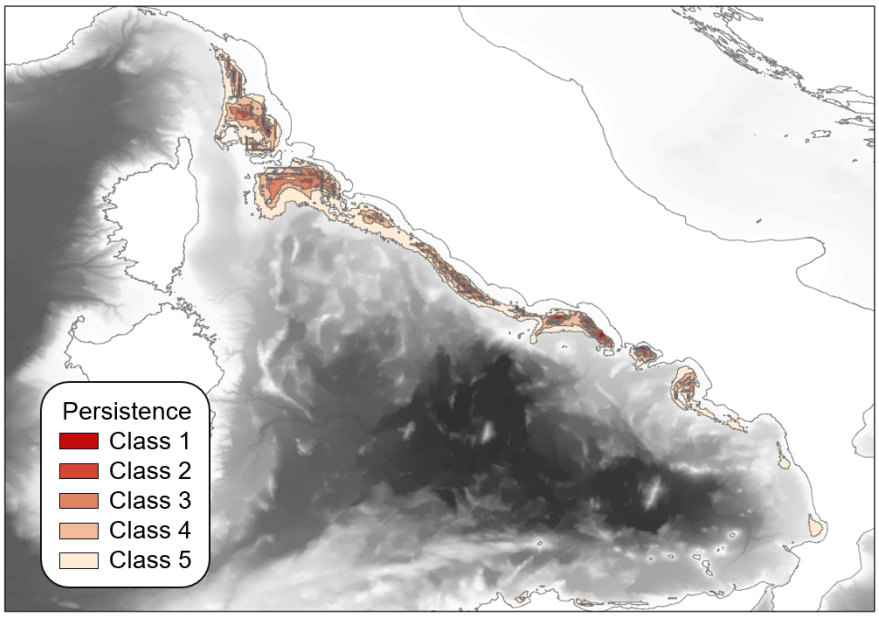

Figure 5.5: Spawning grounds reconstructed in GSAs 9 and 10, with different persistence classes.

Spawning grounds in GSAs 9 and 10, with their persistence classes, were obtained by means of backward Lagrangian simulations and a suitability criterion (depth range).

While nurseries look patchy (fig. 5.1), spawning grounds (fig. 5.5) create a long stripe from La Spezia Gulf (Northern Tuscany) to Punta Licosa (Southern Campania), interrupted only by Elba island in Tuscany and Ischia and Capri islands with their promontories in Campania.

The widest portions of spawning grounds are located off Tuscanian coasts. However, very persistent reproduction areas are located in Gaeta gulf, Naples gulf and off Ostia.

Secundary (and patchy) spawning areas are located off Genoa in Liguria, Sant'Eufemia gulf and Policastro gulf in Calabria, and finally Castellammare and Termini Imerese gulf off Sicilian coasts.

Reproduction areas are located slightly south of the nurseries and farhter from the coast; however, the two layers overlap for a large portion of their extent.

Some spawning grounds around Elba island seem to show an artifact pattern of persistence (fig. 5.6), which suddenly increases or decrease at certain latitudes and longitudes. This behaviour may be due to the discretization of the current fields, which is known to be inaccurate near archipelagos and islands (such as Elba). However, in order to overcome this defect, a coarser grid (fig. 5.4) was used to assess connections betweent different areas, to balance such abrupt changes of persistence.

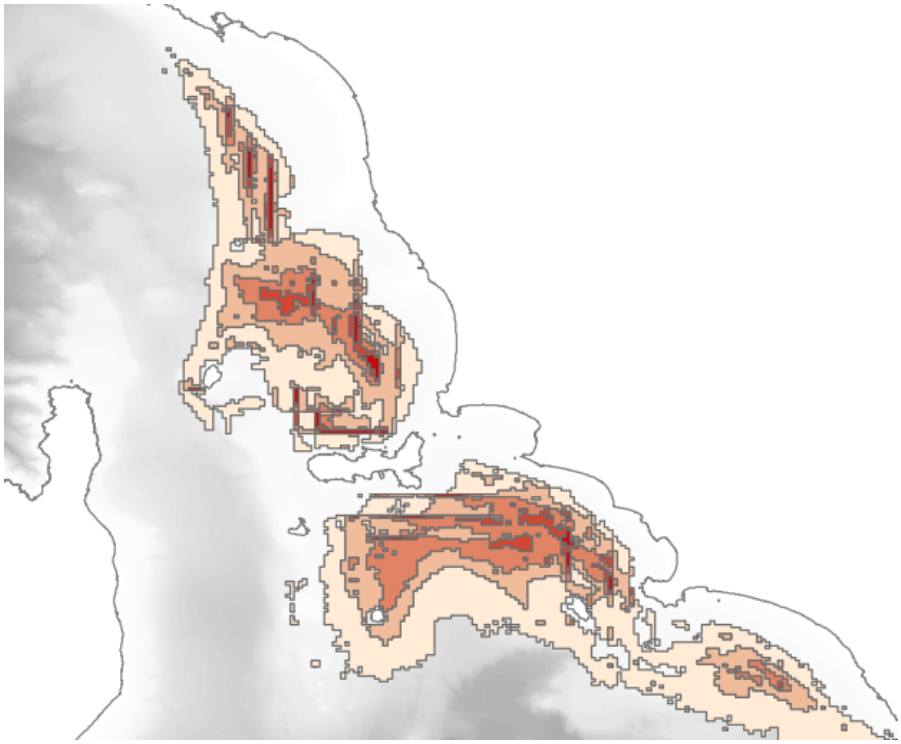

Figure 5.6: Detail of persistent spawning grounds in GSA 9 along the coasts of Tuscany.

A comparison between the reconstructed spawning areas and the locations in which spawners have been actually caught in GSA 9 and 10 is shown in figure 5.7. Hauls from MEDITS program (Bertrand et al., 2017) and LLUCET project (Lleonart, 2002) are reported. Almost every spawner in GSA9 actually falls inside the spawning grounds;

the reconstruction seems to be less accurate in GSA 10, where some individuals were caught very far from Calabrian coasts.

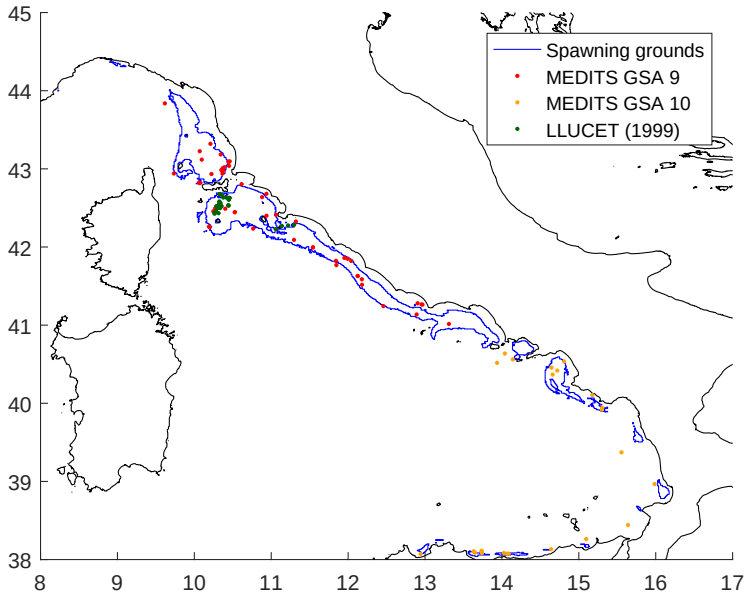

Figure 5.7: Comparison between recostructed spawning grounds in GSAs 9 and 10 and spawners hauls.

5.2.2 *Connectivity matrices*

The main outcome of the connectivity assessment in GSAs 9 and 10 is the construction of connectivity matrices linking spawning cells to nursery cells.

These matrices M_a and M_p are displayed in fig. 5.8. Hotter colours indicate stronger connections between spawning cells (in ordinate) and nursery cells (in abscissa).

The diagonal is evident, showing that retention plays an important role in determining larval dispersal patterns. In addition to this, a general pattern from southern cells toward northern cell is clear.

Larval connectivity matrices provide also a rule of thumb in order to roughly evaluate the travel lengths of the propagules. Most of the particles remain in the cells neighbouring the starting cell, and long travels are impossible; for instance, there are no particles going directly from Liguria to Sicily, or viceversa.

5.2.3 *Analysis of current patterns in the Ligurian and Tyrrhenian Sea*

To investigate the major drivers of connectivity patterns described above, a deeper analysis of the currents fields in the Ligurian and Tyrrhenian Sea was conducted.

Mean monthly vector fields were calculated in an area between 38° N and 44° 30′ N and 8° 30′ and 16 ° 30′ E, for three ranges of depths: 0 - 100 m, 100 - 200, 200 - 300 m. The customary time span, from 2004 to 2013, was considered. The angular pattern was analyzed both by looking at the monthly scale (do currents in one month differ remarkably from those in another month?) and at the interannual scale (do currents recorded in an year differ remarkably from those in another year?).

As a first step, the overall mean pattern was analyzed (fig. 5.9). A main current (A), belonging to the largest counterclockwise cell of the western Mediterranean, starts from western Sicily, proceeds far from the coast until reaches Gaeta Gulf, than follows the coastline. This current is present also in deeper waters (fig. 5.10).

In SE Tyrrhenian sea, isolated by the main counterclockwise cell, the currents arrangement is less clear. A persistent clockwise cell is evident on the extreme south (B in fig. 5.9); this current creates a patter north - south on Calabrian and Sicilian coasts, which is opposed to the one prevailing in northern regions. Other two small cells, a northern clockwise and a southern counterclockwise, describe the circulation in front of Campania region (C). These last cells disappear while proceeding toward deeper waters, where a sort of Campania - Sicilia corridor occurs (C, B, fig. 5.10).

A measure of the overall angular standard deviation is provided in figure 5.11. A quite stable (blue) pattern where the current previulsy labeled as "A" can be easily recognised. On the other hand, two areas are marked in red, indicating deviations around 75°: Tuscanian coasts and the entire eastern Tyrrhenian Sea, from Sicily up to Gaeta gulf. This suggests clear inversions in the direction of the current during the analyzed period.

5.2.3.1 *Changes in monthly patterns*

A first sharp change is observed - especially in the shallowest waters - during summer, from July to September. A clear, sudden inversion of the currents also occurs along Tuscanian coasts; this leads to a southward circulation during these three months (D, fig. 5.12). A series of smaller changes in the eastern Tyrrhenian Sea, instead, create an evident direct connection between central Campania and Calabria (E).

A secundary change occurs at the end of the autumn, in November and in December. An inversion of the currents brushing the coastline from Campania to Sicily is observed; as a result, the current flows clockwise during these months (F, fig. 5.13).

Finally, a change in deep strata only is observed in late spring. From May to June an inversion occurs in different patches far from coasts in Lazio and Campania. In these patches, the current flows downward (G, H, fig. 5.14).

No periodic relevant changes were observed in currents patterns from year to year in the analyzed period.

5.2.4 *Larval dispersal between regions*

A deeper analysis was made upon larval dispersal at the local scale. Which are the overall connections at the regional scale? It was considered interesting to investigate, since a region could significantely benefit from protection measures adopted elsewhere.

Nursery and spawning cells were divided into 6 regions (Sicily, Calabria, Campania, Lazio, Tuscany, Liguria) depending on the closest mainland (fig. 5.15). Two indicators were computed:

1. The proportion $c_{x,y}$ of eggs released in a region x and reaching another region y, with respect to all the eggs arrived to the region y.

2. The proportion $t_{x,y}$ of eggs released in a region x and reaching another region y, with respect to all the eggs released from the region x reaching a favourable habitat[1].

The former indicator should answer to the question "where do recruits growing in this region come from?", while the latter answers to the question "Where do eggs released in this region go?".

Pie charts in fig. 5.17 summarize the results about indicator $c_{x,y}$. Sicily, Calabria and Campania show a similar pattern: more than 98% of particles come from the region of origin (99.2%, 98.6% and 98.2% respectively), while the main remaining contribution is given by the region located immediately north (0.8%, 1.3% and 1.8%).

The interpretation of these results is clear while looking at figure 5.9. Since in these three regions the current flows clockwise, the (although small) external contributions can come only from the first region proceeding counterclockwise.

In Lazio and Tuscany the proportion of locally born recruits is still large, 85.9% and 89.1% respectively, but lower compared to that of southern regions. Moreover, a relevant portion of larvae comes from the region situated immediately south, 13.1% from Campania (to Lazio) and 10.9% from Lazio (to Tuscany). Finally, Lazio shows also a little percentage of particles coming from northward (1.0% from Tuscany). Liguria shows a completely different composition, being the

1 This last clarification is necessary, since many particles are lost out of the domain (i.e. they do not reach any nursery) during the simulations: $t_{x,y}$ does not consider those eggs.

largest part of its recruits (87%) released from Tuscany. This last result is probably due to the fact that Ligurian nurseries and spawning grounds are small and have a low persistence, while Tuscanian ones are both larger and more persistent.

In these northern regions, the current circulation proceeds counterclockwise, and the main contributions arrive from southern regions. The only exception is given by the small flow from Tuscany to Lazio: this latter is probably due to the summer inversion occurring in shallow waters (fig. 5.12).

On the other hand, pie charts in fig. 5.18, summarizing indicator $t_{x,y}$, give complementary results. Eggs released from Sicily - and reaching a nursery - are retained in the same region ($\approx$ 100%), and the same can be said also for Calabria (98.9 %), where a small percentage is transported toward Sicily (0.6%) and Campania (0.5%). A large percentage of eggs released in Campania flows toward Lazio (16.8%), and the remaing part is retained in the same region. A similar pattern can be observed also in Lazio, where 18.8% is transported toward Tuscany, 1.1% toward Campania and the rest remain there, and in Tuscany, where 12.6 % flows toward Liguria, and 0.5% toward Lazio. Finally, 98.9% of the eggs released in Liguria remains there[2], and 1.1% goes back to Tuscany.

All these results are largely in line with what was previously noted about the currents. Two exceptions need to be explained: the small flow from Calabria toward Sicily, and the (again, small) flow from Lazio to Campania. While the latter mat be due to the inversion in shallow waters in eastern GSA 10 (fig. 5.13) in late autumn, the latter is probably due to the patchy inversion occurring in late spring (fig. 5.14).

5.2.4.1 *Transfer efficiency and retention*

To complete this analysis, other two indicators believed to convey interesting information were assessed:

1. The *transfer efficiency* is given by the proportion of eggs released in a certain region and reaching a favourable nursery;

2. The *retention* is given by the proportion of eggs released in a certain cell and reaching a favourable nursery within the same cell.

The purpose of these last two indicators is to evaluate if there are relevant differences between regions in terms of their capability to replenish the hake population, in particular near the spawning grounds of origin. Obviously, the value of the latter indicator is by definition smaller than the former.

2 Always considering only particles haveing reached a nursery. Without this condition this percentage would be sensibly lower, as it will be clear in the next paragraph.

Overall, the mean transfer efficiency is estimated to be around 57.7%, from a minimum value of 28.1% in Liguria to a maximum of 72.9% in Campania. Retention accounts for less than half of the eggs that are successfully released: the mean value is 15.9%, ranging from the lowest, Lazio (10.21%), to the highest, Campania (32.3%).

These last indicators can help in explaining, for example, why the contribution of Ligurian eggs to the Ligurian recruitment is so poor. Liguria has small and low-persistence reproduction areas, and has both the lowest transfer efficiency and retention; next to it, Tuscany has the largest reproduction areas, and a relevant difference between transfer efficiency and retention. The current brings the abundant Tuscanian eggs toward Liguria, while Ligurian eggs are mainly lost in the open sea.

Transfer efficiency and retention (averaged in each region) are shown in fig. 5.16.

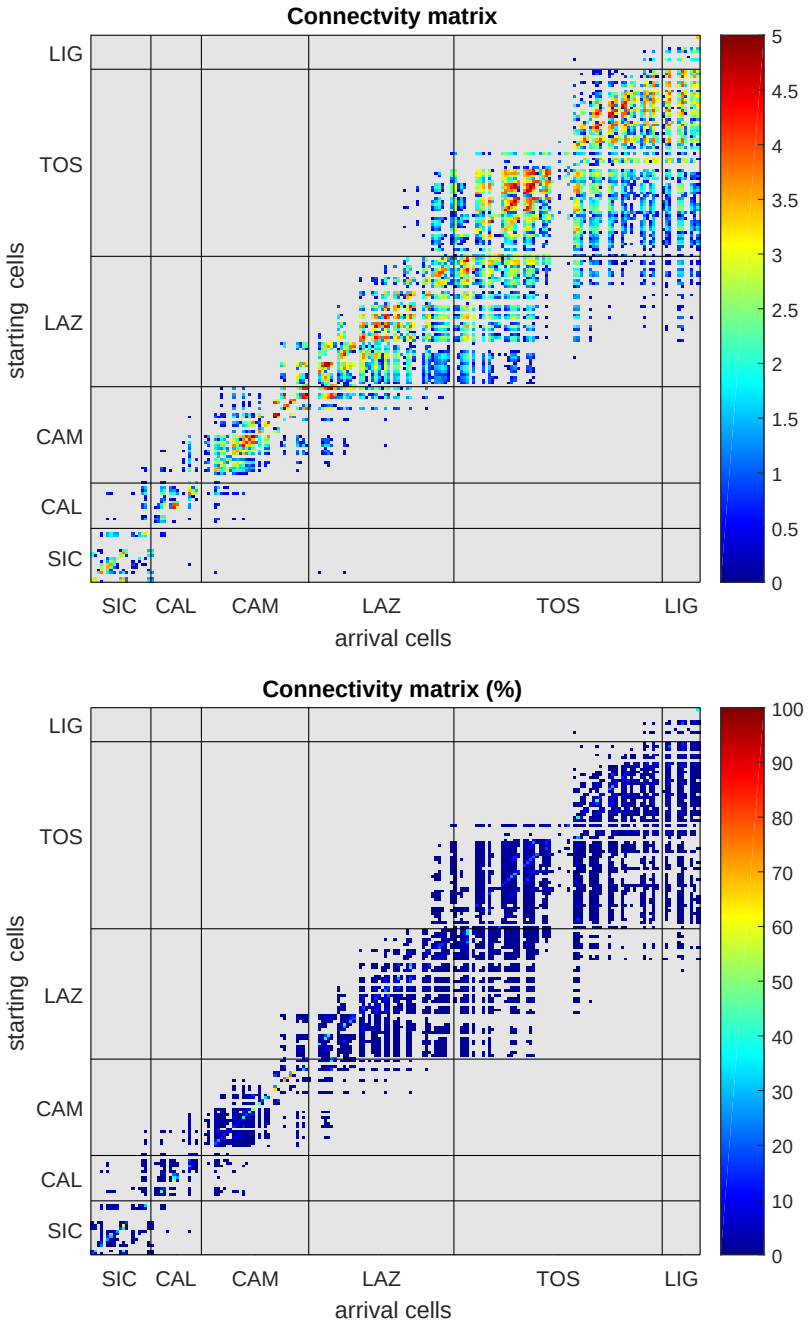

Figure 5.8: Connectivity matrices describing larval dispersal in GSAs 9 and 10. Above, matrix displaying absolute logaritmic frequencies (M_a) is shown; below, the matrix shows the proportion of particles, normalized with respect to the number of released particles in each cell M_p.

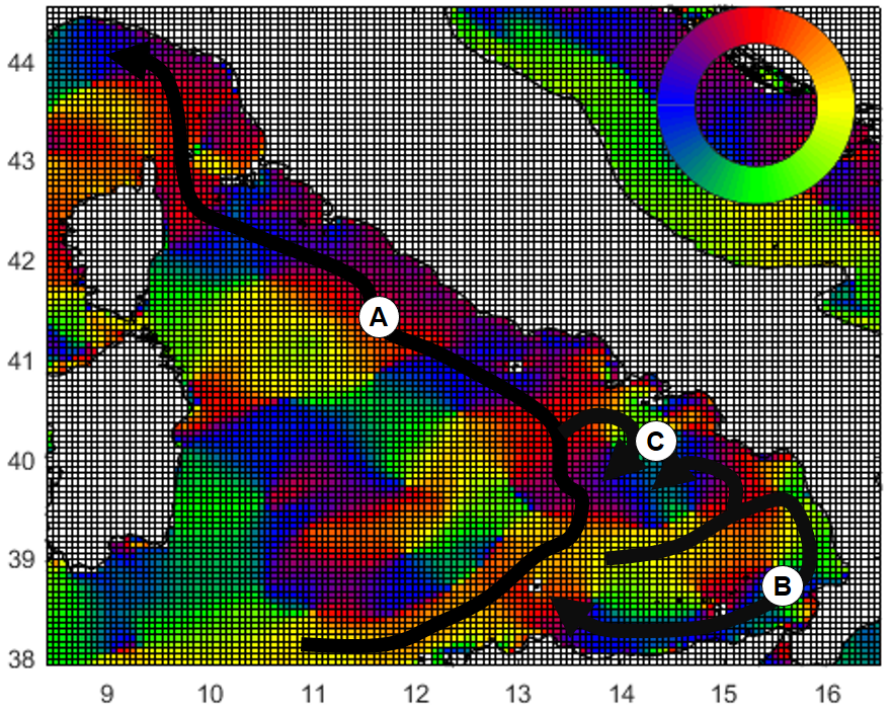

Figure 5.9: Angular patterns in the range 0 - 100 m. Red = northward current; yellow = eastward current; green = southward current; blue = westward current. Three main currents, A, B and C, are highlighted.

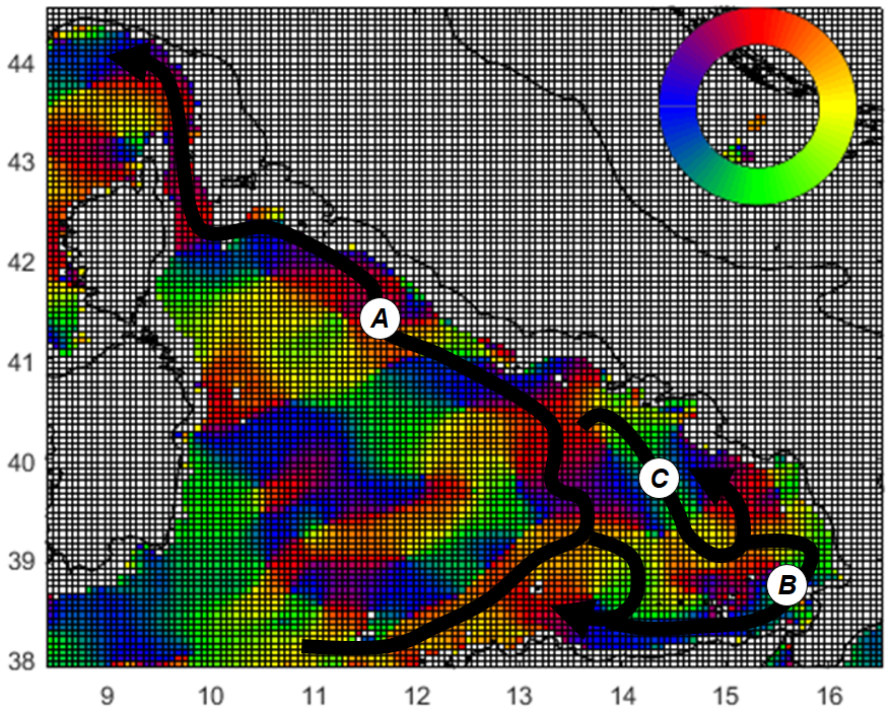

Figure 5.10: Angular patterns in the range 200 - 300 m. Red = northward current; yellow = eastward current; green = southward current; blue = westward current. Three main currents, A, B and C, are highlighted.

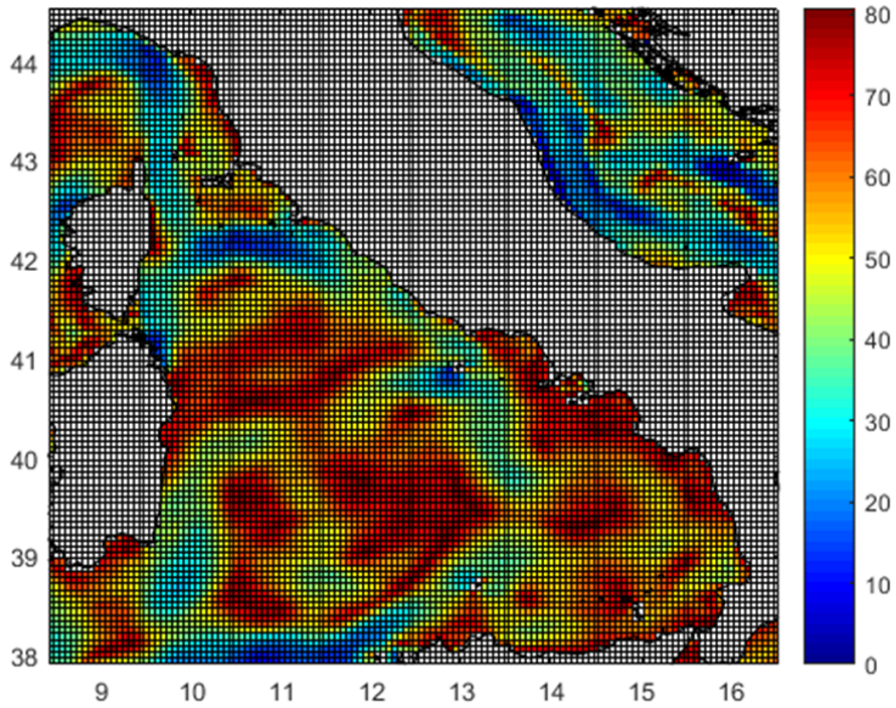

Figure 5.11: Standard deviation of current angle in the range 0 - 100 m. Hotter colours correspond to larger values.

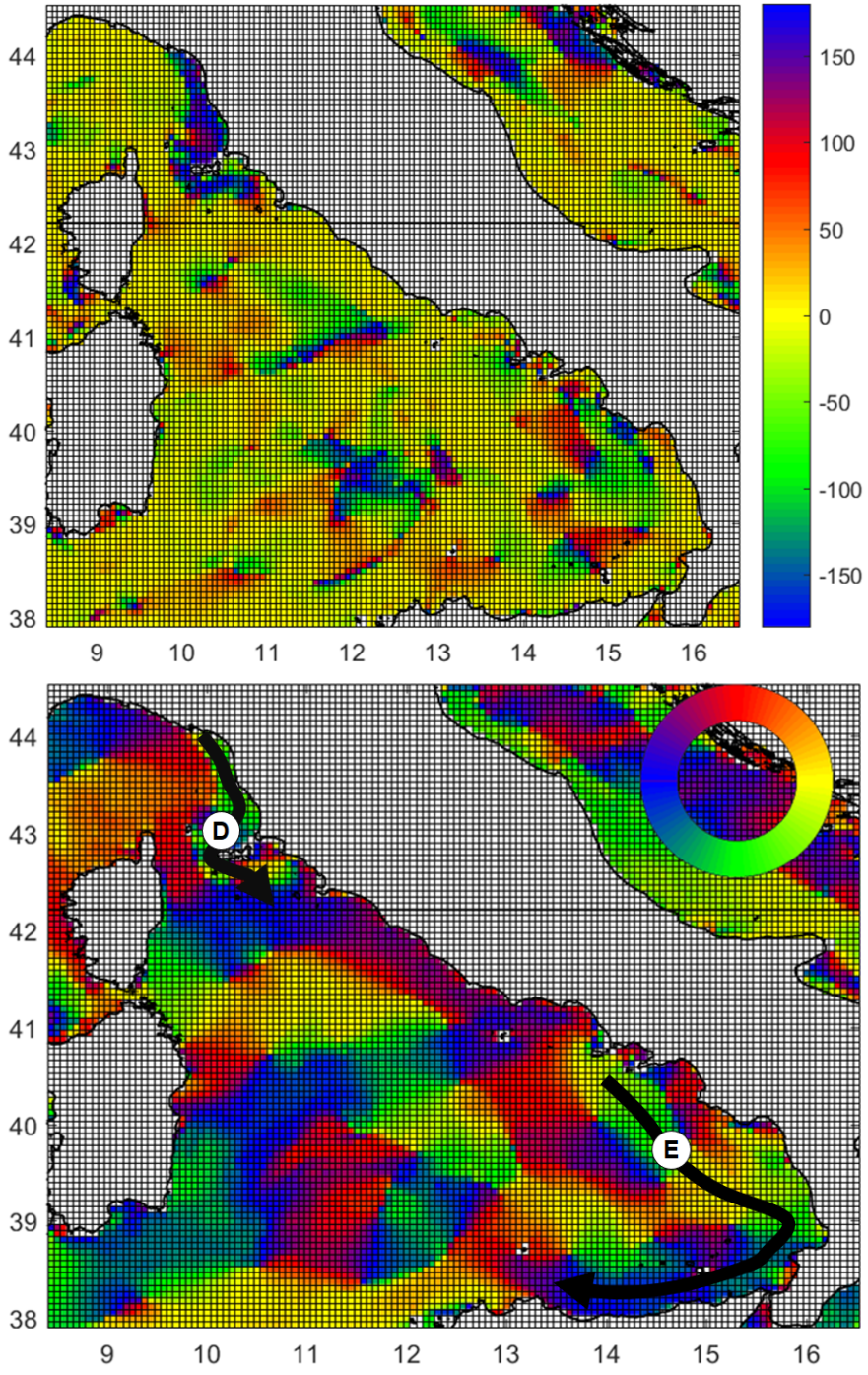

Figure 5.12: Deviation in August current angle in the range 0 - 100 m with respect to the overall average current angle in the same depth range. The figure above shows the absolute difference between the August mean and the overall mean, while the figure below shows the current fields in August.

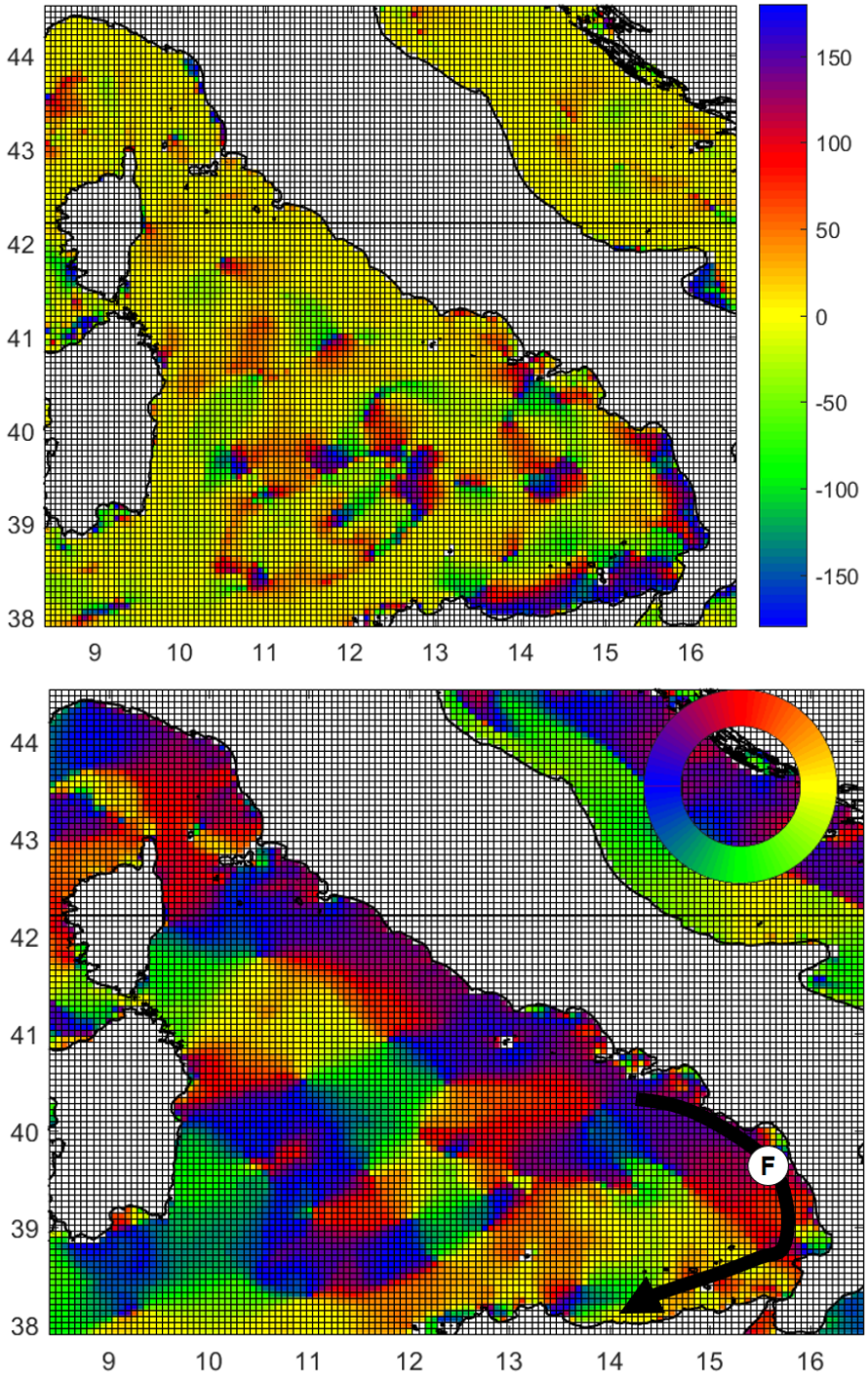

Figure 5.13: Deviation in December current angle in the range 0 - 100 m with respect to the overall average current angle in the same depth range. The figure above shows the absolute difference between the December mean and the overall mean, while the figure below shows the current fields in December.

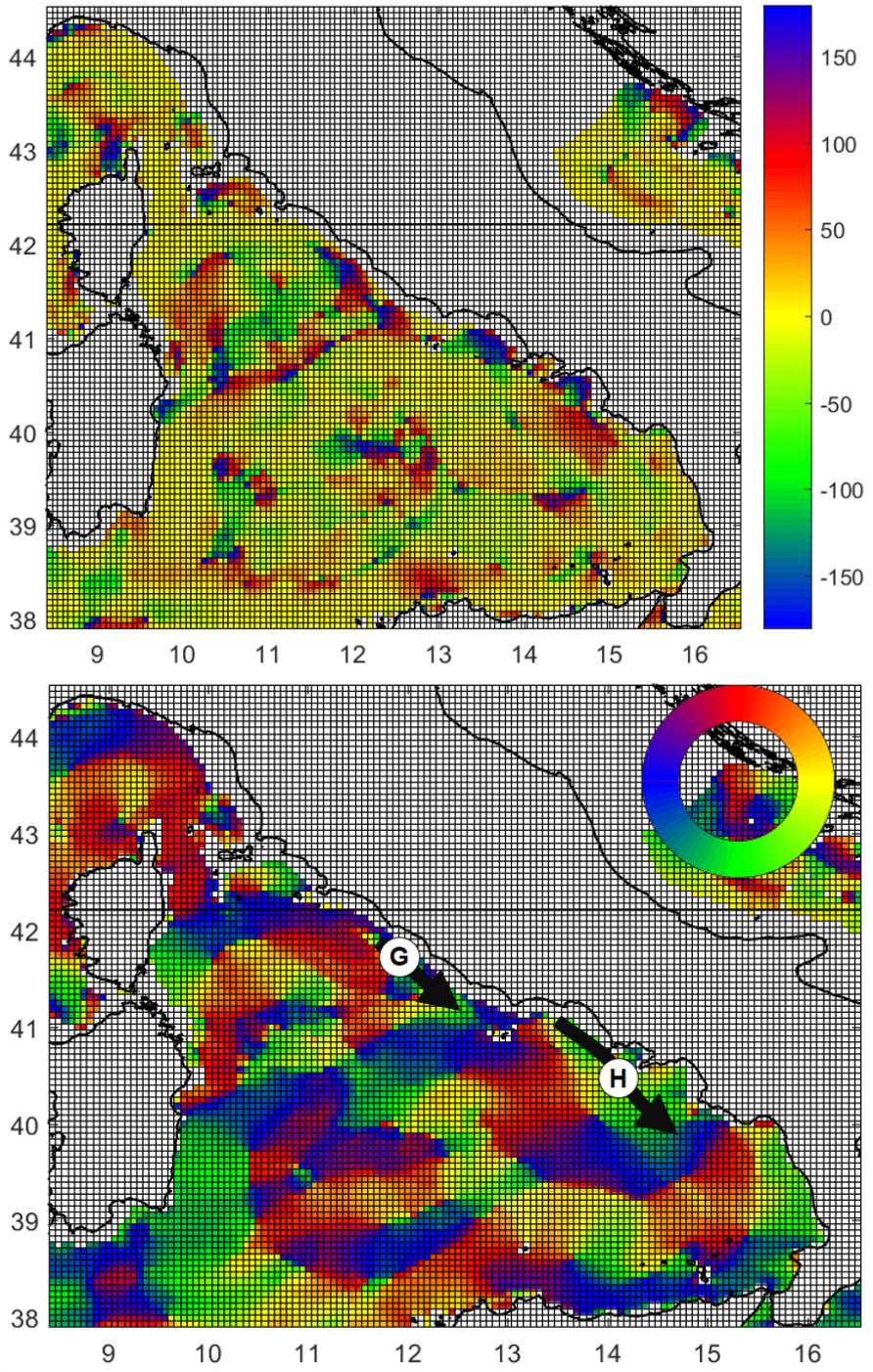

Figure 5.14: Deviation in June current angle in the range 100-200 m with respect to the overall average current angle in the same depth range. The figure above shows the absolute difference between the June mean and the overall mean, while the figure below shows the current fields in June.

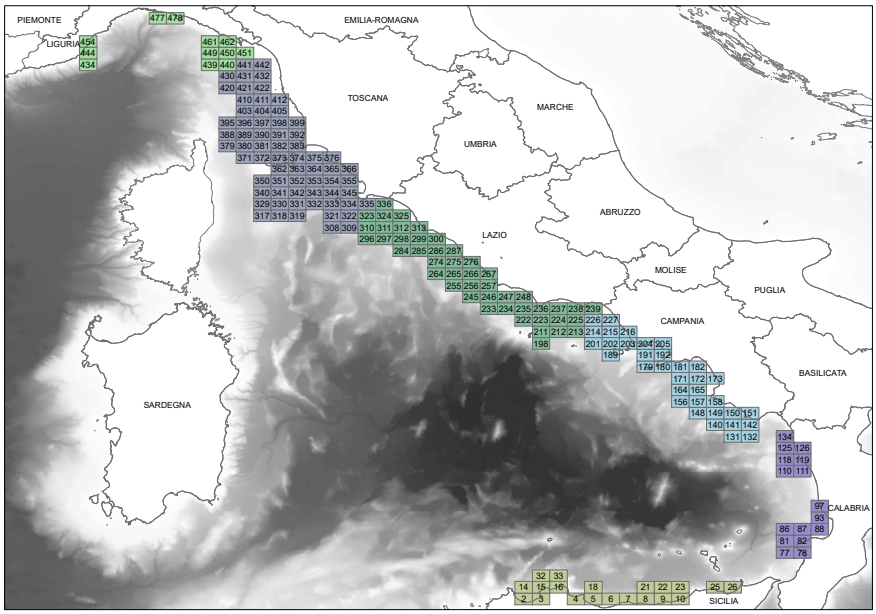

Figure 5.15: Subdivision of cells into regions.

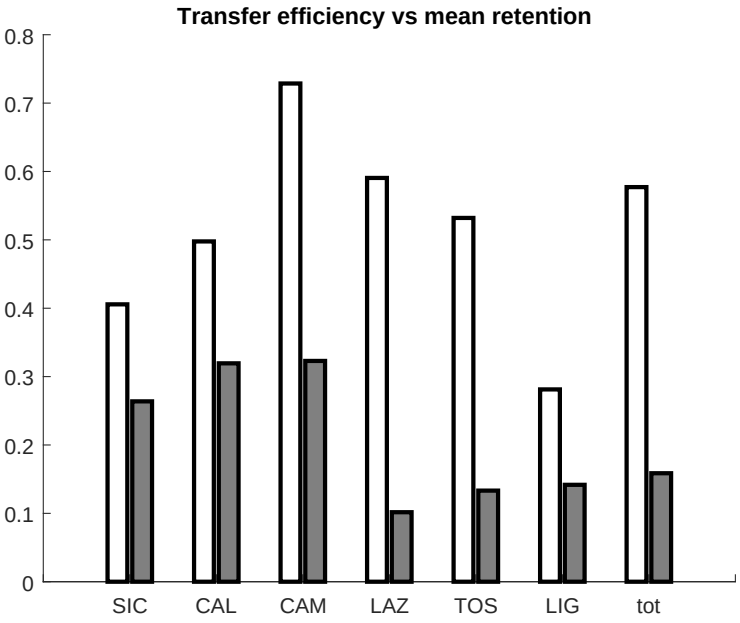

Figure 5.16: Transfer efficiency and mean retention.

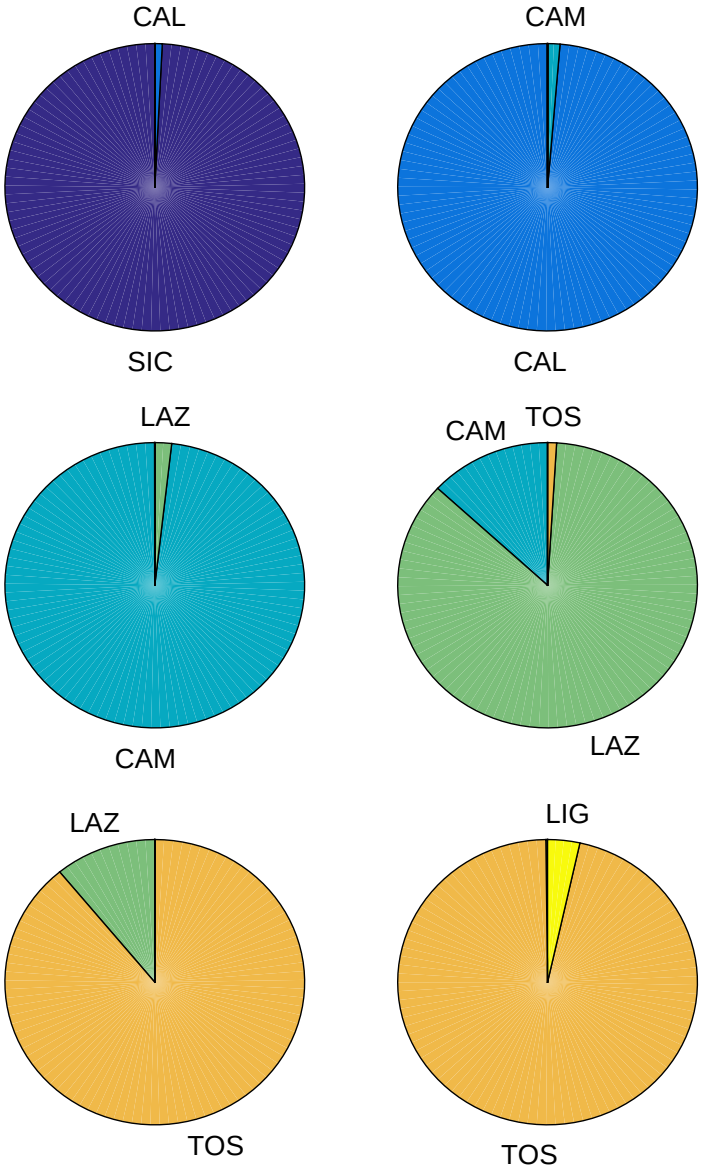

Figure 5.17: Where do eggs come from? These pie charts show theregion of origin of Lagrangian particles arriving in a specific region. First row: Sicily and Calabria; second row: Campania and Lazio; third row: Tuscany and Liguria.

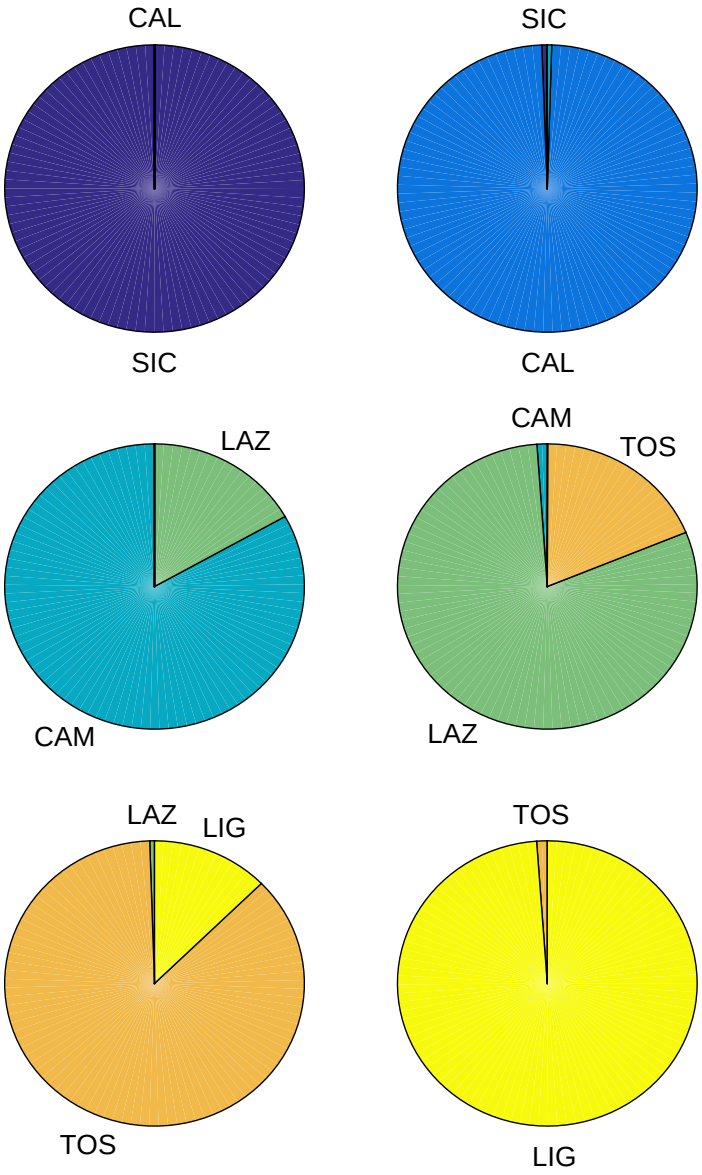

Figure 5.18: Where do eggs go? These pie charts show the region of destination of Lagrangian particles released from a specific region. First row: Sicily and Calabria; second row: Campania and Lazio; third row: Tuscany and Liguria. Only particle reaching a favourable destination are considered.

6 METAPOPULATION MODEL

Designing effective policies for the sustainable management of marine resources requires tools to predict the consequences of different management choices. In this sense, metapopulation models represent a valuable approach to describe the spatiotemporal dynamics of exploited fish stocks under different levels of fishing pressure.

Having reconstructed spawning grounds in Ligurian and Tyrrhenian Sea and having asssessed the larval connections between different locations in the same GSAs, here the focus is placed on GSA 9 only.

6.1 METHODS

To provide a realistic description of the processes at stake, metapopulation models should include:

1. An age-structured description of the demographic dynamics of adult life stages;
2. A stock-recruitment function (S/R), linking the abundance of spawners with that of their offspring;
3. A description of the processes driving the dispersal of eggs and larvae;
4. A description of the dispersal of adult life stages;
5. A description of the spatiotemporal patterns of fishing mortality produced by different fleet segments.

This model was developed for GSA 9 only. Three reasons support the decision to focus only on this area of the Ligurian and Northern Tyrrhenian sub-basin:

1. Given the distribution of currents in Western Mediterranean Sea (see Millot, 1999) it is likely that spawning grounds in the Gulf of Tunis (GSA 12, Bouhlal and Ktari, 1975) replenish nurseries along the northern Sicilian coasts (GSA 10). However, the location of Tunisian spawning grounds is unknown, being outside the range of most scientific surveys carried out in the last decades;
2. Compared to the larval flux from GSA 10 to GSA 9, other contributions to GSA 9 are negligible, as it was explained in Chapter 4;

3. The STECF report (Cardinale, Damalas, and Chato Osio, 2015) does not provide any abundance time series for GSA 10.

Given the existing knowledge gaps on the dynamics of the hake stock of the GSA 10, it seemed reasonable to proceed focusing on the GSA 9 only, using information available for GSA 10 as an external output to set border conditions (i.e. the supply of larvae from outside the domain).

6.1.1 *Age structure*

In the proposed metapopulation model, the hake stock is subdivided into age classes according to the STECF classification (Cardinale, Damalas, and Chato Osio, 2015). Classes range from age 0, i.e. recruits, to 6+, i.e. individuals aged 6 or more years.

Mean body weight, proportion of mature (spawning) individuals and natural annual mortality are summarized in table 6.1. Mortality is a decrescent function of age. Body lenght for each age class was calculated by means of a Von Bertalanffy model ($L_{inf} = 103.9$ cm, $K = 0.212$, $t_0 = 0.031$, Von Bertalanffy, 1938), whose parameterization was provided by the STECF project (Cardinale, Damalas, and Chato Osio, 2015); for the first year, a growth of 1.5 cm/month was assumed.

Age	mature	natural mortality (y^{-1})	weight (kg)	length (cm)
0	0%	1.2	0.008	7.8
1	25%	0.62	0.166	19.3
2	90%	0.44	0.578	35.5
3	100%	0.37	1.2	48.5
4	100%	0.33	1.949	59.1
5	100%	0.31	2.745	67.7
6+	100%	0.29	3.529	≈ 80

Table 6.1: Biological traits of European hake in GSA 9 (Cardinale, Damalas, and Chato Osio, 2015)

6.1.2 *Model initialization*

The overall hake stock of GSA 9 is described as a set of subpopulations distributed over the spatial grid described in Chapter 5 (see fig. 5.4) and exchanging larvae and adult individuals with each other. To initialize the model, it is necessary to know the abundance of the different age classes in each cell. Since data are available only at the GSA level, these should be spread over the spatial domain according to the availability of suitable habitat.

Time series of abundances provied by the STECF project (Cardinale, Damalas, and Chato Osio, 2015) were used to set the initial state. Mature individuals were spread in each cell proportionally to the mean persistence of the spawning grounds of each cell, while immatures individuals were, similarly, spread proportionally to the persistence of the nurseries in that cell.

The rationale behind this procedure is, once again, the possibility to use temporal persistence of a habitat as a surrogate of mean spatial density, as it was explained in Chaper 4.

6.1.3 *Stock-recruitment function*

A stock-recruitment curve is a relation linking the abundance of the (spawning) stock to the abundance of the recruits, i.e. individuals aged 0. Usually, this relation links the spawning stock of a certain year to the recruits of the same year. In this case, however, given the multimodal distribution of recruitment peaks (late autumn/early winter and late spring/early summer; Giannoulaki et al., 2013), the period in which scientific surveys of the MEDITS project are performed (late spring/early summer; Druon et al., 2015), and the fact that the fishing gears used during surveys capture large recruits more easily than small ones (Sbrana et al., 1998, Belcari, 2005), it can be concluded that most of the recruits sampled in a year should be attributed to eggs released during the last months of the previous year.

That being said, the general stock-recruitment curve used in this metapopulation model can be written as (eq. 6.1):

$$N_{0,t+1} = f(N_{1,t}, N_{2,t}, ..., N_{6+,t}, \theta_1, ..., \theta_n) \tag{6.1}$$

The STECF project (Cardinale, Damalas, and Chato Osio, 2015) provides a 9 year time series of the spawning stock biomass, given by the product of abundances, weight and proportion of mature individuals in each age class, at GSA level; a time series of abundance of recruits are provided as well.

In this metapoulation model, the stock-recruitment function is supposed to work with density indices instead of absolute abundances. This approach allows the calibration of a stock-rectuitment function at the GSA level, calculating density indices from time series of abundances and the overall surface of nurseries (or spawning grounds), and apply it at a local (cell) level - since density is an intensive property.

In order to accomplish this requirement, densities of spawning stock biomass in each cell at each time step ($ssb_{i,t}$) were calculated as the ratio between SSB in a certain cell and the persistent area of

spawning grounds in that cell, which should be a measure of the area effectively inhabited by oldest hakes (eq. 6.2):

$$ssb_{i,t} = \frac{\sum_k w_k m_k N_{i,k,t}}{\sum_l A_{i,l} P_l^{spw}} \tag{6.2}$$

Where w_k is the weight associated to age class k, m_k is the proportion of spawners (mature) in the same class, $N_{i,k,t}$ is the abundance of class k in cell i at time t, $A_{i,l}$ is the area with persistence class l in cell i, and P_l^{spw} is the persistence of spawning grounds in class l. Similarly, a density index was defined for recruits too, computed as (eq. 6.3):

$$r_{i,t} = \frac{N_{i,0,t}}{\sum_l A_{i,l} P_l^{nrs}} \tag{6.3}$$

Where $N_{i,0,t}$ is the abundance of recruits in cell i, and P_l^{nrs} is the persistence associated to nurseries in class l, other subscripts being the same.

In the literature, the main types of stock-recruitment curves are used:

1. The linear model (eq. 6.4), which describes the demography as a malthusian dynamics (Leslie model, Leslie, 1945). Recruits are proportional to the SSB of the previous year. It is customary to use a linear model only when density dependent effects are negligible, otherwise it would fail to describe the demographic dynamics in a realistic way.

$$R_{i,t+1} = \alpha SSB_{i,t} \tag{6.4}$$

2. The Beverton-Holt model (eq. 6.5), which is based on the assumptions that juvenile competition results in a survival rate that is decreasing with the number upon the number of the offsprings. The number of recruits saturates whithout discontinuity toward a carrying capacity;

$$R_{i,t+1} = \frac{\alpha SSB_{i,t}}{1 + \beta SSB_{i,t}} \tag{6.5}$$

3. The Ricker model (eq. 6.6), which assumes that the mortality rate of the eggs and juveniles is proportional to the initial spawning stock. Biological traits that might lead to this assumption being met could be cannibalism of the juveniles by the adults or disease transmission. The numer of recruits is not always an

increasing function of SSB, since at high densites the number of survivors decreases:

$$R_{i,t+1} = \alpha SSB_{i,t} e^{-\beta SSB_{i,t}} \tag{6.6}$$

Stock-recruitment parameters (α and β) can be calibrated minimizing the square of the mean squared errors (RMSE) between the expected abundance of recruits and that provided by STECF series (Cardinale, Damalas, and Chato Osio, 2015). All the models described above were calibrated and compared through a model selection procedure, as described in the next paragraphs.

Since the stock-recruitment function is supposed to work with densities instead of absolute abundances, the total number of eggs released in cell i (before larval displacement) is calculated as shown in eq. 6.7:

$$R*^{9}_{i,t+1} = f(ssb_{i,t}) \sum_{l} (A_{i,l} P_l^{nrs}) \tag{6.7}$$

Where $f(ssb_{i,t})$ is the stock-recruitment function.

6.1.3.1 *External contribution*

The larval connectivity matrix M_p introduced in Chapter 5 describes the connectivity in both GSAs 9 and 10. In order to represent a realistic external contribution from GSA 10 to GSA 9, series of STECF abundances of individuals aged 0 have been used, distributed in each cell of the GSA 10 proportionally to the persistence of the nurseries of those cells.

The row vector containing the abundance of recruits in each cell of the GSA 10 is $R*^{10}_t$. The vector containing all the eggs in each cell in both GSAs 9 and 10 before dispersal is defined by eq. 6.8:

$$R*_t = [R*^{9}_t \; R*^{10}_t] \tag{6.8}$$

6.1.4 *Larval dispersal adjustment*

The larval connectivity matrix M_p specifies the proportion of larvae $m_{i,j}$ released from cell i and reaching cell j. The matrix M_p does not reproduce a Markovian process, because a relevant number of larvae is dispersed outside the spatial domain of the model, not reaching any favourable nursery (eq. 6.9):

$$\sum_{j} m_{i,j} \leqslant 1 \tag{6.9}$$

A correction was made to reflect the fact that simply applying the connectivity matrix to the number of eggs which is estimated to be produced in each cell (and that is assumed to contribute to recruitment) would result in a sistematic underestimation of recruitment. At each time step, after displacement, the number of age-0 hakes in every cell is multiplied by a correction factor, given by the ratio between the total number of recruits in GSA 9 before displacement and the same quantity after displacement. This correction factor is always $\geqslant 1$ (eq. 6.10):

$$R_{i,t} = \frac{\sum_i R*_{i,t}}{\sum_i (R *_t M)} (R *_t M)_i \tag{6.10}$$

Being $R*_t$ the vector calculated in eq. 6.8.

6.1.5 *Adult stage dispersal*

No quantitive information is available about adult dispersal (i.e. of the individuals aged 1 or more). However, it is known that adults can move far from nurseries and spawning grounds, and that they are skilled swimmers.

In the absence of information regarding the swimming behaviour of adult hakes, their dispersal was modelled by means of dispersal kernels. Three different shapes of dispersal kernels have been explored:

1. A power law karnel;
2. An exponential kernel;
3. A Gaussian kernel.

6.1.5.1 *Power law dispersal kernel*

In the power law dispersal kernel (fig. 6.1), two parameters have to be calibrated:

1. The proportion of adults moving from cell i to cell j. This should be a decreasing function of the Euclidean distance $d_{i,j}$ between centroids of cells i and j, moduled by the exponent θ_{D2} (eq. 6.11):

$$D_{i,j} = d_{i,j}^{-\theta_{D2}} \tag{6.11}$$

2. The proportion of adults remaining in each source cell i, which is described in eq. 6.12. The definition of this parameter is nec-

essary since the function given by eq. 6.11 can not be computed for $i = j$.

$$D_{i,i} = \theta_{D1} \tag{6.12}$$

Moreover, the adoption of two parameters allows the uncoupling of the retention, dependento on θ_{D1}, from the dispersal, dependent on parameter θ_{D2}. This does not ensure that the dispersal kernel has its maximum in the source cell.

6.1.5.2 *Exponential dispersal kernel*

A dispersal described by an exponential kernel follows this equation:

$$D_{i,j} = e^{-\theta_{D2} d_{i,j}} \tag{6.13}$$

Which is suitably defined also for $i = j$. This shape has a shape that is qualitatively similar to that of the power law, but assumes the dispersal to be confined in a narrower area (fig. 6.1).

6.1.5.3 *Gaussian dispersal kernel*

A dispersal described with a Gaussian kernel follows this law:

$$D_{i,j} = e^{-\frac{d_{i,j}^2}{\theta_{D2}}} \tag{6.14}$$

Which is suitably defined also for $i = j$ as well. This dispersal kernel has its maximum at the source cell, with an inversion of concavity, that usually makes the tail of the distribution thinner than in the other kernels (fig. 6.1).

Another assumption was made about adults dispersal, i.e. that all adults remain inside the domain (eq. 6.15):

$$\sum_j D_{i,j} = 1 \tag{6.15}$$

This assumption was made in order to avoid introducing a fictitious mortality, which would have complicated the calibration of other parameters linked to fishing pressure. As a consequence of this assumption, parameter θ_{D1} in the power law dispersal kernel (and similarly e^0 in exponential and Gaussian) does not account directly for retention, which should be calculated in the aftermath.

A final hypothesis was that adults do not move toward cells which do not contain any spawning ground. This assumption was made

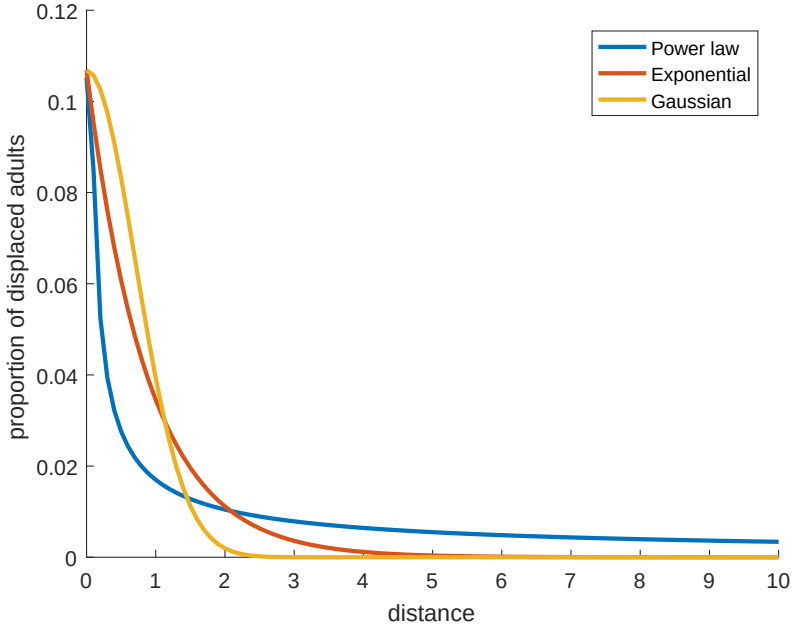

Figure 6.1: Qualitative dispersal kernels.

in order to differentiate the role of cells hosting preferably recruits (nurseries) or older individuals (spawning grounds).

No other assumption has been made upon adults dispersal, which is supposed to occur after reproduction and before applying mortality. All the dispersal kernels described above were calibrated and compared through a model selection procedure, as described in the next paragraphs.

6.1.6 *Fishing pressure*

STEFC (Cardinale, Damalas, and Chato Osio, 2015) reports time series of fishing mortality differentiated by age class, estimated via a software for virtual population analysis, XSA. However, those data refer to the whole GSA 9 and are not disaggregated by area nor fleet segment. In order to disaggregate the fishing pressure in space, time and fleet segment, a different approach, described below, was used.

Fishing mortality can be calculated as (eq. 6.16):

$$F = qE \tag{6.16}$$

Where q represents the catchabily and E is the effort. Catchability is a proportionality constant that represents the fishing mortality per unit effort (Arreguín-Sánchez, 1996). Effort, on the other hand, is a measure of fishing intensity, and can be expressed in terms of the resources employed while fishing (for instance, time spent at sea or fuel consumption).

In this case, it seemed reasonable to express catchability as a function of specific fishing gear (the same in each métier, i.e. a specific fleet segment equipped with a certain gear and, in this case, identified by a LOA range) and on selectivity, which represents the proportion of retained fish as a function of fish size. This depends upon the size of the fish, and can then be modelled using a so-called selectivity curve. Over a short time horizon, in which technological development is not a relevant phenomenon, catchability can be thought as constant in time (and space).

On the other hand, effort has a well specific temporal dynamics, since it depends on the resources employed while fishing. STECF (Cardinale, Damalas, and Chato Osio, 2015) provides time series for métiers targeting European hake in GSA 9, expressed in kW $\times$ days at sea (fig. 6.2).

In this metapopulation model, four different méters were considered:

1. SSC 0-12: small scale fisheries with LOA $\leqslant$ 12 m, including mainly gillnets (GNS);
2. SSC 12-24: small scale fisheries with LOA between 12 and 24 m, including mainly gillnets (GNS);
3. OTB 0-12: otter bottom trawlers with LOA $\leqslant$ 12 m;
4. OTB 12-24: otter bottom trawlers with LOA between 12 and 24 m.

Effort has a spatial dimension too. Fishing grounds identified by the Stockmed project (Fiorentino et al., 2014), introduced in Chapter 3 (fig. 3.4, 3.5, 3.6 and 3.7), were used to subdivide the gridded domain into smaller regions, and to characherize each sub region (or subcell) with a value of fishing footprint (Kavadas et al., 2015) for each fleet segement. More precisely, these fishing grounds map the potential fishing pressure exerted by different métier in all the Mediterranean sea. Each fishing ground is assigned one of the five fishing footprint classes, ranging from $0-0.2$ (the lowest) to $0.8-1$ (the highest). In order to spatially weight the effort exerted by different métiers, each subcell was assigned the mean value of fishing footprint relative to the footprint class of that subcell.

Finally, the classification of the fleet into segments was simplified to make modelling easier. Table 6.2 was elaborated from Deliverable 2.5 of the Safenet project (Sartor et al., 2015). As it is shown, fleet segment OTB 0-12 is negligible with respect to others in terms of landings. In this analysis, OTB 24-40 and OTB 12-24 were merged together.

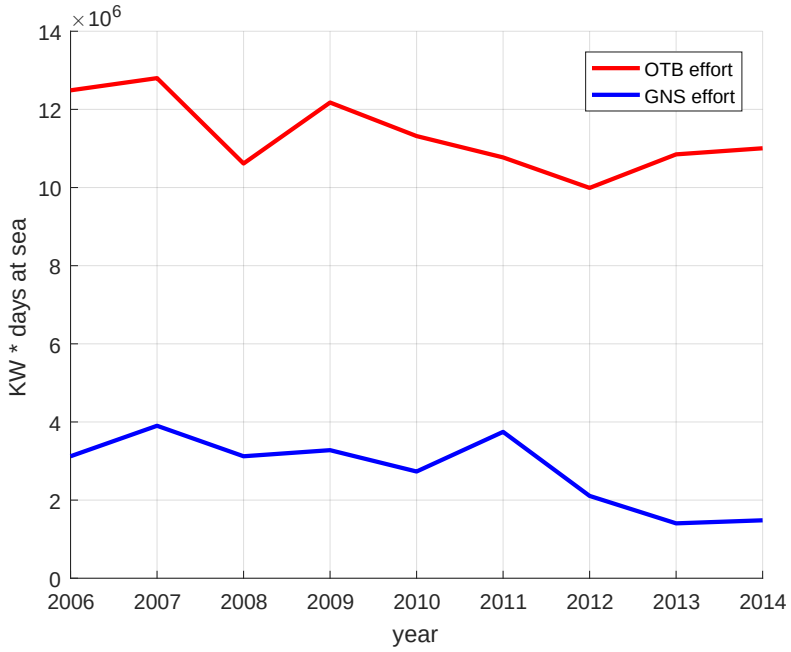

Figure 6.2: Time series of effort in GSA 9, expressed in kW * days at sea, differentiated per métier (Cardinale, Damalas, and Chato Osio, 2015).

Segment	mean landings 2012 - 2014 (tons)
SSC 0-12	193.7
SSC 12-24	82.3
OTB 0-12	0.6
OTB 12-24	783.6
OTB 24-40	339.6

Table 6.2: Landings for fleet segment in GSA 9

6.1.6.1 *Selectivity*

Each net captures fish with a different efficiency depending on fish size. The curve describing the capture efficiency as a function of fish TL is called selectivity function.

Since gillnets are the main métier targeting adult hakes, this métier was considered as representative of the whole small scale fisheries sector. Two different curves were taken:

1. The first (red curve in fig. 6.3) refers to gillnets with mesh size 62.5 mm (Sbrana et al., 2007), estimated with the SELECT method, which provides a bimodal function (Millar and Holst, 1997), due to medium-sized fish entrapped by the body and large fish held by other protusions;

2. The second (blue curve in fig. 6.3) refers to a larger mesh size, around 82 mm (Belcari, 2005), which provides unimodal length frequecies distributions, as it catches only large specimens, and was estimated using the Sechin method (Reis and Pawson, 1992).

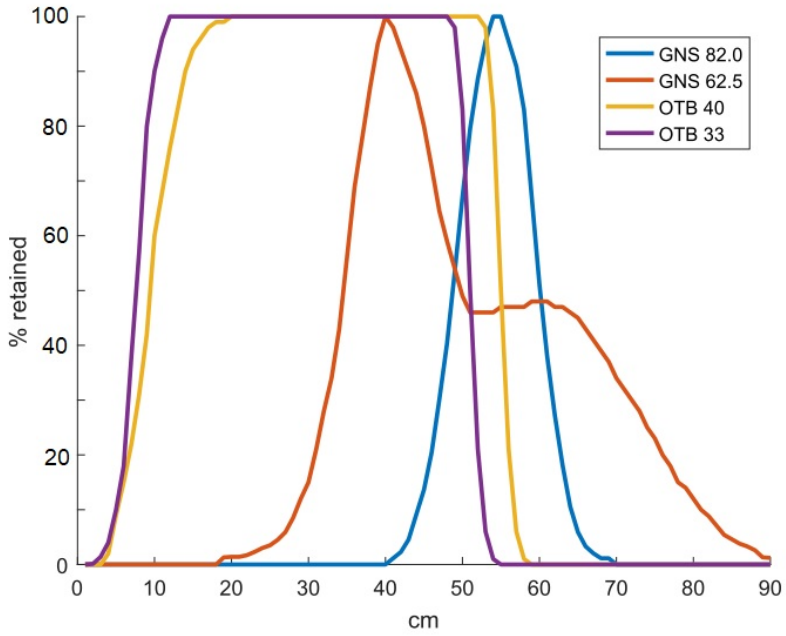

Figure 6.3: Selectivity functions expressing the percentange of retained fish as a function of TL for the four fishing gears.

An article by Russo et al. (2017) is the main source for what concerns OTB selectivity curves. Since otter bottom trawls are the main mérier in GSA 9 targeting *Merluccius merluccius*, in terms of both landings and discards (Cardinale, Damalas, and Chato Osio, 2015), also here two different curves were used to model selectivity:

1. The first was made combining the logistic curve associated to small mesh size (33 mm) developed for individuals from 0 to 15 cm TL (Sbrana et al., 1998) with the curve associated to the lowest selectivity toward large individuals among those used by Russo et al. (2017 purple curve in fig. 6.3) in the GSA 19.

2. The second was built combining the logistic curve associated to medium mesh size (40 mm) developed for individuals from 0 to 30 cm TL (Belcari, 2005) with the curve associated to the highest selectivity toward large individuals between those used by Russo et al. (yellow curve in fig. 6.3).

The rationale behind this subdivision is to differentiate two segments whose selectivity is (as far as possible) strongly directed toward recruits or large individuals.

Selectivity, originally expressed as a function of body size, was then mapped into a function of age to be used within the age-structured model. This was done by inverting the body growth curve (table 6.1). Selectivity for each age class and gear is reported in table 6.3.

Age class	OTB (33 mm)	OTB (40 mm)	GNS (62.5 mm)	GNS (82 mm)
0	61%	49%	0%	0%
1	100%	100%	20%	0%
2	100%	100%	100%	15%
3	24%	60%	59%	100%
4	0%	0%	56%	27%
5	0%	0%	39%	0%
6	0%	0%	12%	0%

Table 6.3: Selectivity of métiers in GSA 9.

Equation defining fishing mortality (6.16) is finally changed into eq. 6.17:

$$F_{\upsilon,k,t,\mu} = \theta_{\mu} sel_{k,\mu} eff^{T}_{t,\mu} eff^{S}_{\upsilon,\mu} \tag{6.17}$$

Where:

1. $F_{\upsilon,k,t,\mu}$ indicates the fishing mortality in subcell υ on individuals aged k at time t by fleet segment μ;
2. $sel_{k,\mu}$ is the selectivity of métier μ on individuals of class k (fig. 6.3);
3. $eff^{T}_{t,\mu}$ is the effort of fleet segment μ at time t (fig. 6.2) given by the STECF series, normalized by dividing it by its mean value over time;
4. $eff^{S}_{\upsilon,\mu}$ is a coefficient weighting the effort of métier μ in subcell υ, derived from Stockmed maps (fig. 3.4 and following).

θ_{μ}, $(\mu = 1, 2, 3, 4)$ are four parameters to be calibrated in order to allocate the overall catches according to the four métiers (OTB with mesh size 33 mm, OTB 40, GNS (SSC) 62.5, GNS 82). The four values θ_{μ}, as well as θ_{D1} and θ_{D2}, are calibrated minimizing the root mean square logarithmic errors (RMSLE) between abundances reconstructed by STECF and those simulated with the model (eq. 6.18):

$$J(\theta) = \sqrt{\frac{1}{KT} \sum_{k,t} [\ln(\hat{N}_{k,t}(\theta)) - \ln(N_{k,t})]^2} \tag{6.18}$$

Where:

1. K is the number of age classes;
2. T is the length of the time series;
3. $\hat{N}_{k,t}(\theta)$ is the calculated abundance of age class k at time t, expressed as a function of parameters θ;
4. $N_{k,t}$ is the abundance of age class k at time t provided by the STECF time series;

This cost function was chosen since it balances errors refered to different age classes (which usually differ by orders of magnitude) and penalizes relative underestimations over overestimations. These characteristics make it preferable to the root mean of square errors (RMSE), since this last metric would give a disproportionate importance to the youngest (and most abundant) age classes.

In each subcell, overall fishing mortality for each age class at each time step is computed with eq. 6.19:

$$F_{v,k,t} = \sum_{\mu} F_{v,k,t,\mu} \tag{6.19}$$

Catches (and deaths) in each cell were calculated with the Baranov equation (eq. 6.20), in which the time step Δ is 1 year (Baranov, 1918). Abundances are set to be proportional to the subcell area A_v.

$$C_{i,k,t} = \sum_{v \in i} \frac{F_{v,k,t}}{F_{v,k,t} + M_k} (1 - e^{-(F_{v,k,t} + M_k)\Delta}) N_{i,k,t} \frac{A_v}{A_i} \tag{6.20}$$

6.2 RESULTS

6.2.1 *Stock-recruitment function*

Three possible recrutiment curves were estimated and are shown in figure 6.4. Table 6.4 shows the details about parameter values and cost functions. The Ricker model and the Beverton-Holt model have a very similar shape, and their cost functions are close to each other. The same cannot be said about the linear model, which has the worst fitting performance.

6.2.2 *Model validation*

Abundances for each age class from year 2006 to 2014 were reconstructed using nine parameterizations, each obtained associating a

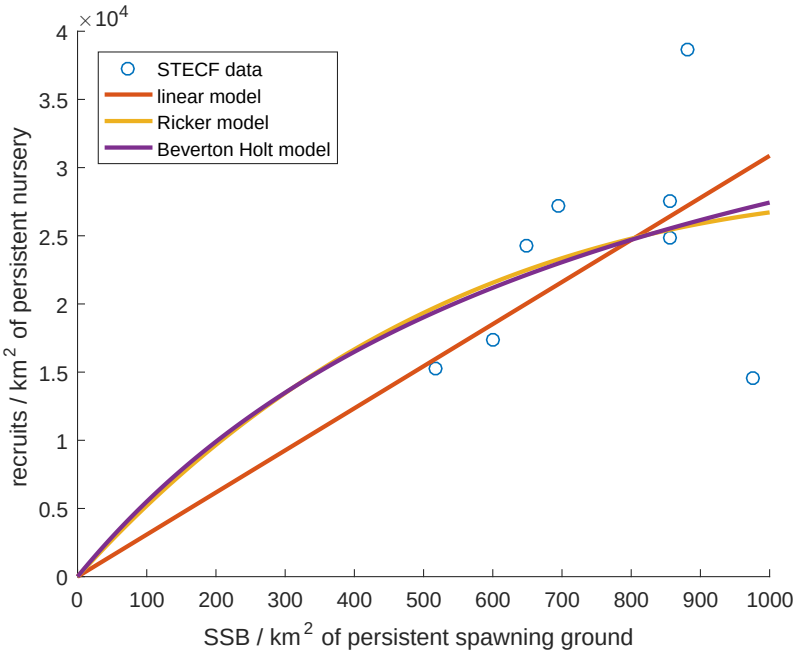

Figure 6.4: Stock-recruitment functions for the hake stock in GSA 9. Spawning stock biomass (kg) and recruits are expressed in terms of spatial density.

Model	α	β	RMSE
Linear	30.91	-	7344.76
Ricker	56.12	74.09×10^{-5}	6822.13
Beverton-Holt	62.07	12.59×10^{-4}	6893.48

Table 6.4: Results of the calibration of the three stock-recruitment functions. α is the proportionality coefficient, β the density dependent coefficient.

stock-recruitment function (linear, Ricker or Beverton-Holt) to a dispersal kernel (power law, exponential or Gaussian). Each of these parameterizations is defined by eight coefficients (α and β for the S/R function; θ_{D1} and θ_{D2} for adult dispersal; θ_{OTB33}, θ_{OTB40}, θ_{GNS625} and θ_{GNS820} for the catchability). In fig 6.5 are shown the simulated abundances for the power law dispersal kernel, in fig. 6.6 for the exponential, and finally in fig. 6.7 for the Gaussian.

These nine recostructions are compared to STECF data (black circles in the same figure). Table 6.5 shows the values of the optimized parameters.

Fishing yields in terms of weight are computed (and shown in fig. 6.8, 6.9, 6.10). Yields were calculated from the number of catches of individuals longer than 20 cm (for semplicity, only individuals aged 0 were considered as shorter than 20 cm), multiplied for the weight

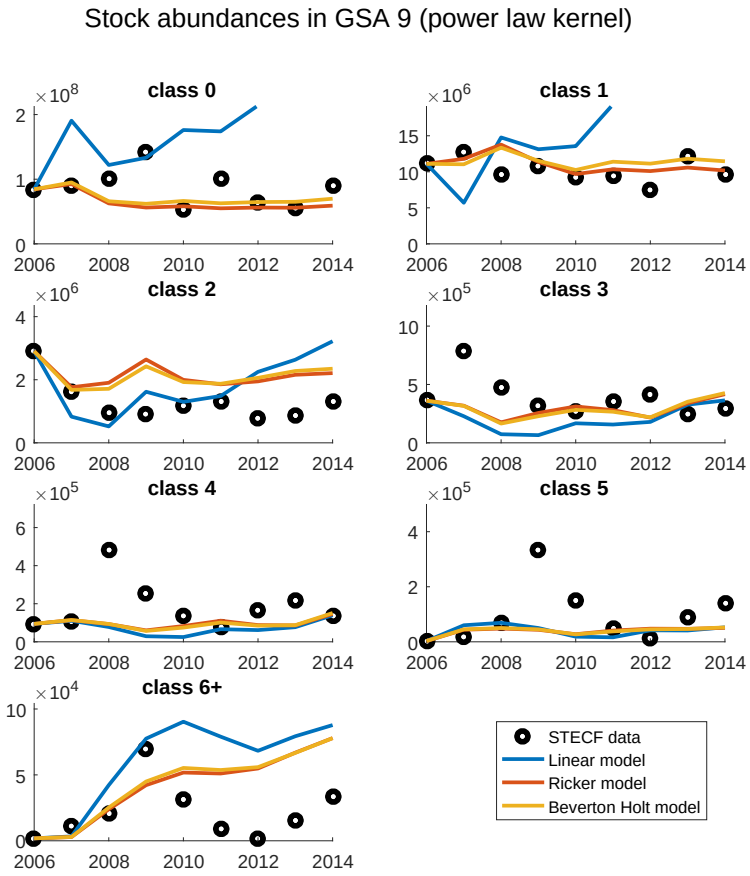

Figure 6.5: Reconstructed abundance of the different age classes in GSA 9 obtained with different S/R functions and a power law dispersal kernel.

provided by table 6.1. These outputs were compared to available data in order to validate the metapopulation model parameterizations (fig. 6.11).

Results obtained with the linear stock-recruitment function (blue line) have always the worst fitting performance, with every dispersal kernel. In fact, they are associated with highest RMSLE both in calibration and in validation (fig. 6.11). Moreover, these parameterizations underestimate gillnet catchability, and overestimate otter bottom trawls catchability (fig. 6.8 and following).

On the opposite, the simulations produced with Ricker (red line) and Beverton-Holt (yellow line) models follow similar trends, underestimating some age classes (such as 0) and overestimating others (such as 2; see fig. 6.5 and following). Consequently, yields provided by the two models are similar: both parameterizations manage to describe those by gillnets, and overestimate those by otter bottom trawls (fig. 6.8 and following).

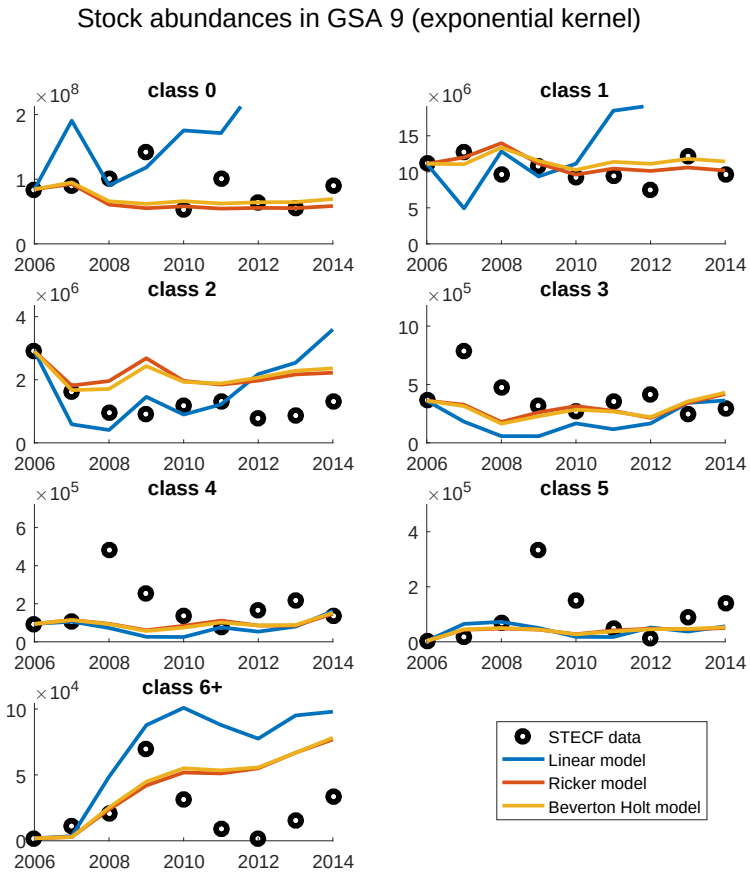

Figure 6.6: Reconstructed abundance of the different age classes in GSA 9 obtained with different S/R functions and an exponential dispersal kernel.

The entity of this overestimation depends on the dispersal kernel. As it is evident from fig. 6.11 and table 6.5, power law and exponential kernels produce a validation error around 0.40, while the Gaussian kernel produces a lower one (0.25), and determines yields trajectories closer to STECF data compared to that of previous kernels.

On the other hand, with the exception of the linear S/R model, there is no relevant difference among models with respect to the calibration error, all values ranging from 0.98 to 1.00.

As a consequence, in the simulations run in Chapter 7 to assess the consequences of different management policies, a Gaussian dispersal kernel was used, coupled either with a Ricker or a Beverton-Holt stock-recruitment relationship.

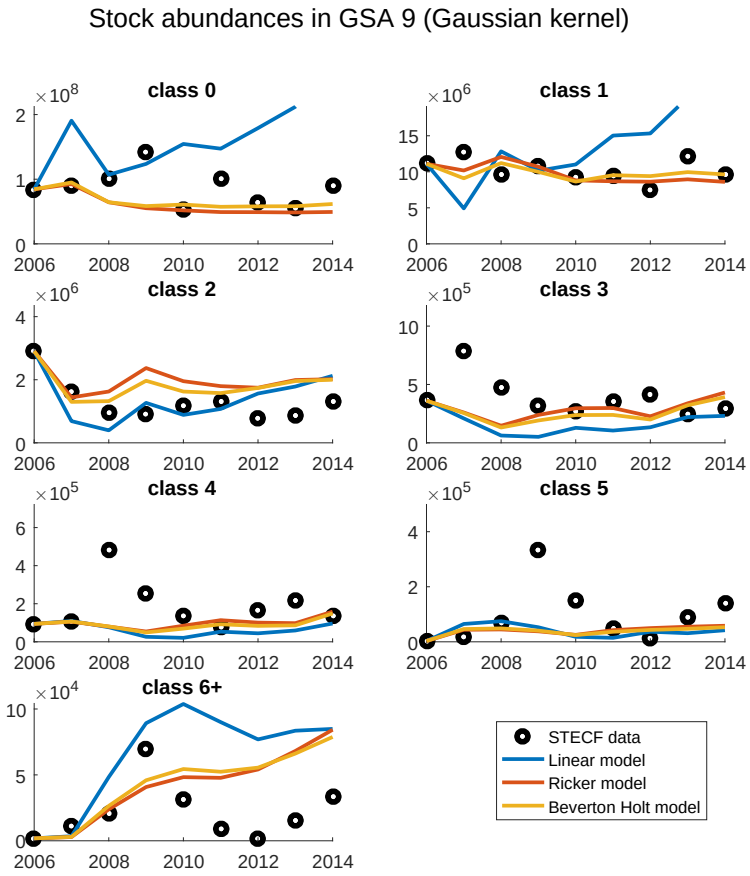

Figure 6.7: Reconstructed abundance of the different age classes in GSA 9 obtained with different S/R functions and a Gaussian dispersal kernel.

6.2.3 *Comments about data quality*

The evident mismatch between peaks in abundances data and reconstructions and the high RMSLE in calibration required further analysis in order to be explained. In figure 6.12 normalized trends of STECF fishing mortalities for classes (0 and 6+) and efforts (OTB and GNS) are reported.

As it is evident from eq. 6.17, fishing mortality of a certain age class should be linearly proportional to efforts of metiér targeting that class. More precisely, since recruits (individuals aged 0) are captured by otter bottom trawls only (tab. 6.3), fishing mortality over class 0 and otter bottom trawl efforts should be linearly correlated. Instead, Pearson's correlation coefficient between these two dataset shows a value of 0.30.

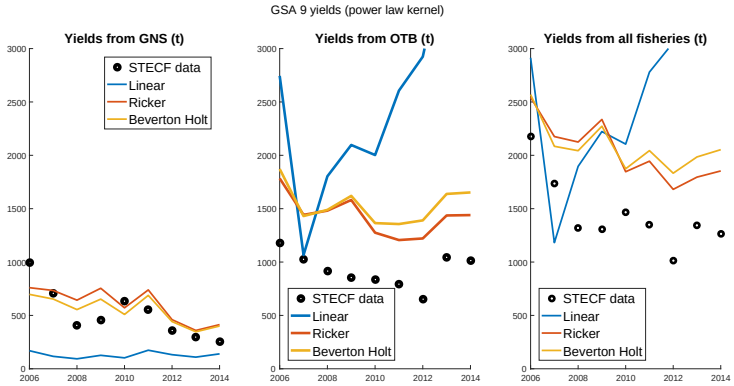

Figure 6.8: Yields data and reconstructions, power law kernel.

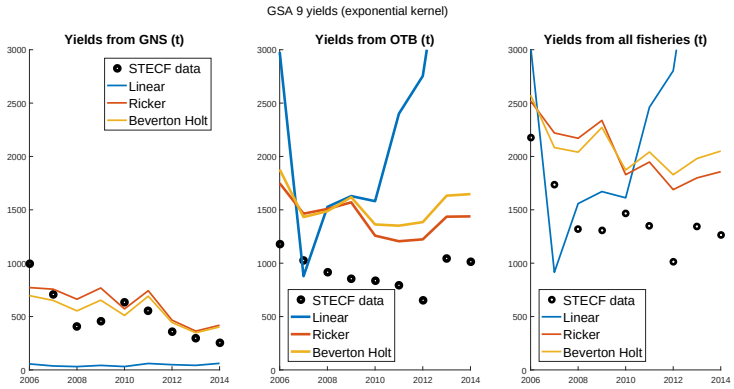

Figure 6.9: Yields data and reconstructions, exponential kernel.

The same procedure was followed for class 6+, fished by gillnets only: in this case, the Pearson's correlation coefficient showed an even lower value of 0.04 (fig. 6.12).

This mismatch between effort data and reconstructed fishing mortalities resulted in a poor calibration of the coefficients θ_μ and in a high RMSLE value.

6.2.4 *Final comments*

Values shown in table 6.5 allow to observe patterns in catchability parameters differentiated by métier. For instance, parameters θ_{GNS82} and θ_{OTB40} are both below 10^{-3}. Models with a linear S/R function have a lower value of θ_{GNS} and a higher value of θ_{OTB} compared with those with a non-linear S/R function: this is probably why the yields provided by the linear model are unbalanced (fig. 6.8 and following). All the other catchability parameters range from 2.9 to 7.8; gillnets catchabilities are regularly lower than those of otter bottom trawls.

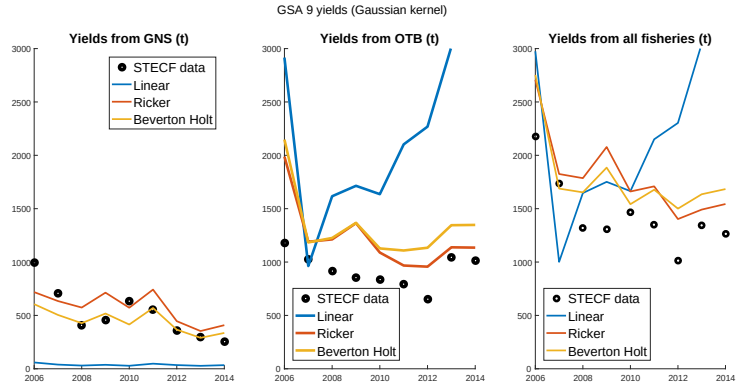

Figure 6.10: Yields data and reconstructions, Gaussian kernel.

Dispersal kernel	S/R model	$\theta_{GNS62.5}$	θ_{GNS82}	θ_{OTB33}	θ_{OTB40}
Power law	linear	8.84×10^{-1}	1.0×10^{-4}	1.30×10	1.0×10^{-4}
Power law	Ricker	3.39	9.9×10^{-4}	5.30	3.0×10^{-4}
Power law	Beverton-Holt	3.14	4.0×10^{-4}	5.89	1.0×10^{-4}
Exponential	linear	3.12×10^{-1}	2.0×10^{-4}	1.49×10	2.0×10^{-4}
Exponential	Ricker	3.42	4.0×10^{-4}	5.15	1.0×10^{-4}
Exponential	Beverton-Holt	3.15	4.0×10^{-4}	5.88	1.0×10^{-4}
Gaussian	linear	3.19×10^{-1}	5.0×10^{-4}	1.49×10	1.0×10^{-4}
Gaussian	Ricker	3.40	4.0×10^{-4}	6.65	1.0×10^{-4}
Gaussian	Beverton-Holt	2.92	2.0×10^{-4}	7.77	1.0×10^{-4}
Dispersal kernel	S/R model	θ_{D1}	θ_{D2}	RMSLE (cal)	RMSLE (val)
Power law	linear	0	1.85	1.252	0.780
Power law	Ricker	2.14	4.40×10^{-1}	0.980	0.381
Power law	Beverton-Holt	1.0×10^{-4}	7.37×10^{-1}	0.982	0.412
Exponential	linear	–	2.0×10	1.356	0.792
Exponential	Ricker	–	5.2×10^{-3}	0.981	0.387
Exponential	Beverton-Holt	–	7.20×10^{-3}	0.983	0.411
Gaussian	linear	–	9.53×10^{2}	1.299	0.589
Gaussian	Ricker	–	1.64×10^{2}	0.992	0.255
Gaussian	Beverton-Holt	–	3.24×10^{2}	0.997	0.251

Table 6.5: Results of model calibration and validation: catchability per métier, coefficients of adult dispersal and errors in calibration and validation.

The coefficients θ_{D1} and θ_{D2} of the dispersal kernels cannot be directly compared between different dispersal kernels, because the adult dispersal matrix D is normalized by rows - which means that parameters in table 6.5 do not define D directly. In order to have ad in idea of the effective retention and diffusion, the average of each coefficients has been calculated on the normalized dispersal matrix. Table 6.6 shows (1) the average percentage of adults retained in the same cell from year to year and (2) a measure of adult dispersal, given by the average percentage of adults moving toward one of the neighbour-

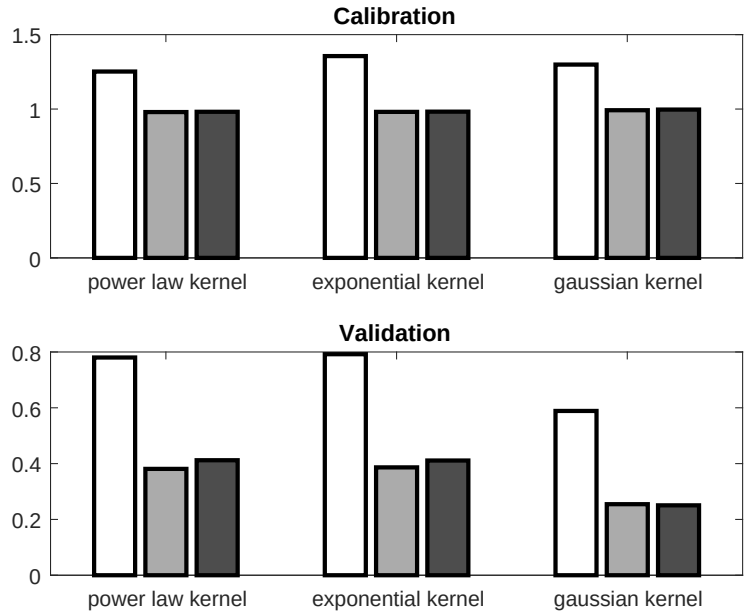

Figure 6.11: Calibration and validation performances of the nine parameterizations considered. White bars represent the linear S/R model RMSLE, light grey bars the Ricker S/R model RMSLE, dark grey bars the Beverton-Holt S/R model RMSLE.

ing cells (or retained in the source cell). The nearest 20-neighbours were chosen to assess dispersal.

As explained in the section 6.1.4, the power law kernel allows to uncouple retention and dispersal: higher retention does not imply a reduction in the dispersal radius - as it is, instead, for exponential and Gaussian kernels, in which a higher retention is regularly followed by a higher value of adults disperded within the 20-neighbours. As expected, Gaussian kernel shows the lowest dispersal radius, since quite all the adults move within the 20-neighbours.

Table 6.6 shows a relevant variability among parameterizations, the retention ranging from 0% to 87 %, and the resulting displacement in the neighbours from 28% to 100 %. Unfortunately, no available data can support a specific value of retention or dispersal.

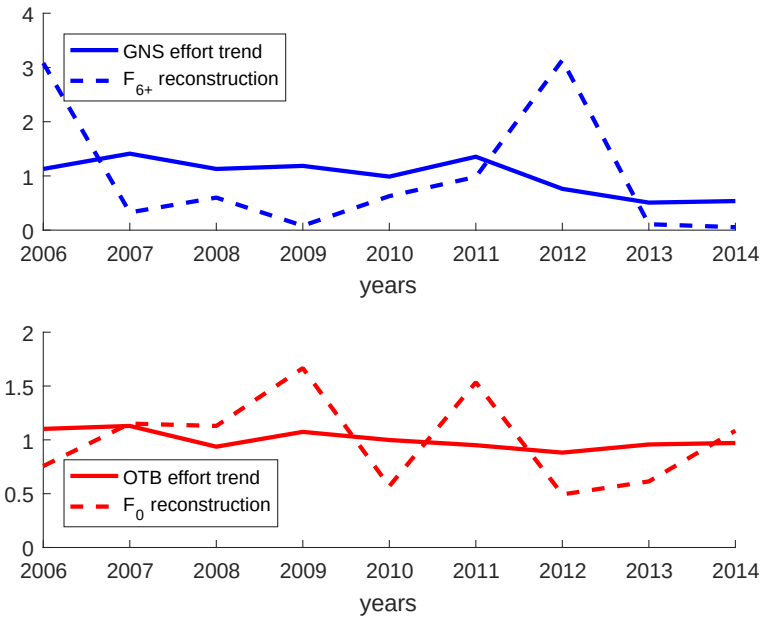

Figure 6.12: Trends of efforts and STECF fishing mortalities, normalized by dividing them by their mean value over time. Red lines refers to STECF mortality on class 0 and OTB efforts; blue lines refers to STECF mortality on class 6+ and GNS efforts (Cardinale, Damalas, and Chato Osio, 2015)

Dispersal kernel	S/R model	retained	disperded within the 20-neighbours
Power law	linear	0%	69.9%
Power law	Ricker	11.9 %	35.0%
Power law	Beverton-Holt	≈ 0%	35.0%
Exponential	linear	87.1%	100%
Exponential	Ricker	1.7 %	27.9%
Exponential	Beverton-Holt	2%	32.3%
Gaussian	linear	13 %	84.9%
Gaussian	Ricker	45.5 %	99.6%
Gaussian	Beverton-Holt	27.2%	96.7%

Table 6.6: Mean adult retention and dispersal in the 20-neighbours for each parameterization.

7

NETWORK ANALYSIS AND POLICIES

The last step of this work was to propose a strategy in order to approach a sustainable exploitment of *Merluccius merluccius* in GSA 9, using the metapopulation model defined in the previous Chapter.

7.1 METHODS

7.1.1 *Policy definition*

The method here proposed consists in simulating, in turn in each cell of the grid described in Chapter 6, the establishment of a marine protected area (i.e. the complete closure of the fishery in that cell), and in evaluating the consequent variation of suitable indicators with respect to a status quo scenario. These indicators should be able to take into account for both the conservation benefits and the impacts on fishing yields of closing the fishery in a single cell.

SSB was chosen as an indicator of conservation benefits. SSB has the advantage of considering an aggregate measure of older classes, without being affected by interannual fluctuation (such as the abundance of recruits does, and consequently the amount of discards) and suitably weighting a key demographic trait - fertility, i.e. the capacitiy of creating new biomass - of all age classes. Fishing yield (in weight), instead, was selected as an indicator accounting for fishers' interests.

Both indicators were computed as the average outputs in the last 10 year of a 50-year long simulation. In each simulation, the parameters related to the fishing pressure of a specific cell have been set to zero, and those of all the other cells have been proportionally increased in such a way as to keep the total fishing effort unchanged:

$$\tilde{eff}^{S}_{\upsilon,\mu} = \frac{\sum_{\upsilon} eff^{S}_{\upsilon,\mu} A_{\upsilon}}{\sum_{\upsilon \in i \neq i*} eff^{S}_{\upsilon,\mu} A_{\upsilon}} eff^{S}_{\upsilon,\mu} \tag{7.1}$$

Where $i*$ is the cell in which fishery is not allowed, $\tilde{eff}^{S}_{\upsilon,\mu}$ is the recomputed fishing effort in subcell υ belonging to cell i (being $i \neq i*$) of métier μ, $eff^{S}_{\upsilon,\mu}$ is the fishing effort in subcell υ of métier μ in the status quo scenario, A_{υ} is the surface of the subcell υ.

7.1.2 *Synthetic time series generation*

In order to provide future time series of model inputs, such as the recruits in GSA 10 or the efforts by otter bottom trawls and gillnets,

resampling techniques have been used, able to reproduce the autocorrelation in generated time series without assuming a parametric generating process. In this simulation, Nearest Neighbor bootstrap (NNB) was used (Lall and Sharma, 1996).

According to this algorythm, overlapping blocks are constructed from each historical time series, in order to generate a new value equal to the one which succeeds the historical block that is "nearest" to the most recent block. NNB requires two parameters to be defined:

1. The length of the blocks, d;
2. The number of nearest blocks to be considered at each iteration, k.

It is customary to use $k = \sqrt{T}$, where T is the length of the historical time series, and $d \leqslant 6$.

Since the dimension of the sample is very short (9 years), both d and k were set to 3. Figure 7.1 shows the results of resampling recruits abundances and efforts by gillnets and otter bottom trawls time series.

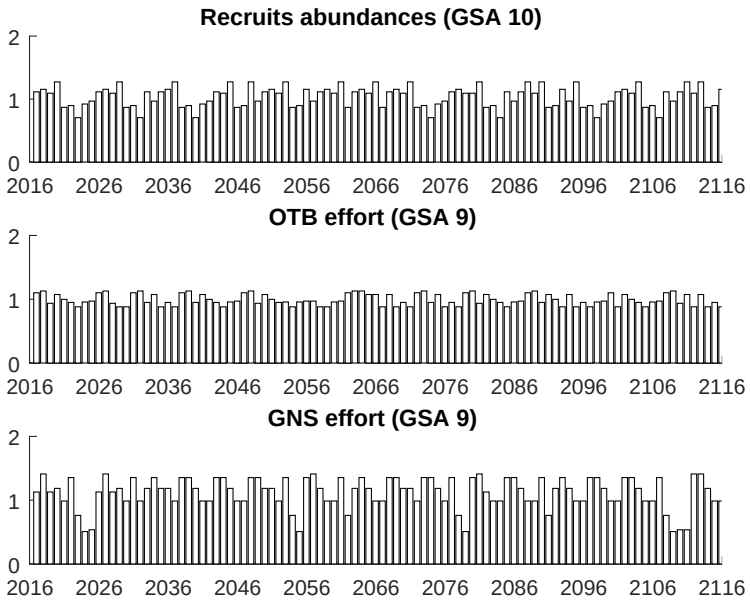

Figure 7.1: Synthetic time series generated for future inputs, normalized with respect to the mean value.

7.1.3 *Network analysis*

In order to explain the results given by temporary closures in different locations, cells have been characterized in term of network centrality indicators (Barabási, 2016).

In the metapopulation model developed in Chapter 6, cells can distribute (and consequently receive) hakes through (a) larval and (b) adult dispersal. This means that cells can be thought as network nodes, and exchanged juvenile or adult hakes as links.

Since the adult dispersal matrix D is the output of a calibration process which provided very different results with different parameterizations (see tab. 6.5), only the (physically based) larval dispersal matrix M_a, which describes fluxes of larvae from and toward GSA 10, was considered in order to evaluate cells properties.

The network described by matrix M_a, defined in Chapter 5, is directed, weighted and provided with many and consistent self loops, representing the retained eggs (fig. 5.8). Links direction is given by currents, carrying particles/larvae from cell i to j; weights are given by the amount of particles/larvae released in cell i and reaching another cell j.

Weights $i \rightarrow j$ are proportional to the mean persistence of the spawning ground of the cell i, to the relative extension of the nurseries of cell j, to the transfer efficiency of cell i (fig. 5.16) and to the proportion of particles flowing from i to j ($M_p(i,j)$).

Matrix M_a does not describe a fully connected network, due to the current circulation which drives particles mainly northward (fig. 5.9); nevertheless, there is a giant strictly connected component (Newman, 2010) of 142 nodes (over a total of 194).

For each cell i, 6 centrality indicators were selected:

1. Indegree, i.e. the amount of cells pointing toward cell i;
2. Outdegree, i.e. the amount of cells pointed by cell i;
3. Instrenght, i.e. the total amount of particles entering cell i;
4. Outstrenght, i.e. the total amount of particles released by cell i and reaching other cells;
5. Betweenness centrality, i.e. the amount of shortest paths between all the pairs of cells (nodes) j and k and passing through i ($j, k \neq i$);
6. Information centrality, i.e. the relative loss of efficiency due to the removal of cell i from the network.

The first four indicators are self explanatory; conversely, betweenness and information centrality need a deeper definition.

Both indicators are based on distances between nodes i j, i.e. the shotest path connecting nodes i, j. While in unweighted networks distances can be immediately computed as the minimum number of links able to connect i to j, in weighted networks several generalized definitions are available, depending on the meaning of the weight on each link $i \rightarrow j$. Since, in this case, a link represents the larval flux

connecting a spawning cell to a nursery cell, a weight is a measure of closeness, affinity. This means that the distance between nodes i and j should be linked to a decreasing function of the weight, so that the shortest path will include the heaviest links. In this case, shortest paths were calculated using the matrix $\tilde{M}_a$ of the reciprocals (eq. 7.2):

$$\tilde{M}_a : \tilde{M}_a(i,j) = \begin{cases} M_a(i,j)^{-1}, & \text{if } M_a(i,j) > 0 \\ 0, & \text{if } M_a(i,j) = 0 \end{cases} \tag{7.2}$$

While the betweenness of a node is just the count of the shortest paths connecting all the pairs of nodes and passing through i, information centrality requires the definition of another network property, the efficency, which is the mean of all the reciprocal of the distances (computed using network $\tilde{M}_a$) between all pairs of nodes[1].

Information centrality is defined as (eq. 7.3):

$$I_i = \frac{E_{\tilde{M}_a} - E_{\tilde{M}_{a,i}}}{E_{\tilde{M}_a}} \tag{7.3}$$

Where $E_{\tilde{M}_{a,i}}$ is the efficientcy calculated in the network $\tilde{M}_a$ after the removal of the i^{th} node. Information centrality is a measure of the relative loss in the efficiency of the global network when the node is removed.

7.1.4 *Other indicators*

Alongside the indicators of network centrality, three indicators accounting for fishing pressures were considered. These indicators average fishing footprint in each cell for segments OTB 12-24, SSC 0-12, SSC 12-24, introduced in Chapter 3 and already used in Chapter 6 (fig. 3.4 and following).

Relative increments of overall SSB and yields due to local fishery restrictions in a certain cell were correlated with both network centrality indicators and fishing pressure indicators. This association was investigated by means of Spearman's rank correlation coefficient, which allows to identify a monotonic relation between two datasets: in this case, static indicators (network centrality and fishing pressure) and dynamic ones (the increments of SSB and yields).

A statistical test was finally performed to assess whether this correlations are significant or not, since, under the null hypothesis, the

1 With respect to the simple mean of all the distances between all the pairs of nodes, efficiency has the advantage of handling unconnected pairs, whose mutual distance is infinite.

Spearman's rank correlation follows approximately a Student's t distribution. A two tailed t-test with $n-2$ degrees of freedom was used:

$$t = \frac{\rho_s}{\sqrt{(1-\rho_s^2)/(n-2)}} \tag{7.4}$$

Where ρ_s represents the Spearman's rank correlation coefficient, and n the sample length (124).

7.2 RESULTS

7.2.1 *Overall performances*

Relative increments in the overall SSB and yield indices due to local fishing restrictions according to models parametrized with Gaussian kernel and either Ricker or Beverton-Holt S/R functions are summarized in fig. 7.2.

According to both parameterizations, restricting fishing activity in cell 450 would provide the highest SSB increases, while closure in cell 354 would provide the highest yield increases. Bar charts in fig. 7.3 and 7.5 show the entity of SSB and yield overall variations, closing the cell indicated on the abscissa. It is evident that results obtained with both parameterizations suggest that closures in southern or nothern Tuscany can provide relevant increases in both indicators, while closures in central and northern Lazio bring to a general decrease of spawners and yields.

This is even more evident if one looks at the geographic distribution of the cells ranked among the top ten according to at least one indicator. Figure 7.4 shows the results obtained with Beverton-Holt model: two clusters of cells are highlighted above and below Elba island, and another small cluster is located off La Spezia Gulf. On the other hand, fig. 7.6, which shows the best performing cells using the Ricker parameterization, identifies also five isolated cells off Lazio coasts, whose closure can improve the overall yields.

7.2.2 *Spatial effects of local closures in the GSA 9*

The establishment of fishing restricted areas in cells 450 and 354 could bring to the highest increase in the overall SSB and yield with respect to a status quo scenario. However, nothing guarantees that this benefit is equally distributed over all the cells of the GSA 9.

For instance, figures 7.7 and 7.9 show that only cells located in southern Tuscany and northern Lazio would benefit from restricting fisheries in cell 354, according to both Beverton-Holt and Ricker models: the reallocation of fishing effort (explained in eq. 7.1) would produce a decrease of both spawning biomass and yields in Liguria and

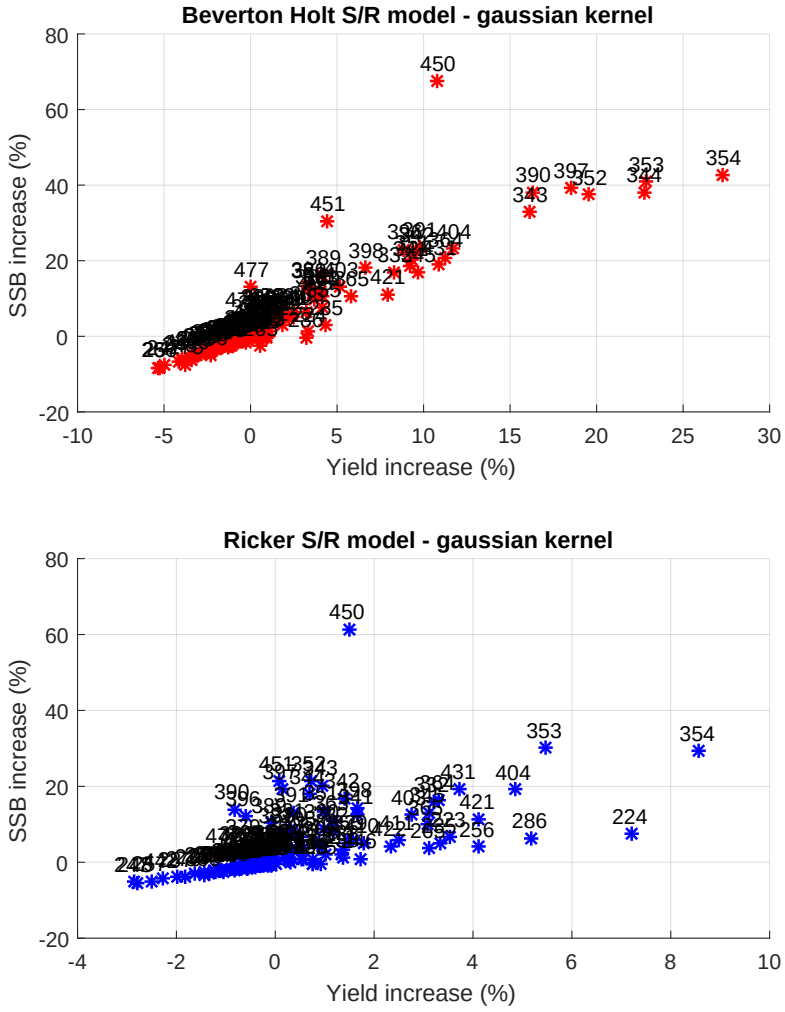

Figure 7.2: Performance of local fisheries restrictions. Each point represents the increment in the overall yields and SSB by means of completely closing fisheries in the labeled cell. Above the results with the Beverton-Holt model, below the results with the Ricker model.

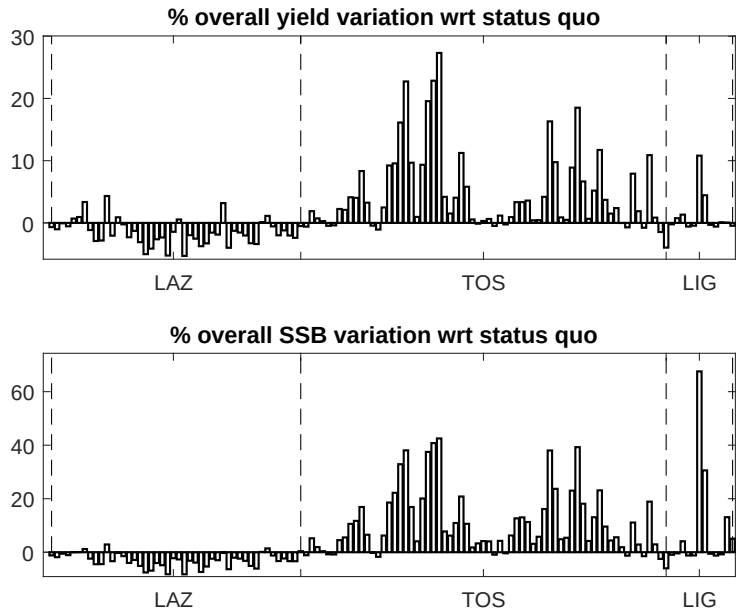

Figure 7.3: Performances of local restrictions with the Beverton-Holt S/R model; above the overall yield increases due to the closure of cell on the abscissa, below the overall SSB increases due to a closure in the same cell.

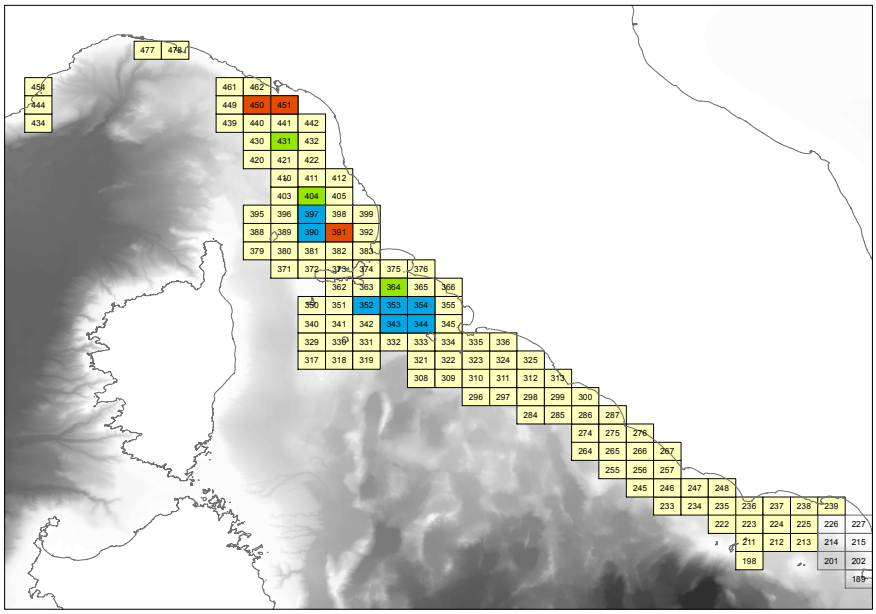

Figure 7.4: Cells whose closure brings high benefits in the overall yields and/or SSB, according to the Beverton-Holt parameterization: red cells are ranked in the top 10 as SSB increase, green cells are ranked in the top 10 as yield increase, blue cells are ranked in the top 10 according to both indicators.

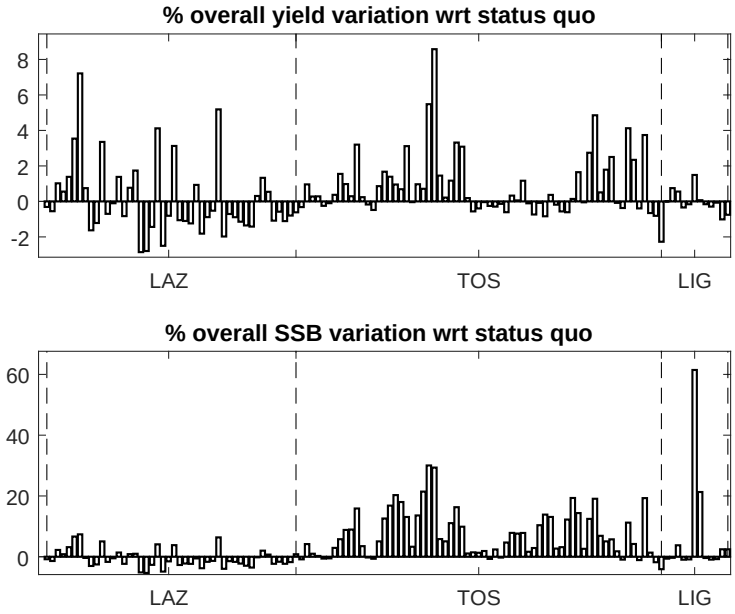

Figure 7.5: Performances of local restrictions with the Ricker S/R model; above the overall yield increases due to the closure of cell on the abscissa, below the overall SSB increases due to the same cell.

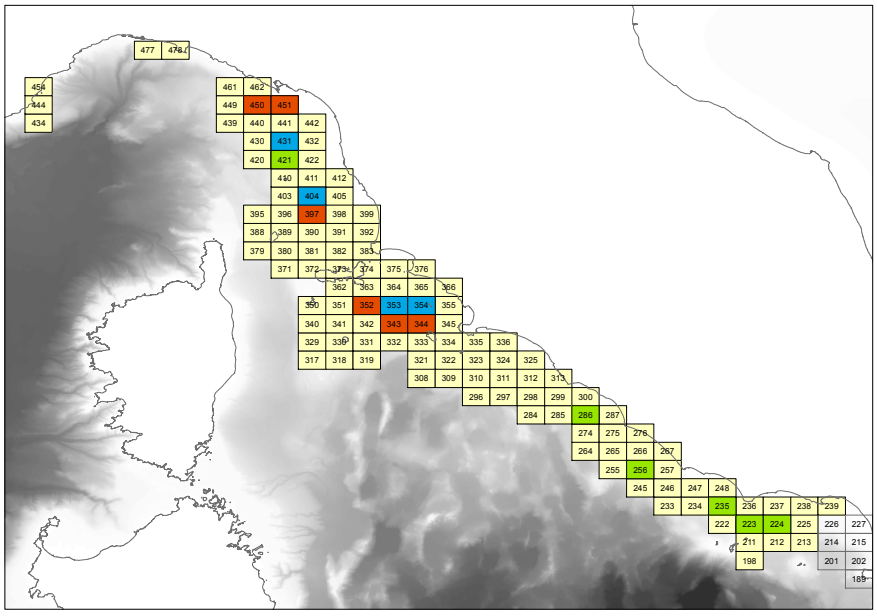

Figure 7.6: Cells whose closure brings high benefits in the overall yields and/or SSB, according to the Ricker parameterization: red cells are ranked in the top 10 as SSB increase, green cells are ranked in the top 10 as yield increase, blue cells are ranked in the top 10 according to both indicators.

southern Lazio. Moreover, as it is shown in the bar charts above, the entity of benefits varies according to the location: cells close to 354 can double or triple their indices of performance with respect to the status quo scenario, on the opposite negative variations in other regions are in the order of a few percentage points.

Consequences of restricting fisheries in cell 410 are less clear to predict, since results vary according to the adopted model. Beverton-Holt parameterization (fig. 7.9) forecasts an increase of an order of magnitude of SSB in the interested cell and in its neighbours, and a slight increase of performances of both indices would be observed barely in all the GSA 9. On the opposite, Ricker parameterization (fig. 7.10) shows a very similar shape of the bar charts, with the difference that, in great part of the domain, both SSB and yield indices perform slightly worse than the status quo scenario. Only few cells in La Spezia Gulf benefits from both SSB and yield increases.

7.2.3 *Robustness analysis*

In order to assess how uncertain the obtained outputs are, local closures of cells have been simulated also with other dispersal kernels, and rankings according to SSB and yields increases have been recorded. The rational behind this analysis is to investigate whether different parameterizations - which underlie different assumptions regarding one of the most uncertain settings of the model, such as adult retention and dispersal (tab. 6.6) - would confirm or disprove the results so far obtained.

Table 7.1 shows the performances of the ten cells providing the highest SSB increments selected by the Ricker model (in the first column) according to all the other parameterizations obtained in Chapter 6 - with the exception of the linear S/R function. Neighbouring cells 450 and 451 display a sudden fall in the ranking; on the opposite neighbouring cells 352, 353 and 354 show much more robust performances, as well as neighbouring cells 397 and 404, all located off Tuscany. Table 7.2, showing the ranking of the ten cell providing the highest SSB increments selected by the Beverton-Holt model, confirms as robust the same cells identified with the Ricker model.

Cells 354, 353 and 404 are confirmed to provide the best and most robust yield increases (tab. 7.4 and 7.3). Also cell 431 produces stable performances with every parameterization.

7.2.4 *Correlation between static and dynamic indicators*

Once assessed the performances of local closures according to different parameterizations, these have been compared with static indicators, i.e. network centrality and fishing pressures indicators.

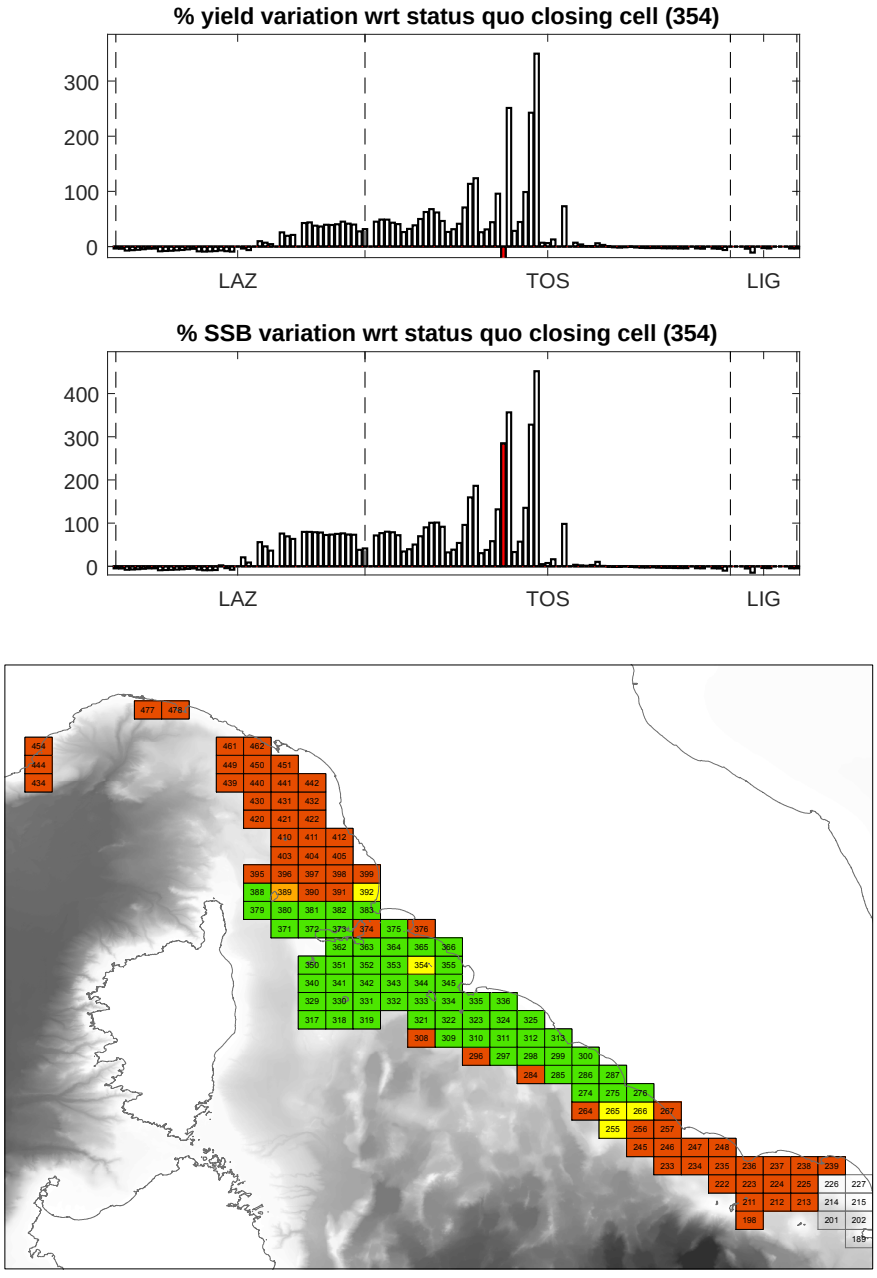

Figure 7.7: Effects of a fishery closure in cell 354, simulated with the Beverton-Holt S/R model. Above, bar corresponding to cell 354 is coloured in red. Below, it is shown the geographical distribution: red cells are penalized according to both indicators; orange cells benefit from an yield increase only; yellow cells benefit from a SSB increase only; finally, green cells benefit from an increase of both indicators.

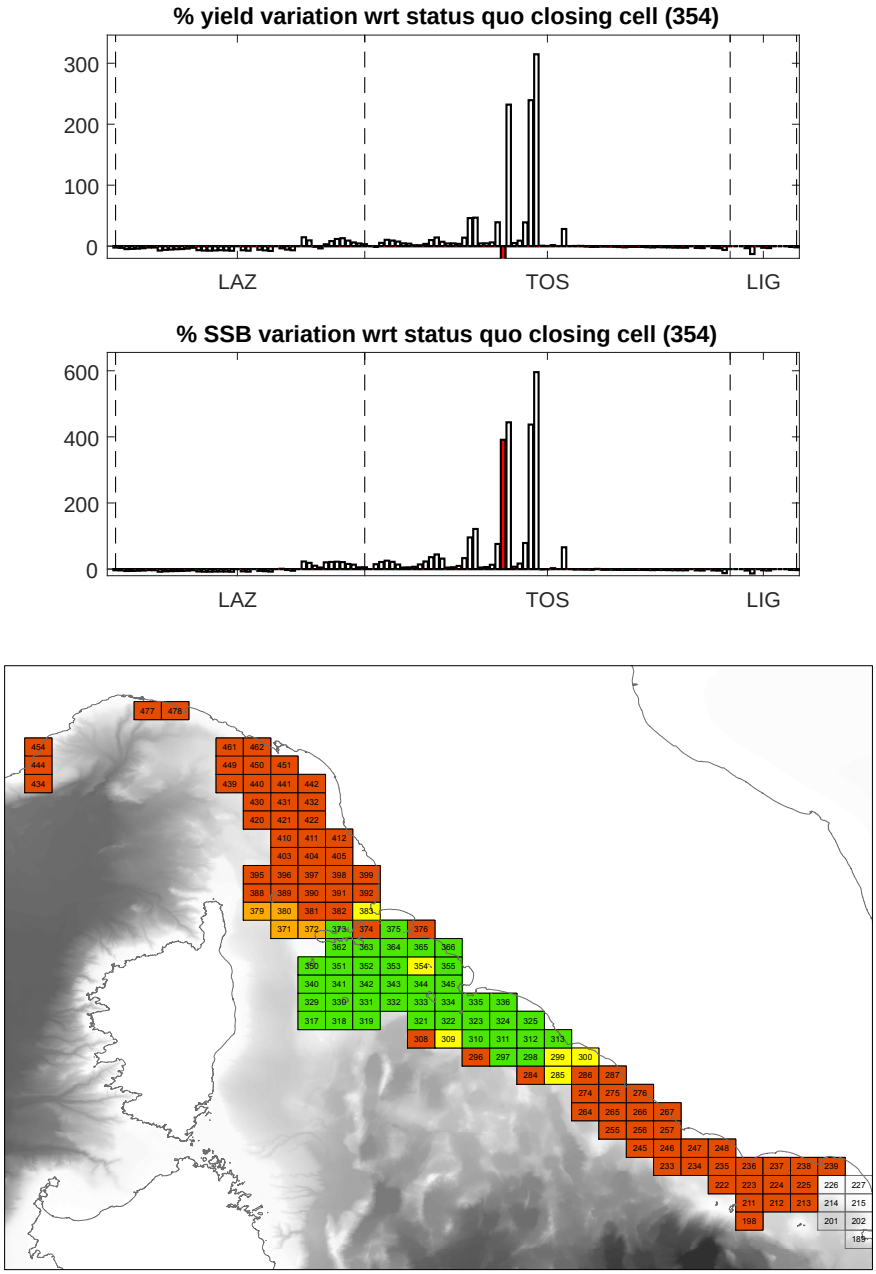

Figure 7.8: Effects of a fishery closure in cell 354, simulated with the Ricker S/R model. Above, bar corresponding to cell 354 is coloured in red. Below, it is shown the geographical distribution: red cells are penalized according to both indicators; orange cells benefit from an yield increase only; yellow cells benefit from a SSB increase only; finally, green cells benefits from both indicators.

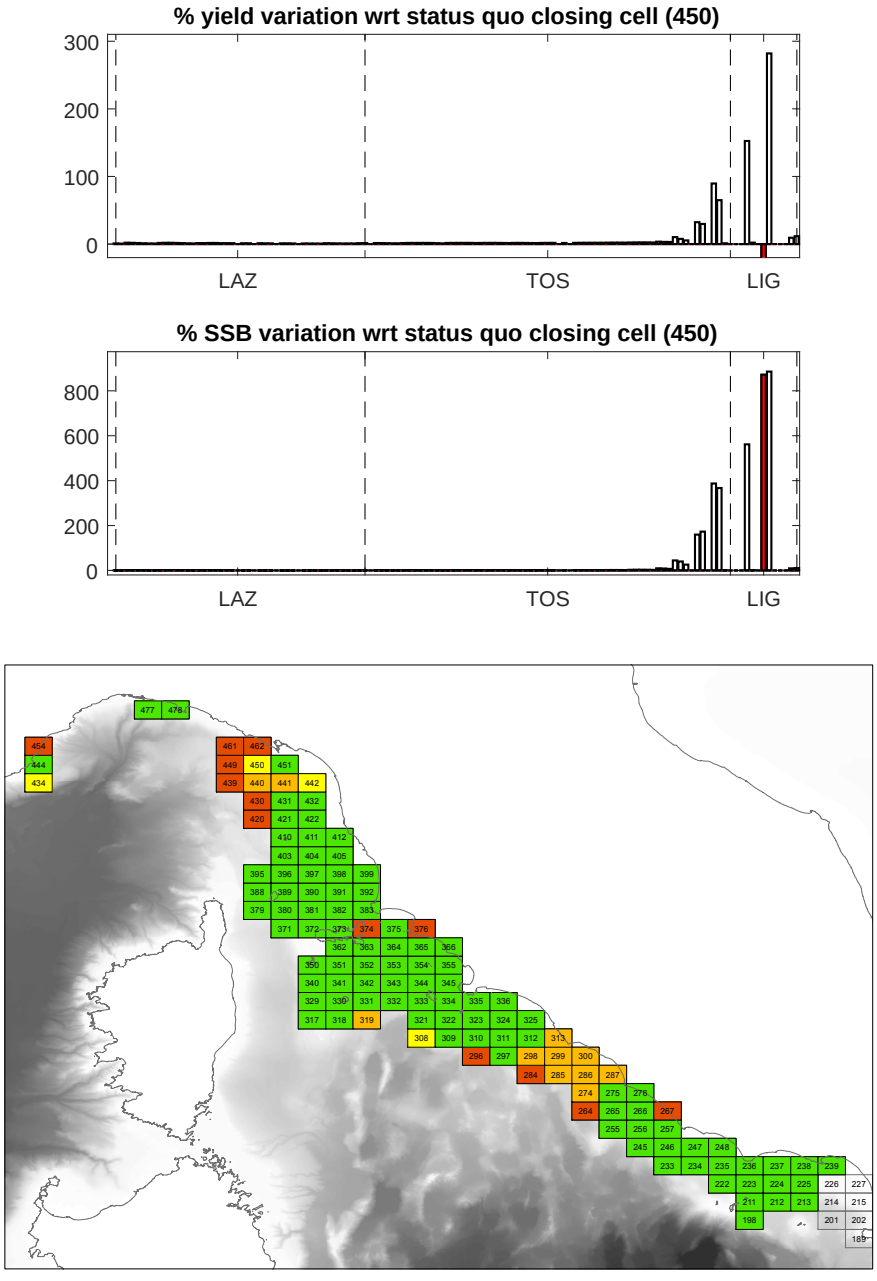

Figure 7.9: Effects of a fishery closure in cell 450, simulated with the Beverton-Holt S/R model. Above, bar corresponding to cell 450 is coloured in red. Below, it is shown the geographical distribution: red cells are penalized according to both indicators; orange cells benefit from an yield increase only; yellow cells benefit from a SSB increase only; finally, green cells benefit from an increase of both indicators.

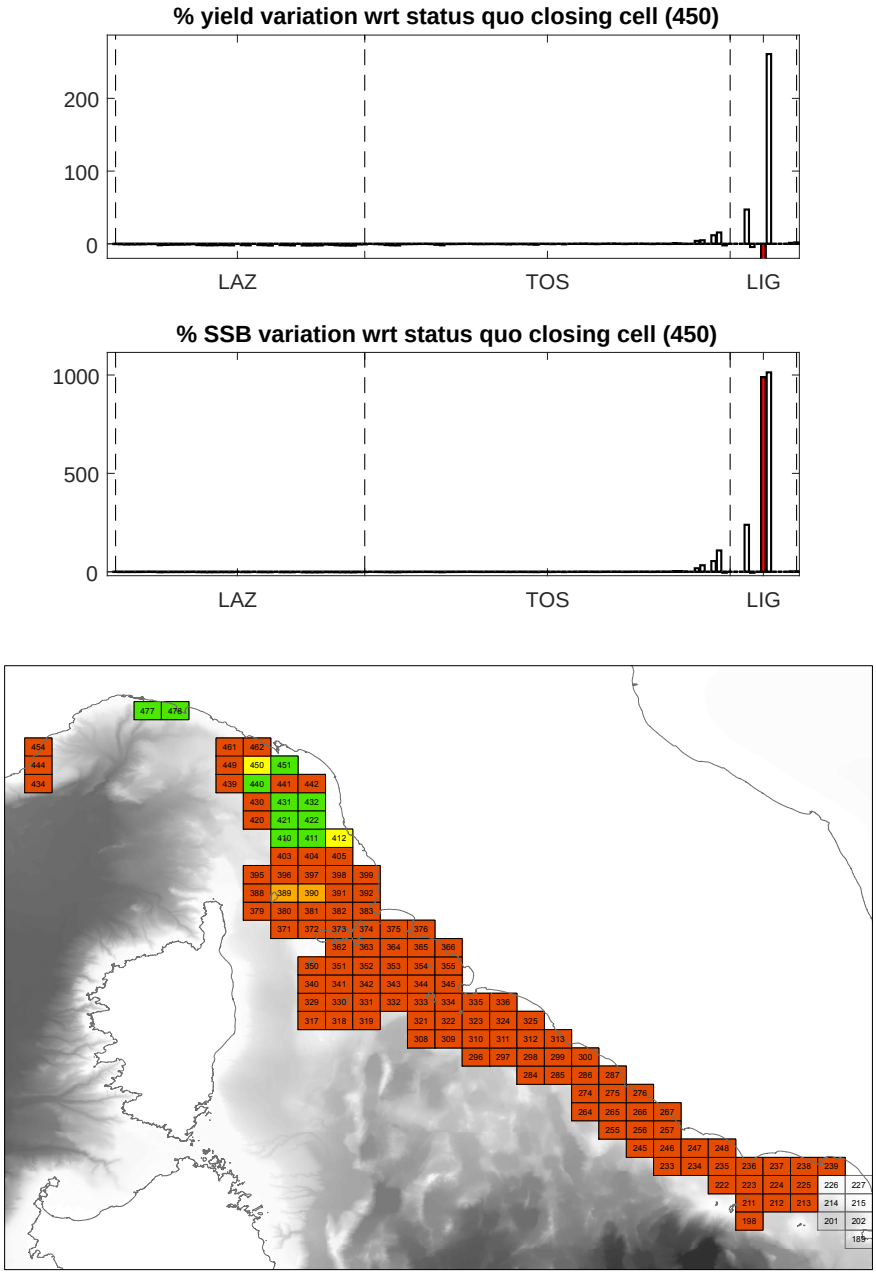

Figure 7.10: Effects of a fishery closure in cell 450, simulated with the Ricker S/R model. Above, bar corresponding to cell 450 is coloured in red. Below, it is shown the geographical distribution: red cells are penalized according to both indicators; orange cells benefit from an yield increase only; yellow cells benefit from a SSB increase only; finally, green cells benefits from both indicators.

dispersal kernel	Gaussian	exponential	exponential	power law	power law
s/r function	Beverton-Holt	Ricker	Beverton-Holt	Ricker	Beverton-Holt
cell id	ranking				
450	1	24	15	17	20
353	3	2	4	2	3
354	2	1	1	1	1
352	7	3	6	3	6
451	9	63	57	64	60
343	8	15	12	13	10
397	4	4	2	4	2
431	16	7	9	8	11
404	11	5	7	5	7
344	5	11	3	14	4

Table 7.1: Performances of the cells giving the highest SSB increases - according to the model with Ricker S/R model and Gaussian kernel parameterization - simulated with other parameterizations. Each element of the table shows the ranking of the cell specified in the first column given as a result of the simulation performed with the parameterization specified in the first and the second row.

dispersal kernel	Gaussian	exponential	exponential	power law	power law
s/r function	Ricker	Ricker	Beverton-Holt	Ricker	Beverton-Holt
cell id	ranking				
450	1	24	15	17	20
354	3	1	1	1	1
353	2	2	4	2	3
397	7	4	2	4	2
344	10	11	3	14	4
390	15	38	5	43	5
352	4	3	6	3	6
343	6	15	12	13	10
451	5	63	57	64	60
391	17	6	8	6	8

Table 7.2: Performances of the cells giving the highest SSB increases - according to the model with Beverton-Holt S/R model and Gaussian kernel parameterization - simulated with other parameterizations. Each element of the table shows the ranking of the cell specified in the first column given as a result of the simulation performed with the parameterization specified in the first and the second row.

dispersal kernel	Gaussian	exponential	exponential	power law	power law
s/r function	Ricker	Ricker	Beverton-Holt	Ricker	Beverton-Holt
cell id	ranking				
354	1	1	1	1	1
353	3	2	4	2	3
344	43	12	2	21	2
352	42	3	6	3	6
397	58	4	3	5	4
390	104	43	5	82	5
343	36	15	10	18	9
404	5	5	7	4	7
364	11	11	11	10	10
431	8	8	8	9	11

Table 7.3: Performances of the cells giving the highest yield increases - according to the model with Beverton-Holt S/R model and Gaussian kernel parameterization - simulated with other parameterizations. Each element of the table shows the ranking of the cell specified in the first column given as a result of the simulation performed with the parameterization specified in the first and the second row.

dispersal kernel	Gaussian	exponential	exponential	power law	power law
s/r function	Beverton-Holt	Ricker	Beverton-Holt	Ricker	Beverton-Holt
cell id	ranking				
354	1	1	1	1	1
224	32	19	45	12	32
353	2	2	4	2	3
286	36	9	19	8	22
404	8	5	7	4	7
421	19	14	12	17	13
256	108	27	79	20	79
431	10	8	8	9	11
223	49	63	80	37	70
235	24	18	33	16	27

Table 7.4: Performances of the cells giving the highest yield increases - according to the model with Ricker S/R model and Gaussian kernel parameterization - simulated with other parameterizations. Each element of the table shows the ranking of the cell specified in the first column given as a result of the simulation performed with the parameterization specified in the first and the second row.

Figure 7.11 shows the linear correlations between rankings in SSB increases due to fishing restrictions in a cell - simulated with Ricker model - and that cell static indicators. Table 7.5 lists all the Spearman's ranking coefficients, while tab. 7.6 shows the two tailed p-values of the cumulated Student's t distribution. Correlation is positive for all network indicators, with highest values for instrenght (0.57), betweenness (0.54) and information centrality (0.53), implying that higher indices are related to good performances associated with the establishment of a fishing restricted area.

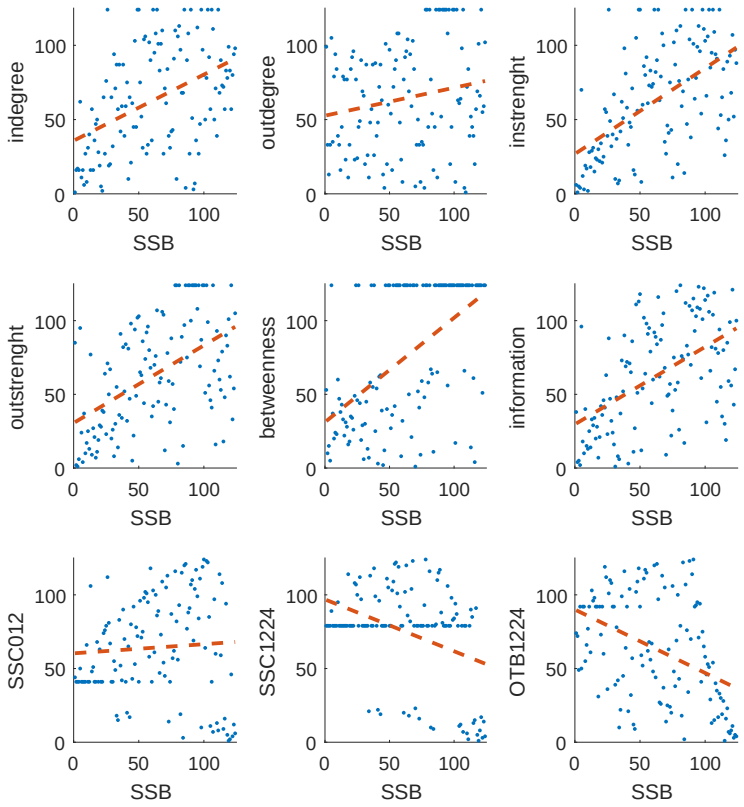

Figure 7.11: Linear correlation between rankings of the overall SSB increase due to closure of a cell (on the abscissa) and its ranking according to static indicators (in ordinate), with the Ricker parameterization.

For what concerns a possible link between static indicators and yields, figure 7.12 confirms that instrenght, betweenness and information centralities are the most correlated.

The same analysis, repeated with Beverton-Holt model's outputs, is reported in fig. 7.13 and in the last two columns of tables 7.5 and 7.6. In the case of SSB increments, the correlation is generally weaker: instrenght and betweenness emerge again, but information centrality is replaced by indegree. Instead, yields increments confirm to be

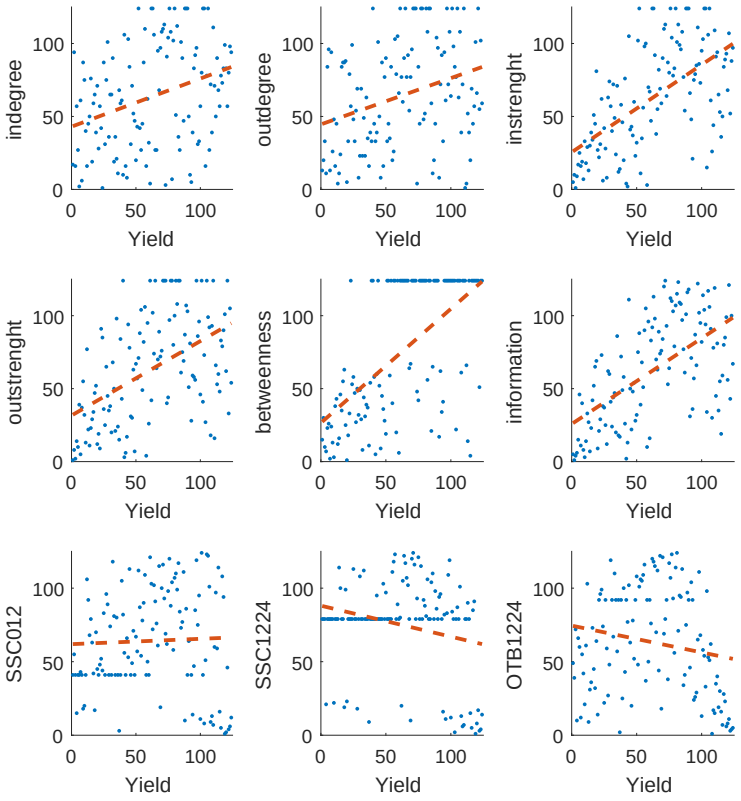

Figure 7.12: Linear correlation between rankings of the overall yields increase due to closure of a cell (on the abscissa) and its ranking according to static indicators (in ordinate), with the Ricker parameterization.

correlated mainly with instrenght, betweenness and information centralities. Among the pool of network indicators, outdegree shows the lowest significance.

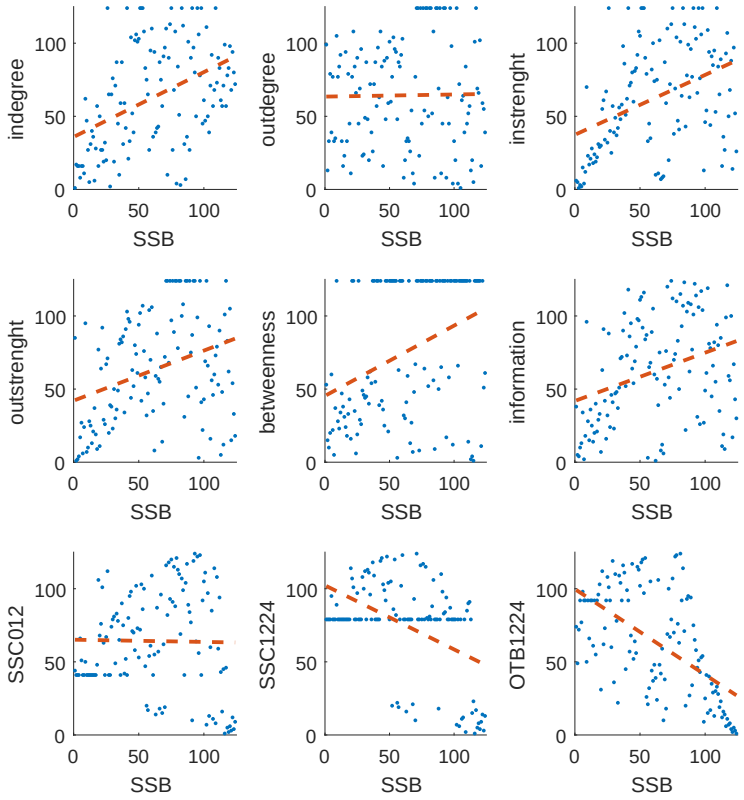

Figure 7.13: Linear correlation between rankings of the overall SSB increase due to closure of a cell (on the abscissa) and its ranking according to static indicators (in ordinate), with the Beverton-Holt parameterization.

Negative correlation coefficients were obtained between dynamic indices and fishing pressures indices OTB 12-24 and SSC 12-24, for both Ricker and Beverton-Holt parameterizations; in this latter case, absolute values were particularly high for OTB 12-24 segment and SSB. This suggests that prohibiting fishing in areas particularly frequented by fisheries - and consequently reallocating the effort across the entire domain - would result in an overall SSB and yield decrease. The correlation coefficient between dynamic indices and fishing pressure indicator SSC 0-12 is never significant, p-values ranging from 0.48 to 0.86.

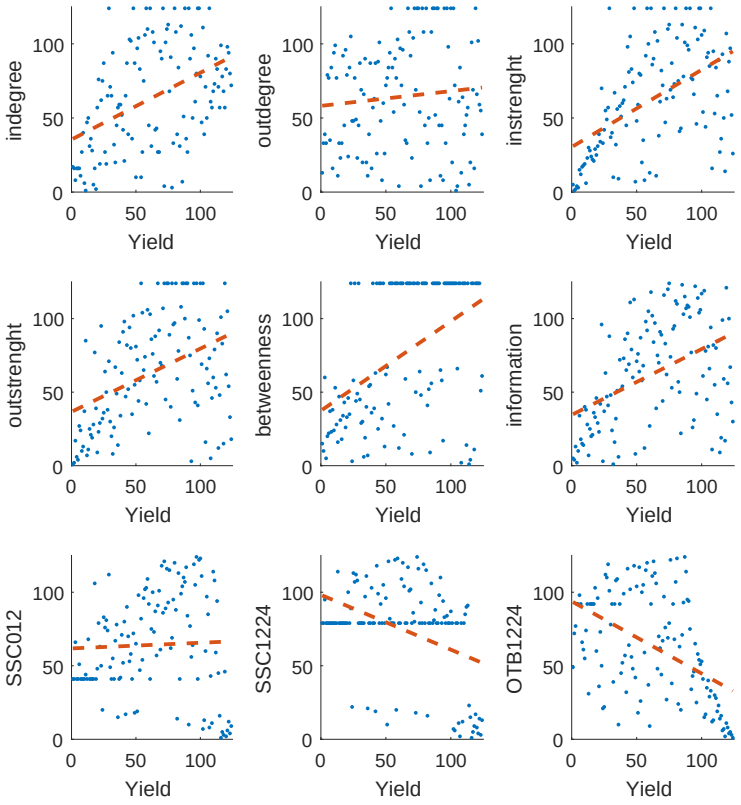

Figure 7.14: Linear correlation between rankings of the overall yields increase due to closure of a cell (on the abscissa) and its ranking according to static indicators (in ordinate), with the Beverton-Holt parameterization.

s/r function	Ricker	Ricker	Beverton-Holt	Beverton-Holt
dynamic indicator	SSB	yields	SSB	yields
static indicator	ρ_s			
Indegree	0.44	0.32	0.44	0.44
Outdegree	0.18	0.31	0.01	0.10
Instrenght	0.57	0.59	0.40	0.51
Outstrenght	0.51	0.49	0.33	0.41
Betweenness	0.54	0.59	0.37	0.46
Information	0.53	0.59	0.33	0.45
SSC 0-12	0.06	0.04	-0.02	0.04
SSC 12-24	-0.38	-0.23	-0.47	-0.41
OTB 12-24	-0.43	-0.18	-0.58	-0.48

Table 7.5: Spearman's correlation coefficients between static indicators and dynamic indicators according to different parameterizations.

s/r function	Ricker	Ricker	Beverton-Holt	Beverton-Holt
dynamic indicator	SSB	yields	SSB	yields
static indicator	p-values			
Indegree	10^{-7}	10^{-4}	10^{-7}	10^{-7}
Outdegree	0.04	10^{-3}	0.87	0.29
Instrenght	10^{-11}	10^{-12}	10^{-6}	10^{-9}
Outstrenght	10^{-9}	10^{-8}	10^{-4}	10^{-6}
Betweenness	10^{-10}	10^{-13}	10^{-5}	10^{-8}
Information	10^{-10}	10^{-12}	10^{-4}	10^{-7}
SSC 0-12	0.48	0.68	0.86	0.66
SSC 12-24	10^{-5}	0.01	10^{-8}	10^{6}
OTB 12-24	10^{-6}	0.05	10^{-12}	10^{-7}

Table 7.6: P-values of Spearman's correlation coefficients between static indicators and dynamic indicators according to different parameterizations.

8

CONCLUSION

In the present work, a modelling approach has been developed to (1) investigate the spatiotemporal dynamics of the European hake in the Mediterranean Sea and (2) support the identification of candidate locations to be protected in order to pursue the long term conservation of this species and the profitability of the fishery.

As a first step, Lagrangian simulations at a wide geographic scale (NW Mediterranean Sea) were conducted in order to assess the extent to which different reproduction areas across the basin are connected by the dispersal of eggs and larvae through ocean currents. The fraction of propagules exchanged between different GSAs was estimated to be below 1% of the releases, and hence almost negligible compared to the fraction retained in the same GSA, the only exception being GSAs 9 and 10 that are connected by a more intense flux of propagules (2.7% of the particles released in GSA 10 reach nurseries in GSA 9). The quality of the results presented in Chapter 4 is strongly dependent on the reliability of the assumptions made to describe the temporal distribution of larval releases over the year, and on the lack of information regarding the actual location of many reproduction sites, especially spawning areas along African shores. Despite a high degree of uncertainty caused by numerous knowledge gaps, the modelling setting on which the simulations were based relies on a thorough review of the information available in the primary and grey literature on the subject.

As second step, a detailed connectivity assessment was carried out on GSAs 9 and 10. Chapter 5 illustrated the method developed for the reconstruction of spawning grounds from the available information regarding the distribution of nurseries in this area. The most likely locations of spawning grounds across the region (which encompasses the Ligurian Sea and the Tyrrhenian Sea) were identified using backward Lagrangian simulations and suitability maps. Although this reconstruction is inevitably affected by a high degree of uncertainty (since it is not based directly on survey data, which are considered to be insufficently reliable to describe accurately the distribution of spawners), the results obtained have been judged to be sufficently realistic by the fisheries scientists that have been consulted. Reconstucted spawning grounds were set as a basis to assess connectivity at the regional scale. An indepth analysis of ocean circulation patterns was performed to investigate the possible oceanographic features affecting the most peculiar results obtained, such as the main flux of particles from central Tyrrhenian Sea toward Ligurian Sea.

The third step of the research was the development of a metapopulation model (Chapter 6) for the hake stock of the GSA 9, with the aim to describe the spatiotemporal dynamics of the stock under the combined effect of dispersal (of both juvenile an adult life stages) and the fishing pressure exerted by different fleet segments. The model is age-structured, based on the current knowledge about the life cycle of the species, and describes fish dispersal across a grid with cells of 0.125° (latitude) × 0.1875° (longitude). The model was calibrated against data collected by STECF (Cardinale, Damalas, and Chato Osio, 2015) between 2006 and 2014, and validated against a time series of catch data. Different stock-recruitment functions and adult dispersal kernels were tested; the model showing the best performances described a Gaussian dispersal kernel and included a non-linear stock recruitment function (either a Ricker or a Beverton-Holt relationship). A critical analysis of the results highlighted some important inconsistencies between available data regarding, on the one hand, the abundance and the structure of the population and, on the other hand, reconstructed time series of fishing effort data. Also, the lack of information about the behaviour of adult hakes, as well as the brevity of the time series, further affect the quality of the metapopulation model. Possibly for these reasons, the model selection procedure did not identify a single best parameterization structure. Nevertheless, the result of this phase of the thesis represents the first attempt to describe the spatiotemporal dynamics of this species at this geographic scale.

The metapopulation model was used (Chapter 7) to assess the log-term effect of stock protection (implemented via local closures) on both the viability of the stock and the productivity of the fishery. Results are very encouraging, as the closure of fisheries in specific sites (such as some cells in the proximity of Elba island) has the potential to increase both the overall spawning stock biomass and the fishing yields compared to a status quo scenario. Interestingly, local closures showed an uneven geographical distribution of benefits. A network theoretical approach was then used to investigate more in depth the contribution of each cell to connectivity across the whole GSA. To this end, network centrality indicators were used to characterize the properties of each cell from a network perspective: instrenght and betweenness (and, partially, information centrality) are shown to be significantely associated to the performances of a cell (stock protection and fisheries productivity), hence providing a valuable tool to preliminary identify candidate sites for protection.

Future developments of this thesis should certainly include the assessment of a broader range of protection policies than those that could be considered in the present work. In particular, these include the possible rotation closures, in order to balance benefits and draw-

backs across regions, or to combine several closures (possibly with a smaller geographic extent) at the same time.

In order to improve the results of this work, more research effort would be needed to bridge major knowledge gaps, in paricular regarding the dispersal behaviour of adult hakes, and to build a wider and more coherent set of time series.

BIBLIOGRAPHY

URL: https://it.wikipedia.org/wiki/Merluccius_merluccius (visited on 03/23/2018) (cit. on p. 7).

URL: http://safinacenter.org/2015/08/fishing-gear-101-longlines-the-snaggers/ (visited on 03/25/2018) (cit. on p. 10).

URL: http://www.fao.org/docrep/003/x6935e/x6935e00.htm (visited on 03/25/2018) (cit. on p. 11).

URL: http://www.memphisnet.net/trammelnets (visited on 03/25/2018) (cit. on p. 12).

URL: http://www.gulfofmaine-census.org/education/research-technology/sampling-tools-for-physical-capture/ (visited on 03/25/2018) (cit. on p. 13).

Abella, A, F Serena, and JF Caddy (1998). "Estimation of the parameters of the Caddy reciprocal M-at-age model for the construction of natural mortality vectors." In: *Cahiers Options Mediterraneennes (CIHEAM)* (cit. on p. 18).

Abella, Alvaro, Fabrizio Serena, and Michela Ria (2005). "Distributional response to variations in abundance over spatial and temporal scales for juveniles of European hake (Merluccius merluccius) in the Western Mediterranean Sea." In: *Fisheries Research* 71.3, pp. 295–310 (cit. on pp. 6, 26).

Abella, Alvaro, Fabio Fiorentino, Alessandro Mannini, and Lidia Orsi Relini (2008). "Exploring relationships between recruitment of European hake (Merluccius merluccius L. 1758) and environmental factors in the Ligurian Sea and the Strait of Sicily (Central Mediterranean)." In: *Journal of Marine Systems* 71.3-4, pp. 279–293 (cit. on pp. 6, 8, 27, 37).

Adams, Douglas (1979). *Hitchhiker's Guide to the Galaxy*. Ban Books. ISBN: 0-330-25864-8 (cit. on p. v).

Alkemade, Rob, Patricia Balvanera, Céline Bellard Ben ten Brink, Neil Burgess, Silvia Ceausu, et al. (2014). "Global Biodiversity Outlook 4 - A mid-term assessment of progress towards the implementation of the Strategic Plan for Biodiversity 2011-2020." In: p. 155 (cit. on p. 1).

Arneri, E and B Morales-Nin (2000). "Aspects of the early life history of European hake from the central Adriatic." In: *Journal of Fish Biology* 56.6, pp. 1368–1380 (cit. on pp. 7, 8, 26).

Arreguín-Sánchez, Francisco (1996). "Catchability: a key parameter for fish stock assessment." In: *Reviews in Fish Biology and Fisheries* 6.2, pp. 221–242. ISSN: 1573-5184 (cit. on p. 74).

Barabási, Albert-László (2016). *Network science*. Cambridge university press (cit. on p. 90).

Baranov, Fedor I (1918). *On the question of the biological basis of fisheries*. 1, 81—128 (cit. on p. 79).

Bartolino, Valerio, Alessandro Ottavi, Francesco Colloca, Gian Domenico Ardizzone, and Gunnar Stefánsson (2008). "Bathymetric preferences of juvenile European hake (Merluccius merluccius)." In: *ICES Journal of Marine Science* 65.6, pp. 963–969 (cit. on p. 8).

Belcari, Paola (2005). "Sperimentazione e sviluppo di reti a strascico con maglie quadre come mezzo di riduzione dell'impatto sulle risorse demersali." In: (cit. on pp. 69, 77).

Belcari, Paola, Alessandro Ligas, and Claudio Viva (2006). "Age determination and growth of juveniles of the European hake, Merluccius merluccius (L., 1758), in the northern Tyrrhenian Sea (NW Mediterranean)." In: *Fisheries Research* 78.2-3, pp. 211–217 (cit. on pp. 7, 26).

Bertrand, Jacques, Luis Gil De Sola, Costas Papacostantinou, Giulio Relini, and Arnauld Souplet (2017). *International bottom trawl survey in the Mediterranean - Instruction manual*. SIBM (cit. on pp. 5, 18, 24, 46, 51).

Bjelland, Reidun Marie and Anne Berit Skiftesvik (2006). "Larval development in European hake (Merluccius merluccius L.) reared in a semi-intensive culture system." In: *Aquaculture Research* 37.11, pp. 1117–1129 (cit. on pp. 7, 8).

Borges, Jorge Luis (1952). *El idioma analítico de John Wilkins*. Editorial Pra (cit. on p. v).

Bouhlal, M and MH Ktari (1975). "Croissance du merlu de la région du golfe de Tunis." In: *Bulletin de l'Institut National Scientifique et Technique d'Océanographie et de Pêche, Salammbo* 4, pp. 5–47 (cit. on pp. 38, 67).

Bozzano, Anna, Francesc Sardà, and José Ríos (2005). "Vertical distribution and feeding patterns of the juvenile European hake, Merluccius merluccius in the NW Mediterranean." In: *Fisheries Research* 73.1-2, pp. 29–36 (cit. on p. 8).

Bruin, Frans (1970). *Royal Purple and the dye industries of the Mycenaeans and Phoenicians*. M. Mollat (cit. on p. 1).

Calvino, Italo (1979). *Se una notte d'inverno un viaggiatore*. Einaudi (cit. on p. v).

Campana, Steven E and Cynthia M Jones (1992). "Analysis of otolith microstructure data." In: *Otolith microstructure examination and analysis. Edited by DK Stevenson and SE Campana. Can. Spec. Publ. Fish. Aquat. Sci* 117, pp. 73–100 (cit. on p. 28).

Carbonara, P., W. Zupa, G. Lembo, A. Ligas, and P. Sartor (2015). *SafeNet deliverable 2.4 - Review of the existing information on MPAs and other areas with different levels of protection*, p. 94 (cit. on p. 13).

Carbonara, Pierluigi (unpublished). "Unpublished." In: (cit. on p. 28).

Cardinale, Massimiliano, Dimitrios Damalas, and Giacomo Chato Osio (2015). "Scientific, Technical and Economic Committee for Fish-

eries (STECF) - Mediterranean assessment part 1 (STECF-15-18)." In: (cit. on pp. 6, 8, 9, 18, 19, 39, 40, 68, 69, 71, 74–77, 87, 110).

Carenti, Gabriele (2012). *La pesca nell'antichitá. L'apporto dell'archeozoologia negli studi storico-archeologici: un esempio da Sulky - Sant'Antioco*. Universitá degli studi di Sassari (cit. on p. 1).

Cervantes, Miguel Saavedra (1605). *El ingenioso hidalgo don Quijote de la Mancha* (cit. on p. 121).

Colloca, Francesco, Germana Garofalo, Isabella Bitetto, Maria Teresa Facchini, Fabio Grati, Angela Martiradonna, Gianluca Mastrantonio, Nikolaos Nikolioudakis, Francesc Ordinas, Giuseppe Scarcella, George Tserpes, M. Pilar Tugores, Vasilis Valavanis, Roberto Carlucci, Fabio Fiorentino, Maria C. Follesa, Magdalena Iglesias, Leyla Knittweis, Eugenia Lefkaditou, Giuseppe Lembo, Chiara Manfredi, Enric Massutí, Marie Louise Pace, Nadia Papadopoulou, Paolo Sartor, Christopher J. Smith, and Maria Teresa Spedicato (2015). "The Seascape of Demersal Fish Nursery Areas in the North Mediterranean Sea, a First Step Towards the Implementation of Spatial Planning for Trawl Fisheries." In: *PLOS ONE* 10.3, pp. 1–25 (cit. on p. 15).

Coombs, SH and CE Mitchell (1982). "The development rate of eggs and larvae of the hake, Merluccius merluccius (L.) and their distribution to the west of the British Isles." In: *ICES Journal of Marine Science* 40.2, pp. 119–126 (cit. on p. 7).

Copernicus, Marine Environment Monitoring System (2017). URL: http://marine.copernicus.eu/ (visited on 07/25/2017) (cit. on p. 15).

Darby, CD and S Flatman (1994). *Virtual population analysis: version 3.1 (Windows/Dos) user guide*. Great Britain, Ministry of Agriculture, Fisheries and Food, Directorate of Fisheries Research (cit. on pp. 6, 19).

Druon, Jean-Noël, Fabio Fiorentino, Matteo Murenu, Leyla Knittweis, Francesco Colloca, Chato Osio, Bastien Mérigot, Germana Garofalo, Alessandro Mannini, Angélique Jadaud, et al. (2015). "Modelling of European hake nurseries in the Mediterranean Sea: an ecological niche approach." In: *Progress in oceanography* 130, pp. 188–204 (cit. on pp. 6, 8, 16, 26, 69).

EC (2003). "Commission Regulation (EC) No 2244/2003 of 18 December 2003 laying down detailed provisions regarding satellite-based Vessel Monitoring Systems." In: *O. J. Eur. Union L333*, pp. 17–27 (cit. on pp. 6, 19).

— (2008). "Council Regulation (EC) No. 199/2008 concerning the establishment of a Community framework for the collection, management and use of data in the sheries sector and support for scientic advice regarding the Common Fisheries Policy." In: *O. J. Eur. Union L60*, pp. 1–12 (cit. on pp. 6, 19).

European Marine Observation and Data Network (2017). URL: http://www.emodnet-bathymetry.eu/ (visited on 11/23/2017) (cit. on pp. 18, 47).

FAO (2016). "The State of Mediterranean and Black Sea Fisheries." In: *Journal of Natural Resources Policy Research*, p. 152 (cit. on p. 1).

Fiorentino, Fabio, Enric Massutí, F. Tinti, S. Somarakis, G. Garofalo, T. Russo, M.T. Facchini, P. Carbonara, K. Kapiris, P. Tugores, R. Cannas, C. Tsigenopoulos, B. Patti, F. Colloca, M. Sbrana, R. Mifsud, V. Valavanis, and M.T. Spedicato (2014). *Stock units: Identification of distinct biological units (stock units) for different fish and shellfish species and among different GFCM-GSA. STOCKMED Deliverable 03: FINAL REPORT. September 2014*, p. 310 (cit. on pp. 5, 20, 23, 75).

Giannoulaki, M, A Belluscio, F Colloca, S Fraschetti, M Scardi, C Smith, P Panayotidis, V Valavanis, and M Spedicato (2013). "Mediterranean Sensitive Habitats (MEDISEH), final project report." In: *DG MARE Specific Contract SI2* 600741, p. 557 (cit. on pp. 5, 7, 8, 15, 18, 23, 25–27, 35, 46, 48, 69).

Hardin, Garrett (1968). "The tragedy of the commons." In: *Science* 162.3859, pp. 1243–1248 (cit. on p. 1).

Hidalgo, Manuel, Enric Massutí, Joan Moranta, Joan Cartes, Josep Lloret, Pere Oliver, and Beatriz Morales-Nin (2008). "Seasonal and short spatial patterns in European hake (Merluccius merluccius L.) recruitment process at the Balearic Islands (western Mediterranean): the role of environment on distribution and condition." In: *Journal of Marine Systems* 71.3-4, pp. 367–384 (cit. on pp. 6, 37).

Hidalgo, Manuel, Enric Massutí, Beatriz Guijarro, Joan Moranta, Lorenzo Ciannelli, Josep Lloret, Pere Oliver, and Nils Christian Stenseth (2009). "Population effects and changes in life history traits in relation to phase transitions induced by long-term fishery harvesting: European hake (Merluccius merluccius) off the Balearic Islands." In: *Canadian Journal of Fisheries and Aquatic Sciences* 66.8, pp. 1355–1370 (cit. on p. 26).

Jardas, I (1996). "Adriatic ichthyofauna." In: *Školska knjiga dd, Zagreb*, pp. 29–36 (cit. on pp. 6, 9).

Kavadas, S, I Maina, D Damalas, I Dokos, M Pantazi, and V Vassilopoulou (2015). "Multi-Criteria Decision Analysis as a tool to extract fishing footprints and estimate fishing pressure: application to small scale coastal fisheries and implications for management in the context of the Maritime Spatial Planning Directive." In: *Mediterranean Marine Science* 16.2, pp. 294–304 (cit. on pp. 6, 19, 20, 75).

Lall, Upmanu and Ashish Sharma (1996). "A nearest neighbor bootstrap for resampling hydrologic time series." In: *Water Resources Research* 32.3, pp. 679–693 (cit. on p. 90).

Leslie, Patrick Holt (1945). "On the use of matrices in certain population mathematics." In: *Biometrika* 33.3, pp. 183–212 (cit. on p. 70).

Ligas, A, P Belcari, D Bertolini, and C Viva (2003). "Growth of juveniles of European hake, Merluccius merluccius (L., 1758), in the northern Tyrrhenian Sea." In: *Biol. Mar. Medit* 10.2, pp. 853–855 (cit. on p. 26).

Ligas, Alessandro and Paolo Sartor (2015). *SafeNet deliverable 2.2 - Report on the status of exploitation of selected stocks*, p. 18 (cit. on pp. 1, 14).

Lleonart, Jordi (2002). *Impact of fishery and environment on hake recruitment in Northwestern Mediterranean (LLUCET)*, pp. 129–131 (cit. on pp. 5–8, 27, 28, 30, 51).

Massutí, Enric, Sebastià Monserrat, Pere Oliver, Joan Moranta, José Luis López-Jurado, Marta Marcos, Manuel Hidalgo, Beatriz Guijarro, Aina Carbonell, and Pilar Pereda (2008). "The influence of oceanographic scenarios on the population dynamics of demersal resources in the western Mediterranean: hypothesis for hake and red shrimp off Balearic Islands." In: *Journal of Marine Systems* 71.3-4, pp. 421–438 (cit. on p. 27).

Melià, Paco, Marcello Schiavina, Marisa Rossetto, Marino Gatto, Simonetta Fraschetti, and Renato Casagrandi (2016). "Looking for hotspots of marine metacommunity connectivity: a methodological framework." In: *Scientific Reports* 6, p. 23705 (cit. on p. 23).

Millar, Russell B and René Holst (1997). "Estimation of gillnet and hook selectivity using log-linear models." In: *ICES Journal of Marine Science* 54.3, pp. 471–477 (cit. on p. 76).

Millot, Claude (1999). "Circulation in the Western Mediterranean Sea." In: *Journal of Marine Systems* 20.1, pp. 423 –442. ISSN: 0924-7963 (cit. on pp. 37, 67).

Mood, Alexander McFarlane (1974). "Introduction to the Theory of Statistics." In: (cit. on p. 34).

Morales-Nin, Beatriz and Yvonne Aldebert (1997). "Growth of juvenile Merluccius merluccius in the Gulf of Lions (NW Mediterranean) based on otolith microstructure and length-frequency analysis." In: *Fisheries Research* 30.1-2, pp. 77–85 (cit. on pp. 26, 27).

Morales-Nin, Beatriz and Joan Moranta (2004). "Recruitment and postsettlement growth of juvenile Merluccius merluccius on the western Mediterranean shelf." In: *Scientia Marina* 68.3, pp. 399–409 (cit. on pp. 7, 25, 26).

Munro, Gordon R (1979). "The optimal management of transboundary renewable resources." In: *Canadian Journal of Economics*, pp. 355–376 (cit. on p. 1).

Newman, Mark (2010). *Networks: an introduction*. Oxford university press (cit. on p. 91).

Olivar, MP, G Quilez, and M Emelianov (2003). "Spatial and temporal distribution and abundance of European hake, Merluccius

merluccius, eggs and larvae in the Catalan coast (NW Mediterranean).” In: *Fisheries Research* 60.2-3, pp. 321–331 (cit. on pp. 7, 24, 26, 27).

Oliver, Pere and Enric Massutí (1994). “Biology and fisheries of western Mediterranean hake (M. merluccius).” In: (cit. on pp. 6, 23).

Ostrogorski, Georgije (1969). *History of the Byzantine state*. Rutgers University Press (cit. on p. 1).

Palomera, Isabel, M Pilar Olivar, and Beatriz Morales-Nin (2005). “Larval development and growth of the European hake Merluccius merluccius in the northwestern Mediterranean.” In: *Scientia Marina* 69.2, pp. 251–258 (cit. on pp. 8, 26).

Raffaele, Federico (1888). *Le uova galleggianti e le larve dei Teleostei nel golfo di Napoli*. Stazione zoologica di Napoli (cit. on pp. 1, 7).

Recasens, Laura, Velia Chiericoni, and Paola Belcari (2008). “Spawning pattern and batch fecundity of the European hake (Merluccius merluccius (Linnaeus, 1758)) in the western Mediterranean.” In: *Scientia Marina* 72.4, pp. 721–732 (cit. on pp. 7, 26–29).

Reis, EG and MG Pawson (1992). “Determination of gill-net selectivity for bass (Dicentrarchus labrax L.) using commercial catch data.” In: *Fisheries research* 13.2, pp. 173–187 (cit. on p. 77).

Relini, G, J Bertrand, and A Zamboni (1999). “Synthesis of the knowledge on bottom fishery resources in central Mediterranean (Italy and Corsica).” In: *Biologia Marina Mediterranea* 6.suppl 1, pp. 314–322 (cit. on p. 6).

Russo, Tommaso, Antonio Parisi, Marina Prorgi, Fabrizio Boccoli, Innocenzo Cignini, Maurizio Tordoni, and Stefano Cataudella (2011). “When behaviour reveals activity: Assigning fishing effort to métiers based on VMS data using artificial neural networks.” In: *Fisheries Research* 111.1, pp. 53 –64. ISSN: 0165-7836 (cit. on p. 19).

Russo, Tommaso, Isabella Bitetto, Pierluigi Carbonara, Roberto Carlucci, Lorenzo D’Andrea, Maria T Facchini, Giuseppe Lembo, Porzia Maiorano, Letizia Sion, Maria T Spedicato, et al. (2017). “A holistic approach to fishery management: Evidence and insights from a Central Mediterranean case study (Western Ionian Sea).” In: *Frontiers in Marine Science* 4, p. 193 (cit. on pp. 9, 46, 77).

Sabates, Ana (1990). “Distribution pattern of larval fish populations in the Northwestern Mediterranean.” In: *Marine Ecology Progress Series*, pp. 75–82 (cit. on p. 25).

Sartor, Paolo, Pierluigi Carbonara, Giuseppe Lembo, Maria Teresa Spedicato, and Alessandro Ligas (2015). *SafeNet deliverable 2.5 - Report on the main socio-economic indicators and structure of the selected fisheries*, p. 65 (cit. on pp. 2, 5, 6, 9, 75).

Sbrana, Mario, Franco Biagi, Paolo Sartor, and Stefano De Ranieri (1998). “Selectivity of a commercial bottom trawl net in the tuscan arcipelago (northern Tyrrhenian sea).” In: *Biologia Marina Mediterranea* 5.2, pp. 449–456 (cit. on pp. 69, 77).

Sbrana, Mario, Paola Belcari, Stefano De Ranieri, Paolo Sartor, and Claudio Viva (2007). "Comparison of the catches of European hake (Merluccius merluccius, L. 1758) taken with experimental gillnets of different mesh sizes in the northern Tyrrhenian Sea (western Mediterranean)." In: *Scientia Marina* 71.1, pp. 47–56 (cit. on p. 76).

Velasco, F and I Olaso (1998). "European hake Merluccius merluccius (L., 1758) feeding in the Cantabrian Sea: seasonal, bathymetric and length variations." In: *Fisheries Research* 38.1, pp. 33–44 (cit. on p. 8).

Von Bertalanffy, Ludwig (1938). "A Quantitative Theory of organic growth (Inquires on Growth Laws. II)." In: *Human Biology* 10.2, pp. 181–213. ISSN: 00187143, 15346617 (cit. on pp. 18, 68).

...Vengamos ahora a la citación de los autores que los otros libros tienen, que en el vuestro os faltan. El remedio que esto tiene es muy fácil, porque no habéis de hacer otra cosa que buscar un libro que los acote todos, desde la A hasta la Z, como vos decís. Pues ese mismo abecedario pondréis vos en vuestro libro; [...] y más, que no habrá quien se ponga a averiguar si los seguistes o no los seguistes, no yéndole nada en ello...

— Cervantes, *El ingenioso hidalgo don Quijote de la Mancha*